

UNCLASSIFIED

## REPORT DOCUMENTATION

AD-A236 231

ed  
M-0188

Public reporting burden for this collection of information is estimated to average 1 hour per record, including gathering the data needed, and completing and reviewing the collection of information, including suggestions for reducing this burden. To Washington, D.C. 20503, and to the Office of Management and Budget, Paperwork Project, Washington, D.C. 20503.



Existing data sources,  
by other aspect of this  
report, 1215 Jefferson  
: 20503.

1. AGENCY USE ONLY (Leave blank)		2. REPORT DATE 24 April 1991		3. REPORT TYPE AND DATES COVERED FINAL REPORT June 89 to June 90	
4. TITLE AND SUBTITLE Stochastic Estimation of Coherent Structures and Their Dynamics in Transitional and Turbulent Boundary Layers				5. FUNDING NUMBERS PE - 61102F PR - 2307 TA - A2	
6. AUTHOR(S) Y. G. Guezennec, T. J. Gieseke and N. Trigui				8. PERFORMING ORGANIZATION REPORT NUMBER AFOSR-TR- 91 011	
7. PERFORMING ORGANIZATION NAME(S) AND ADDRESS(ES) Mechanical Engineering Department Ohio State University				10. SPONSORING/MONITORING AGENCY REPORT NUMBER AFOSR-89-0434	
9. SPONSORING/MONITORING AGENCY NAME(S) AND ADDRESS(ES) AFOSR/NA Building 410 BOLLING AFB, DC 20332-6448				11. SUPPLEMENTARY NOTES DTIC	
12a. DISTRIBUTION / AVAILABILITY STATEMENT Approved for public release; distribution is unlimited				12b. DISTRIBUTION CODE	
13. ABSTRACT (Maximum 200 words) The structure of transitional and turbulent boundary layers was investigated experimentally using the stochastic estimation technique. The two-point space-time full correlation tensor was measured at various Reynolds numbers in the near wall region of a boundary layer, and the outer region of a regular and LEBU manipulated boundary layer. It was found that multi-point stochastic estimates yield a far more realistic picture of the turbulent structures than conventional one-point conditional averages. A new technique was developed, whereby the pseudo-dynamic evolution of the flow field is reconstructed by means of the stochastic estimation for a measured time sequence of velocity at one or more points. This yields a very realistic kinematic evolution of the flow structures. Prospects for deriving dynamical evolution equations for the stochastic estimates have also been explored.					
14. SUBJECT TERMS TURBULENCE, TRANSITION, BOUNDARY LAYER				15. NUMBER OF PAGES 92	
17. SECURITY CLASSIFICATION OF REPORT UNCLASSIFIED				18. SECURITY CLASSIFICATION OF THIS PAGE UNCLASSIFIED	
19. SECURITY CLASSIFICATION OF ABSTRACT UNCLASSIFIED				20. LIMITATION OF ABSTRACT UL	

AFOSR-TR- 91 05 11

Approved  
distributed

Final Report on Grant AFOSR 89-0434

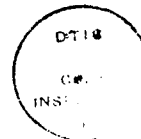
Submitted to the  
Air Force Office of Scientific Research

on

**STOCHASTIC ESTIMATION OF COHERENT STRUCTURES  
AND THEIR DYNAMICS IN TRANSITIONAL  
AND TURBULENT BOUNDARY LAYERS**

by

Y. G. Guezennec  
T. J. Gieseke  
and  
N. Trigui



Mechanical Engineering Department  
The Ohio State University

April 1991

Accession For	
DTIC GRA&I	<input checked="" type="checkbox"/>
DTIC I&M	<input type="checkbox"/>
Unclassified	<input type="checkbox"/>
Justification	
By	
Distribution	
Availability	
Availability	
Dist	Special

A-1

91 6 6 006

91-01380



## TABLE OF CONTENTS

	Page
I. INTRODUCTION	3
II. DESCRIPTION OF EXPERIMENTS	5
Case 1: Wall Layer Structure as a Function of Reynolds Number	7
Case 2: Outer Layer Structure and Large Eddy Break Up Devices	14
III. RESULTS	17
Calibration and Use of Triple Hot-Wire Probes	17
Case 1: Wall Layer Structure as a Function of Reynolds Number	18
Case 2: Outer Layer Structure and Large Eddy Break Up Devices	18
IV. CONCLUSIONS	19
V. APPENDICES	
A. Paper accepted to Experiments in Fluids (1991): An Experimental Approach to the Calibration and Use of Triple Hot-Wire Probes, T. J. Gieseke and Y. G. Guezennec	A-1
B. Paper presented to 29th AIAA Aerospace Sciences Meeting, Reno, Nevada (1991): Detailed Documentation of the Near Field Effects of Large Eddy Break Up Devices on the Oncoming Vortical Structures in Turbulent Boundary Layers, N. Trigui and Y. G. Guezennec	B-1
C. Transparencies presented at the 1991 AFOSR Meeting on Turbulence Structure and Control, Columbus, Ohio (1991): The Stochastic Estimation: A Versatile Tool to Study and Predict (?) Turbulent Flows, Y. G. Guezennec, T. J. Gieseke W. C. Choi and N. Trigui	C-1

## I. INTRODUCTION

Although turbulent boundary layers are very common flows in engineering, the physical mechanisms responsible for the production and sustenance of turbulence are still ill-defined. Largely due to visual studies, the traditional view of turbulence as a random field has evolved in the past twenty years into a more mechanistic description of the turbulent processes through the identification of so-called coherent structures. Among the various structures identified in the context of turbulent boundary layers are the low-speed streaks (Schraub and Kline, 1965; Kline et al., 1967; Blackwelder, 1978 and others), the hairpin vortices (Kim et al., 1971; Smith, 1978; Head and Bandyopadhyay, 1981, Moin and Kim, 1985 and others) and the large-scale outer structures (Blackwelder and Kovaznay, 1972; Brown and Thomas, 1977; Chen and Blackwelder, 1978 and others). It has also been recognized that most of the turbulence production occurs near the wall (Klebanoff, 1954) during very localized random events (in space and time) called bursts (Kline et al, 1967; Kim et al, 1971; Blackwelder and Kaplan, 1976 and others). Due to the complexity of these unsteady three-dimensional processes, and the lack of universally accepted definition of their spatio-temporal structure, most of the evidence gathered from measurements or visual studies has been incomplete and often hard to meld into a unified view of the boundary layer.

Recent advances in computational and instrumentation means have triggered new approaches to improve our understanding of boundary layers: first, the possibility of undertaking full Navier-Stokes simulations for simple turbulent flows (Moin and Kim, 1982, etc...); second, the possibility of processing efficiently large images of flow fields to obtain quantitative information about their instantaneous structures (Brodkey, 1986 and others); and third, the possibility of acquiring large amounts of experimental data to map (at least in the statistical sense) the three-dimensional flow field (Guezennec, 1985 and others). It is only through the convergence of these efforts that the dynamics of the boundary layers will be fully elucidated, and that previous findings will be integrated into a more mechanistic description.

It is very important from a technological standpoint to understand the physical processes in turbulent boundary layers, especially to achieve desired characteristics by modifying their structure. For example, the recent results in drag reduction through suppression of large scales (Corke et al, 1982; Plesniak et al., 1985 and others) could be further optimized if the mechanisms at play were better understood. Other potential applications include heat and mass transfer modification and boundary layer noise

reduction. The ubiquity of these wall-bounded turbulent flows in technological applications justifies the need for a more fundamental understanding of the underlying physics.

An other important aspect is to bridge the gap between transitional and turbulent boundary layers. Recent studies seem to indicate that similar structures and physics may be present in both flows (Kim and Moin, 1986; Williams, 1985 and others), but no direct attempt at tracing these structures over a range of Reynolds number in both regimes has yet been undertaken. It is clear that if the same physical processes are responsible for the breakdown of transitional boundary layers and the turbulence production in turbulent boundary layers, major advances in the modeling of such flows way can be achieved by a unified approach.

Nagib and Guezennec (1986) performed the first attempt to map experimentally the three-dimensional structure of some turbulence producing events. Their results indicate the presence of two counter-rotating roller structures with a scale of the order of half the boundary layer thickness. Based on these results, a conjectured model of the turbulent boundary layer was proposed. However, a number of questions remained unanswered. The origin of those rollers was not clearly established, nor was their evolution. In addition, the mapped events were only reconstructed for two classes of events due to the particular detection technique used (wall-shear). Although they conclusively proved that the events detected by this technique were second and fourth quadrant Reynolds stress events, a broader class of events than the conventional quadrant technique may have been averaged, which could have led to some smearing of the spatial maps. This was later shown to be true particularly for the second quadrant motions by Guezennec, Piomelli and Kim (1987). Moreover, due to experimental limitations, the transverse component of velocity was not measured, but inferred from continuity assuming symmetry about the center plane. This symmetry which reflects the homogeneity of the statistics in the spanwise direction does not need to be true instantaneously, but only on the average. In addition, it has been speculated that that instantaneous structures may come isolated rather than in pairs, as implied by statistical averages. Guezennec, Piomelli and Kim (1987) and Choi and Guezennec (1990) quantified this asymmetry and found that instantaneous structures are more likely to be asymmetric. Based on this, they designed new ensemble averaging procedures to respect this marked asymmetry.

More recently, Guezennec (1988) reprocessed his database using the stochastic estimation technique (Adrian, 1979; Adrian and Tung, 1980,...). The results obtained

by this technique compared very well with those obtained by conventional ensemble averaging. The stochastic estimation offers many advantages over conventional processing. In particular, it allows to examine any number of "conditions" selected *a posteriori* without reprocessing the raw data base, since the procedure relies upon unconditional statistics (two-point spatial correlations). This represent a real computational advantage when dealing with large, three-dimensional data bases. Time evolution for a given condition can be obtained by a simple extension of the technique and the use of space-time correlation functions instead of spatial correlations. Due to the unconditional nature of the underlying statistics, the estimates of the conditional averages also tend to be smoother than those obtained by conventional means (with limited number of realizations).

It has been observed that single point conditional averages (conventional or else) tend to yield structures which scale with the integral scale of the flow. One way around this problem is to perform multi-point conditional averages, i.e. specifying conditions at more than one point. This allows to examine events with a specific length scale governed by the separation between the two or more points at which conditions are specified. However, such conditional measurements are hard to obtain in practice by ensemble averaging. On the other hand, the stochastic estimation is easily generalized to estimate multi-point conditional averages. Preliminary applications of two-point conditional averages have been performed by Adrian and Moin (1987) and Guezennec (1988) to examine events characterized by a sharp interface such as VITA events corresponding to the rapid interaction between second and fourth quadrant motions. The multi-point conditional averages is a very valuable new tool to study "realistic" average structures which bear some resemblance to the instantaneous ones (see Adrian, Moser and Moin, 1987).

## II. DESCRIPTION OF EXPERIMENTS

The experimental research performed was aimed at gaining a better understanding of the structure of turbulent boundary layers and the mechanisms responsible for the sustenance of turbulence. In addition, the relationship between structures observed in turbulent and transitioning boundary layers were to be examined. These objectives were addressed by performing three-dimensional mappings of the flow field at various Reynolds numbers ranging from the transition regime to the fully turbulent one.

One of the key aspects of this study was not only to extract the important flow

structures, but also to study their evolution. Due to the ease of estimating the conditional flow fields for a large number of conditions by means of the stochastic estimation, the evolution of the structures can then be obtained by reconstructing a sequence of flow fields corresponding to a real (measured) time sequence of conditions (*pseudodynamics*). Essentially, this procedure allows to examine the average evolution of structures corresponding to real sequences of events. This approach should enhance our fundamental understanding of the dynamics of the turbulence, while eliminating some of the unnecessary details which contributed to the event-to-event variability. The realism of such pseudo-dynamic reconstruction is particularly enhanced by using multi-point conditional estimates as described earlier.

Based on the limitations of the previous work, it is felt that all three components of velocities had to be measured both at the detection probe and at the moving probe. The penalty paid for having a intrusive detection probe (as opposed to flush-mounted shear sensors) is outweighed by the benefits of the full determination of the velocity vector and allows to discriminate a broader range of motions, in particular the more likely asymmetric structures. The experiments consisted of measuring the full three-dimensional two-point correlation tensors for all velocity components in the boundary layer at various Reynolds numbers and various reference heights. The measurements were performed using a three-component miniature hot-wire probe located at a fixed position above the wall and acquiring data simultaneously with another three-component probe located at various positions around the fixed probe. The movable probe scanned a full three-dimensional grid around the fixed probe. All data was acquired digitally and calibrated on-line. Due to the large amount of data required to obtain converging statistics, those statistics (two-point spatial correlations of second and third order) were also computed on-line and stored for each grid point. Nonetheless, the raw hot-wire signals were archived on magnetic tapes after calibration to allow future reprocessing of the data by other means.

Only the linear estimation technique mentioned earlier was used to process the correlations and obtain the spatial arrays of coefficients required to estimate the average flow field for any given condition. While the quadratic estimates which involve third order statistics have been found somewhat better to examine flow fields characterized by a high skewness (Guezennec, 1988), this advantage disappears when *multipoint* linear stochastic estimates are used.

As mentioned earlier, the evolution of the important structures was investigated by measuring real time sequences of conditions at the fixed probe and using those to

generate dynamic sequences of the corresponding averaged flow fields. This novel procedure which we call *pseudo-dynamics* allows to obtain a animated sequence of kinematic reconstruction of the flow fields consistent with a dynamic (measured) time sequence of conditions. Animated display and movies of such sequences of events are currently being generated to facilitate the interpretation of such data.

Since the mappings of the boundary layer were performed for all velocity components, it is more efficient to measure simultaneously all three components of the velocity. However, the large amount of data required for the three-dimensional mappings necessitate very efficient calibration and velocity extraction procedures for the triple hot-wire probes. Such probes are known to be very difficult to calibrate and use. The extraction of the velocity components from the three anemometer voltages is a complex task involving solving a stiff system of non-linear equations for every velocity triplet. Hence, a considerable amount of time was devoted at the beginning of the project to establish efficient calibration procedures and develop a novel table look-up technique for the velocity extraction. The details of such techniques can be found in T. J. Gieseke's Masters Thesis (1990) and are summarized in a paper presented at the Symposium on Turbulence at the University of Rolla, Missouri in September 1990 and accepted for publication in Experiments in Fluids. A copy of this paper is included in Appendix A.

Two case studies were conducted. One corresponded to the experiments described originally in the proposal, namely a mapping of a regular boundary layer with respect to a probe located in the near wall region and performed at various Reynolds numbers. The other one was a comparative study of the large scale structures in a regular turbulent boundary layer and the changes imposed on such structures in the near field of flow manipulators, namely Large Eddy Break Up Devices.

#### **Case 1: Wall Layer Structure as a Function of Reynolds Number**

For this experiment, simultaneous readings of velocity were taken with two triple hot-wire probes placed in the turbulent boundary layer. One was fixed in space being attached to the measurement plug (the reference probe) and one was attached to the traversing mechanism (the grid or mapping probe). The mapping probe was moved over a grid of locations. These experiments were performed for Reynolds numbers of 3700, 2540, and 960. For each  $R_\theta$ , the experiment was repeated for two reference probe locations, each location depending on Reynolds number and experimental grid specifications. A triple wire probe attached to the traversing mechanism, a

triple wire probe was mounted beneath the test plate with the hot-wire array and body protruding through a small hole in the measurement plug as shown in Figure 1. This probe could be moved vertically, toward or away from the test plate, by sliding it in a specially designed mount. This allowed the probe to be moved out of the boundary layer for calibration or to any vertical location for use as a reference probe in the conditional eddy estimation. Only one reference probe was mounted in the test section at a given time. Additional reference points were added by repeating the experiments and combining the results in processing.

The probe mounted to the traversing mechanism was type AHWP-3-2-OSU (Probe 1). The stationary probe was type AHWP-3-1-OSU (Probe 2). Physical limitations of the arrangement came from the size of the probes. The delicate structure of the hot-wire arrays required that extreme care be taken not to allow the probes to come into contact with each other which would cause damage to the probes. A telescope mounted on a manual positioning mechanism with a range of 0 to 1.3 cm in each direction was used to accurately measure the dimensions of each probe (Figure 2). This allowed definition of a safe range for the moving mapping probe around the stationary probe. The motion of the probes was most limited in the  $z$  direction where the probe bodies interfered with each other. A computer controlled the probe motion using an algorithm designed to avoid objects. These objects were defined in space by the user and the control of probe motion prevented probe contact while allowing minimum probe separation.

The grid over which the moving probe was traversed varied with test Reynolds number. For all Reynolds number cases, the reference probe was positioned as close to the wall as possible, 0.81 mm when measured from the wall to the center of the probe measurement volume. This brings the lowest probe prongs nearly in contact with the wall at a height of 0.43 mm. The grid for each case is described by the information: grid corner location  $(x_h, y_h, z_h)$ , grid size  $(s_x, s_y, s_z)$ , number of grid points  $(n_x, n_y, n_z)$ , reference probe location  $(x_p, y_p, z_p)$ , and bounds of the box around the reference probe to be avoided  $(x_h - x_s < x < x_h + x_s, 0 < y < y_s, z_h - z_s < z < z_h + z_s)$  as shown in Figure 3. Grid dimensions were selected to capture the behavior of large scale eddies in space and time as found in the experiments by Choi and Guezennec (1989). Digital sampling of the anemometer readings was conducted with a  $\Delta t$  of two viscous time units. This frequency varies roughly like the square of the Reynolds number as the turbulent time scales do. The number of samples chosen for statistical convergence had to be reduced from 20,000 to 10,000 for the lowest Reynolds number case in order to

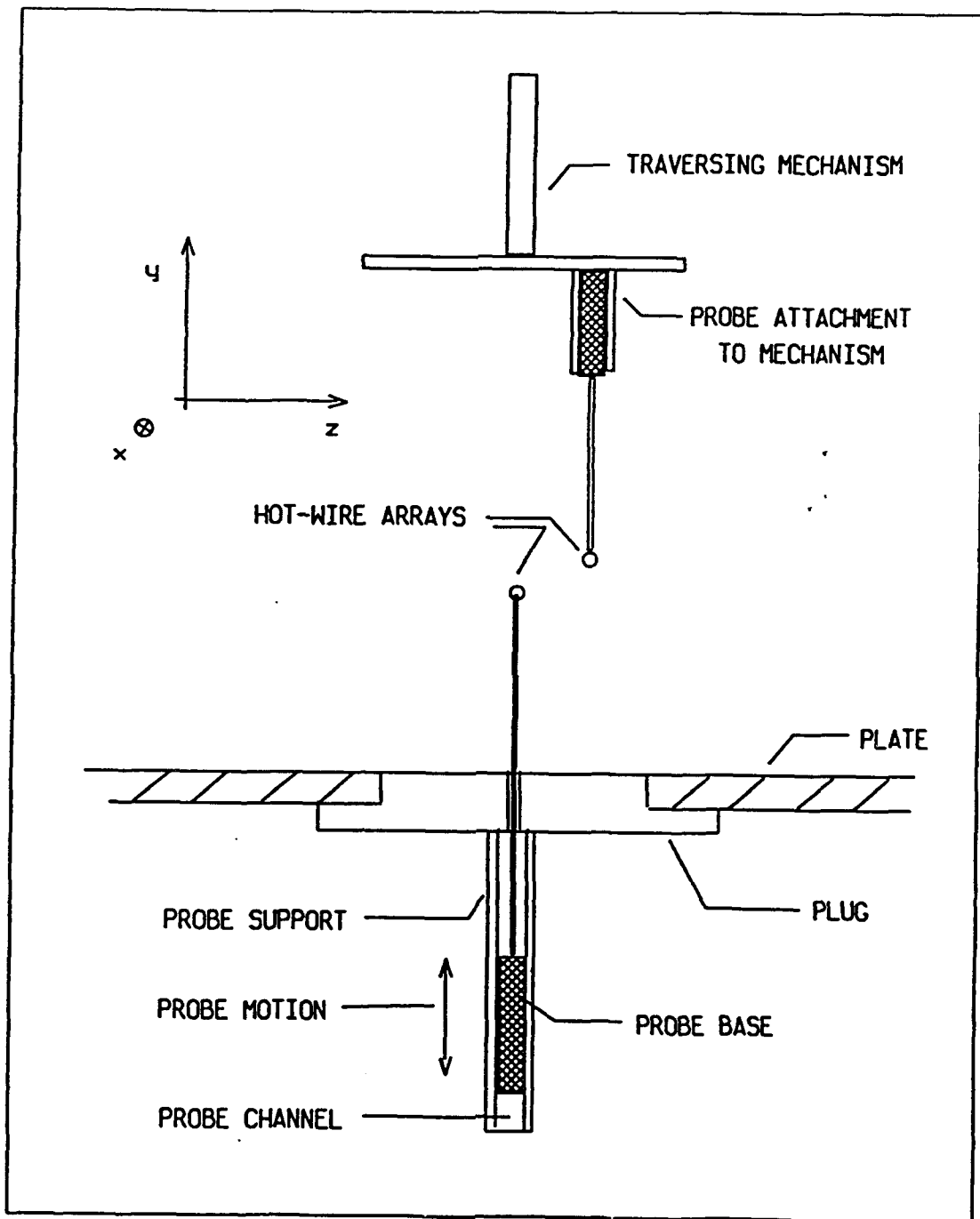


Figure 1. Schematic Diagram of Probe Mounting

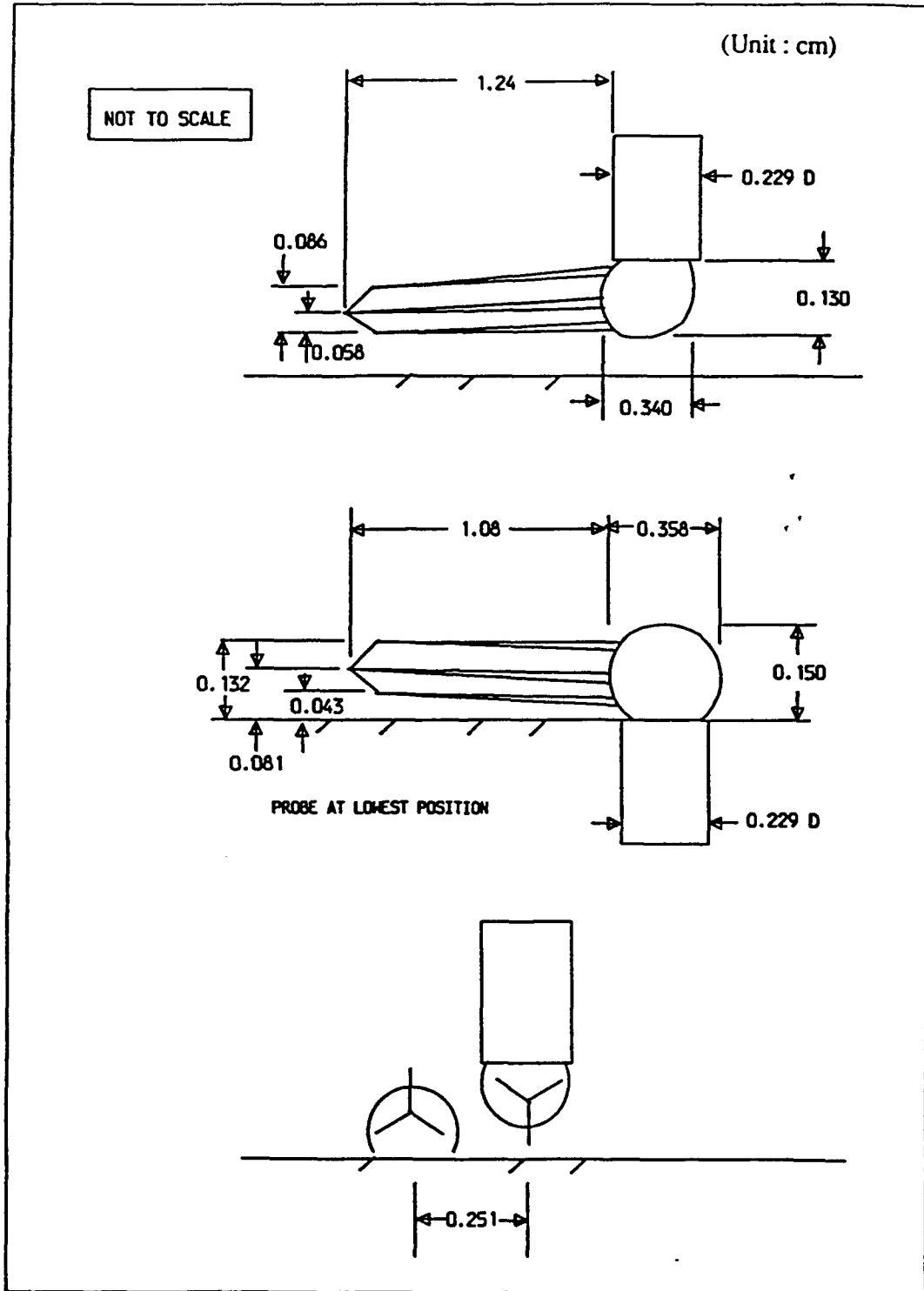


Figure 2. Schematic Diagram of Subminiature Triple Hot-Wire Probes

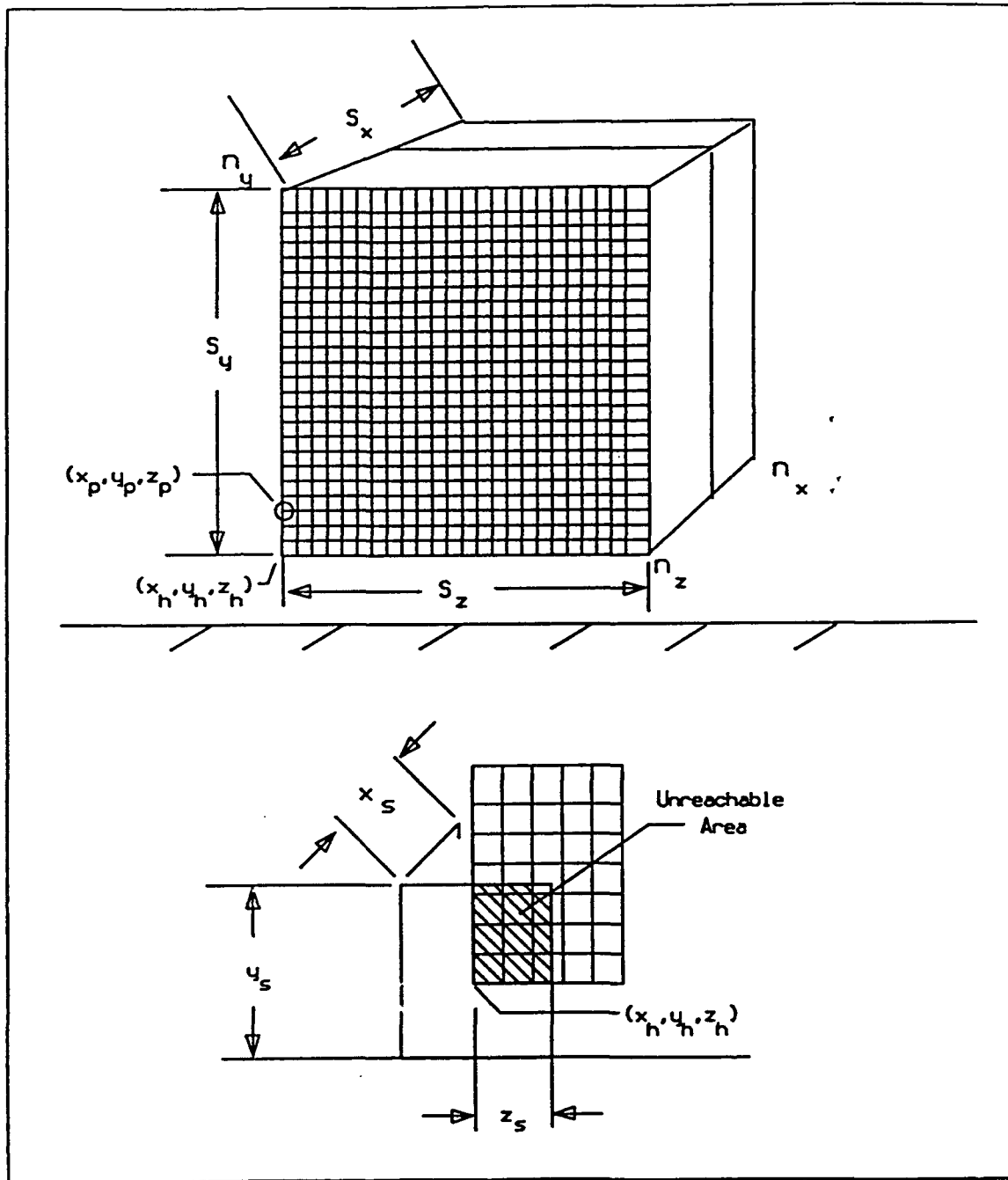


Figure 3. Physical Acquisition Grid for Wall Layer Mappings

	CASE					
	1	2	3	4	5	6
$R_\theta$	3700	3700	2540	2540	900	900
N	20000	20000	20000	20000	10000	10000
f (Hz)	7240	7240	2240	2240	240	240
$x_p^+$	0	0	0	0	0	0
$y_p^+$	20	60	13	53	5	35
$z_p^+$	0	0	0	0	0	0
$x_h^+$	0	0	0	0	0	0
$y_h^+$	20	20	10	10	5	5
$z_h^+$	0	0	0	0	0	0
$s_x^+$	0	0	0	0	0	0
$s_y^+$	400	400	400	400	210	210
$s_z^+$	400	400	400	400	210	210
$n_x^+$	1	1	1	1	1	1
$n_y^+$	21	21	21	21	15	15
$n_z^+$	21	21	21	21	15	15
$x_s^+$	300	300	208	208	80	80
$y_s^+$	59	99	42	82	19	34
$z_s^+$	39	39	39	39	14	14

Table 1. Mapping Grid Characteristics

allow the experiment to be completed in a reasonable time. These variables for all experiments are shown in Table 1 with values in wall units. Owing to the usual symmetric structure of the correlation tensor in the spanwise direction, the measurements were only conducted on one side of the reference probe.

With the grid definition based on the wall variables and the physical limitations, the experiments proceeded in a straightforward fashion. Both the reference and the moving probes were first calibrated to determine their sensitivities and the information was stored as a set of coefficients from the polynomial that best fit measured voltages and freestream velocities. The reference probe was then moved into position in the boundary layer and the mapping probe moved to a known location near the reference probe. With the free-stream velocity set to the desired value the computer was given control of the experiment. The mapping probe traveled from point to point on the grid where the record of discrete voltages output from each of the six anemometers was stored on disk. No processing of the readings was conducted during the experiments. The raw data and calibration information was transferred to an alternate computer system where calculations could be conducted more rapidly.

All the processing took place on a DEC-3100 workstation rather than on the Masscomp system used to acquire the data. This was primarily done because the Masscomp, although ideal for data acquisition, is much slower computationally than the DEC. The DEC, however, is not equipped with a large data storage system like the Masscomp 350 MB hard disk drive which is capable of storing data from several experiments before a tape backup is required. Because of the limitations of both systems, they had to be used in tandem. Data was stored on the large disk and transferred a parcel at a time to the DEC for processing. The data parcels were organized according to experimental grid location and contain all data acquired while the mapping probe was at that location. Each parcel of data consisted of six sampled traces, each trace containing 10,000 or 20,000 data points.

Using the sensitivity calibration and angular calibration tables generated for the experiment, the voltage readings were transformed into discrete velocity vector traces at the reference and grid locations. After the mean velocity components were removed, correlations between the fluctuating velocity components were calculated to generate the stochastic estimation matrices at each location. In addition to calculating the correlations between simultaneously occurring velocities, the correlations were also computed between velocities at the reference position and at the moving probe with some time separation. Because turbulence within the boundary layer is nearly

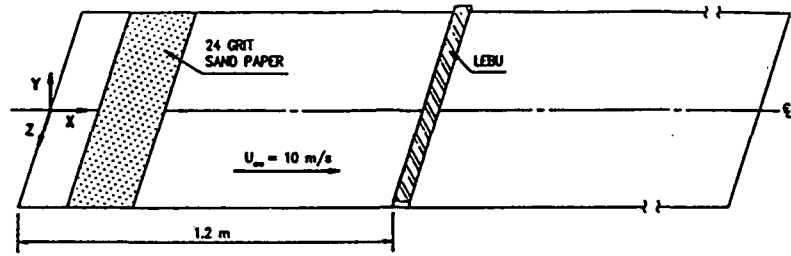
homogeneous in  $x$  and convecting downstream, time separation can be used to estimate correlation measurements in the streamwise direction (Taylor's hypothesis).

Because of the physical limitations preventing the mapping probe from reaching all of the grid points, correlations at these points had to be measured using additional experiments or by interpolating between known values. Making use of symmetry in  $z$ , some missing values were estimated using data from experiments with the reference probe at other locations. For locations that could not be reached, either linear or parabolic interpolation, depending on the knowledge of the correlation variation behavior in space and time, was used between nearby data points on the grid to estimate the values.

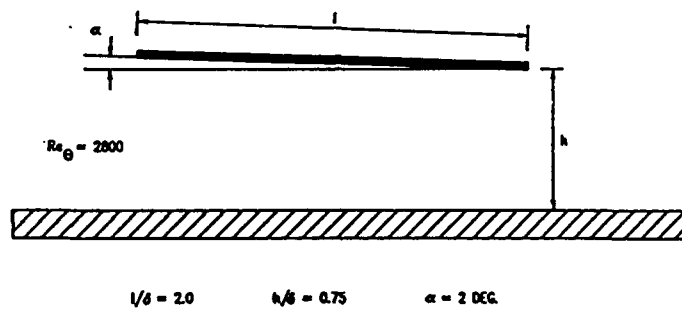
### **Case 2: Outer Layer Structure and Large Eddy Break Up Devices**

The boundary layer investigated was nominally a zero pressure gradient, flat plate boundary layer with a free-stream velocity of 10 m/s and Reynolds number based on momentum thickness ranging from 2000 to 8000. A flat plate manipulator was placed 1.2 m from the leading edge at a small angle of attack of approximately 2 degrees. This location,  $x_L$ , corresponds to a Reynolds number based on momentum thickness  $Re_\theta$  of about 2500. The LEBU was made out of 5 cm wide, 0.127 mm thick blued spring steel strip. It was suspended 1.9 cm above the plate and was carefully tensioned to avoid any vibration. The regular boundary layer thickness,  $\delta_0$ , at that location was nominally 2.5 cm. In other words, the LEBU configuration corresponded to a chord length of  $2 \delta_0$  and a height of  $0.75 \delta_0$ . A schematic diagram of the boundary layer test plate and of the LEBU configuration is given in Figure 4. For more details, the reader is referred to Trigui (1991).

The main part of the experiment consisted in acquiring six simultaneously sampled hot-wire signals: three velocity components at a fixed reference point ("detection probe") and three velocity components at a mapping probe traversed over a coarse three-dimensional sampling grid. In order to study the evolution of the large-scale vortical structures as they pass over the manipulator, the fixed probe was positioned 0.635 cm ( $0.25 \delta_0$ ) upstream of the leading edge of the manipulator at the same height. A mapping was performed on a  $3 \times 15 \times 31$  mesh in the streamwise, normal and spanwise directions, respectively. The first cross-stream ( $y-z$ ) plane corresponded to a zero streamwise separation between the detection and the mapping probes. The second and third cross-stream planes corresponded to separation of 1.27 cm and 2.54 cm ( $0.5$  and  $1.0 \delta_0$ ), respectively.



TEST PLATE



LEBU CONFIGURATION

Figure 4. Schematic Diagram of Boundary Layer Test Plate and LEBU Configuration

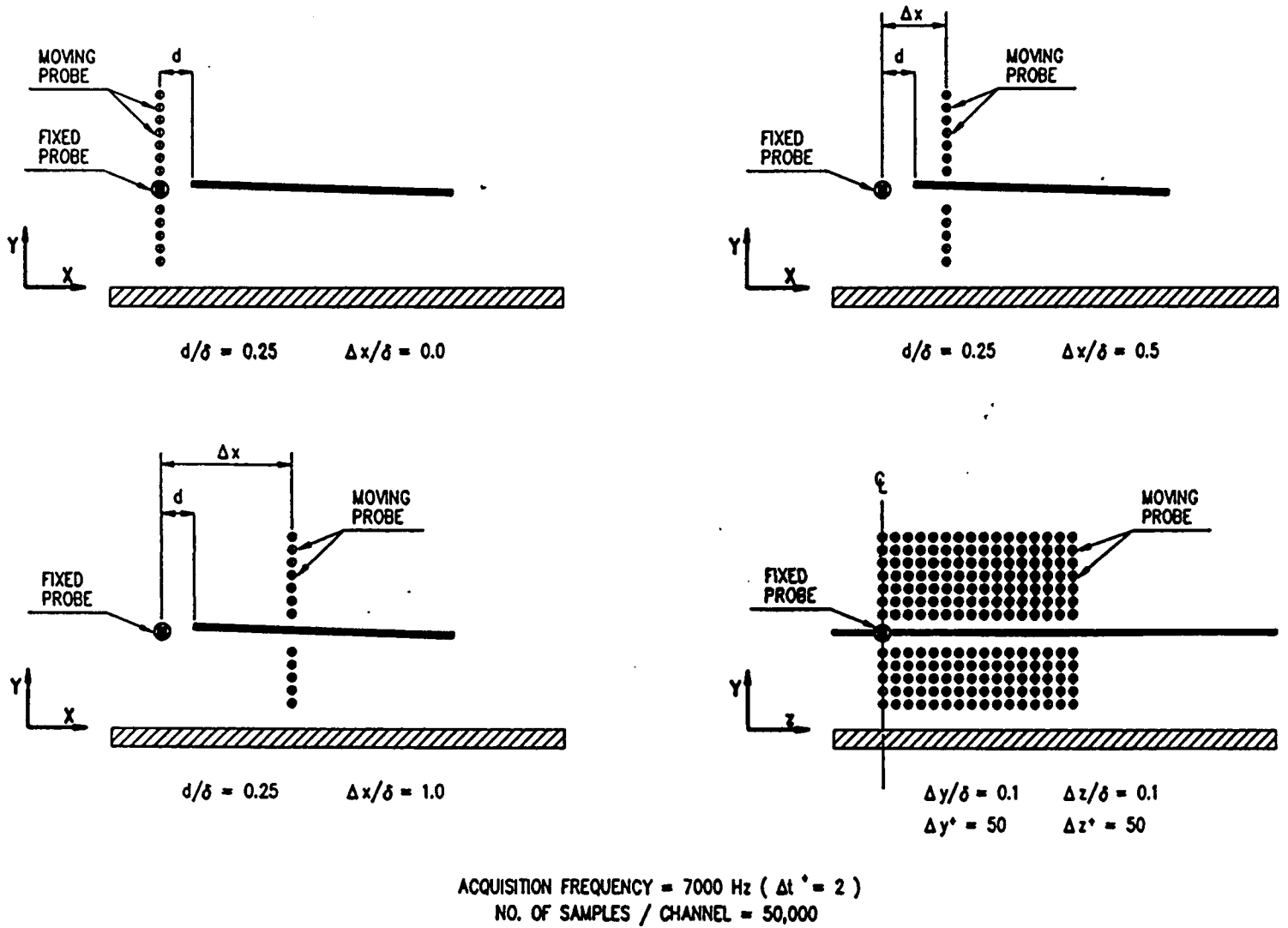


Figure 5. Schematic Diagram of Data Acquisition Grid for Outer Layer Mappings

In each of the cross-stream planes, the mapping span a total distance ranging from 0.508 cm to 3.81 cm away from the surface of the plate in the normal direction, and 3.81 cm on either side of the test plate centerline in the spanwise direction. These distances correspond to distances ranging from  $0.2\delta_0$  to  $1.5\delta_0$  in the normal direction, and from  $-1.5\delta_0$  to  $1.5\delta_0$  in the spanwise direction. The spatial resolution in either the normal or spanwise direction was therefore equal to 0.254 cm ( $0.1\delta_0$ ). As mentioned above, the spatial resolution in the streamwise direction was much coarser, namely 1.27 cm ( $0.5\delta_0$ ). The data acquisition grid is schematically shown in Figure 5. At each grid point, long time records of the six velocity components were acquired at a frequency of 7,000 Hz, corresponding to 2 viscous unit time units between samples. A total of 50,000 samples was acquired at each spatial point. The digital acquisition and processing procedures were very similar to those described for in the previous section for the Case 1 experiments.

In addition to all the usual statistical quantities, such as means, and first and second order moments, all nine components of the space-time correlation tensor were computed, yielding  $R_{\alpha\beta}(\Delta x, \Delta y, \Delta z; \Delta t)$  in both the regular case and the manipulated case. From this, inference about the underlying spatio-temporal structure of the flows can be made, and other quantities such as convection velocities, integral scales in space and time can be computed in the usual fashion. Furthermore, a more physical interpretation of these extensive correlation measurements was made by using the stochastic estimation technique.

### III. RESULTS

#### Calibration and Use of Triple Hot-Wire Probes

A considerable effort was devoted to establishing a convenient and reliable calibration for arbitrary geometry triple hot-wire probes, and for extracting the three velocity components from anemometer voltages in an accurate and fast manner. The conventional models to represent the cooling velocity on inclined sensors (Jorgensen, 1971; and others) were extended to circumvent some of the known limitations. In addition, a novel technique was designed to perform the inversion of the non-linear calibration equations, regardless of the form of such calibration equations. The procedure relies on a clever decomposition of the three-dimensional problem into a series of two-dimensional one, which are then solved by a table look-up and interpolation scheme. This new technique is computationally efficient and has errors which are much smaller than those of the calibration and modelling aspects of the problem. The

results of the overall procedure were presented at the Symposium on Turbulence at the University of Rolla, Missouri in September 1990 and at the 1990 APS Meeting. A paper has subsequently been submitted and accepted for publication in Experiments in Fluids (1991). A preprint of this paper is included in Appendix A, which describes all the details of the technique.

#### **Case 1: Wall Layer Structure as a Function of Reynolds Number**

The bulk of this aspect of the project is described in details in the Masters Thesis of Thomas J. Gieseke (1990). Unfortunately, the extensive data base collected for this experiment was later found to be contaminated by cross-talk among the hot wire channels and has not yet led to any good results. The cross-talk problem has been identified as coming from the use of the sub-miniature triple hot-wire probes, where one of the prong is common to all three wires to minimize the probe size. We were well aware of the possibility of cross-talk at the time of the experiments and had made significant changes to our setup and anemometer operations to eliminate the problem. Unfortunately, some cross-talk remained in the data and was only later identified, thus invalidating the data as it stands. Attempts are currently being made to design some post-processing schemes to eliminate or minimize the problem *a posteriori*. We have also ordered some new subminiature probes with no common prong (at the expense of a slightly larger size). These probes are ordered for a different project, but we expect to redo the boundary layer experiment in the coming summer to gather a new data set (at no cost to the current project!). We believe that this data set will yield very valuable information, particularly in light of the progress on the other aspects of the project (pseudo-dynamics and multipoint conditional averages).

#### **Case 2: Outer Layer Structure and Large Eddy Break Up Devices**

A very extensive study of the outer structure of the turbulent boundary layer and its modification by Large Eddy break Up Devices (LEBU's) was carried out in conjunction with the originally proposed tasks. The results of this study are described in details in the PhD Dissertation of N. Trigui (1991) and a summary of the some of the results were presented at the 1990 APS Meeting and the 29th Aerospace Sciences Meeting in Reno, Nevada in January 1991. A copy of the AIAA Paper 91-0519 is included in Appendix B.

## V. CONCLUSIONS

Based on our composite experience from the various studies, it has become clear that the stochastic estimation technique is an extremely valuable tool to study the structure and dynamics of turbulent wall bounded flows. The "pseudo-dynamics" reconstruction, coupled with the use of multipoint conditional averages provides realistic description of the real flow structure, otherwise unavailable and masked by conventional conditional sampling (single condition at one point). The richness of the turbulence and the dynamic interaction of the various structures is completely obliterated by standard technique and lead an erroneous (or at least very incomplete) picture of the flow. The results obtained thus far in the outer region of the boundary layer point to a succession of single-sided eddies arranged loosely in a staggered pattern in space and time, very similar to the conceptual picture postulated by Stretch and Kim based on DNS of turbulent channel flow. This type of structural organization is very different from the conventional symmetric structure picture usually discussed. Consequently, the mechanisms for the evolution of the structures may be entirely different from those postulated earlier (for example, lift-off away from the wall by mutual interaction, etc.).

Furthermore, we have recently proposed a new idea (cf. AFOSR Workshop on Turbulence Structure and Control, 1991) which potentially can extract real dynamics from the stochastic estimation formalism, alike the POD and dynamical system approach of Aubry *et al.* (1990). Some of these ideas are briefly described in Appendix D. In essence, it involves using as "modes" individual sets of stochastic estimation coefficients from a multipoint stochastic estimate and plugging those "modes" into the Navier Stokes equations to derive a truncated system of dynamical equations. Unlike POD modes, these stochastic estimation "modes" have semi-compact support and are not unlike an optimal wavelet basis. While this approach is very speculative at this stage, it has the potential for major breakthrough in our understanding of wall bounded flows and approximate numerical prediction for control purposes.

## **Appendix A**

**Paper accepted to Experiments in Fluids (1991): An Experimental  
Approach to the Calibration and Use of Triple Hot-Wire Probes,  
T. J. Gieseke and Y. G. Guezennec**

# AN EXPERIMENTAL APPROACH TO THE CALIBRATION AND USE OF TRIPLE HOT-WIRE PROBES

Thomas J. Gieseke and Yann G. Guezennec  
The Ohio State University  
Department of Mechanical Engineering  
Columbus, OH 43210

## NOMENCLATURE

$d$	Diameter of hot-wire
$e_i$	Anemometer voltage output for the $i^{th}$ hot-wire
$l$	Length of hot-wire
$u, v, w$	Orthogonal components of velocity
$D_{R1}$	Velocity ratio $v/u = \tan(\psi)$
$D_{R2}$	Velocity ratio $w/(u^2+v^2)^{1/2} = \tan(\phi)$
$D_{R3}$	Variable ratio $Q_{mag}/U_{mag}$
$Q$	Estimated cooling velocity from a response model
$Q_i$	Cooling velocity associated with the $i^{th}$ hot-wire
$Q_{mag}$	Cooling velocity magnitude $(Q_1^2 + Q_2^2 + Q_3^2)^{1/2}$
$Q_{ref}$	Estimate for the cooling velocity associated with the anemometer output at a known probe orientation
$Q_{R1}$	Cooling velocity ratio $Q_1/Q_3$
$Q_{R2}$	Cooling velocity ratio $Q_2/(Q_1^2 + Q_3^2)^{1/2}$
$Re_d$	Reynolds number based on $d$ and $U_{mag}$
$U$	Velocity vector
$U_b$	Velocity component normal to a wire and perpendicular to the plane of the wires supports

$U_{mag}$	Magnitude of the velocity vector
$U_n$	Velocity component normal to a wire and in the plane of the wires supports
$U_t$	Velocity component tangent to a wire
$\epsilon$	Measure of error
$\theta_i$	Sweep angle for the $i^{th}$ hot-wire
$\omega_i$	Angular rotation for the $i^{th}$ hot-wire
$\phi, \psi$	Angles in spherical coordinates describing the flow direction with respect to the probe

## INTRODUCTION

Hot-wire anemometry has long been accepted as one of the most accurate and affordable methods to study velocity fields in turbulent and unsteady flows. Modern experimental methods in conjunction with powerful computers for use in data reduction have allowed for the development of probes designed to measure the three components of velocity concurrently by using an array of three hot-wires. Each wire in the array responds to the cooling effects of the flow by some function  $Q_i = f_i(u, v, w, \theta_i, \omega_i)$  where  $\theta_i$  and  $\omega_i$  describe the orientation of the wire with respect to a reference coordinate system and the subscript  $i$  denotes a specific wire in the array. The inversion of the calibration equations is required to obtain  $u = g_1(Q_1, Q_2, Q_3, \theta_1, \theta_2, \theta_3, \omega_1, \omega_2, \omega_3)$ ,  $v = g_2()$ , etc. This inversion is usually complicated and tedious because the cooling equations are coupled and nonlinear, depend on probe geometry, and contain unknown constants. Furthermore, they usually yield multiple solutions for some range of cooling velocities, thereby limiting the effective flow angles which can be determined with a given probe.

Few ad-hoc algorithms have been developed (Chang, Adrian and Jones, 1984; Lekakis, 1988; Vukoslavcevic, Balint and Wallace, 1987; Choi, 1989;

Lekakis, Adrian and Jones, 1989; Russ and Simon, 1990; and others) to extract the velocity components from triple hot-wire measurements and most rely on certain simplifying assumptions. The most crucial assumption is the choice of the model to describe how the heat transfer from each wire depends on the direction and magnitude of the impinging velocity vector. The most common model takes several forms, but essentially is a weighted sum of the velocities normal and tangential to the wire. The probe geometry and some model constants must be experimentally determined, but the form is generally accepted because of its physical basis and reasonable agreement with experiment (Morgan, 1975).

The resulting set of equations must be solved point by point for the velocity components using special inversion techniques. Iterative techniques have been used successfully, but multiple solutions often exist and the solution time is lengthy (Choi, 1989; and others). Instead of computing velocity vectors from hot-wire measurements, researchers at Stanford University (Yavuzkurt *et al*, 1977) developed an analog circuit to solve the set of equations in real time. Once again, the governing model equations had to be simple and the use of the circuits was limited to a specific arrangement of wires. Lekakis, Adrian, and Jones (1989) developed a method to analytically invert the three cooling velocities making use of variable transformations very similar to the methods used in the present analysis. The inversion procedure requires that the form of the wire response model, or cooling law, be the Jorgensen's form. As will be discussed later, other models may be better representations of the cooling law when prong interference and wire wakes have significant influences.

Presented here is a set of procedures designed to be generally applicable to any triple-wire probe. Wire response models based on a generalization of the physical concepts and experimental analysis are developed for each individual wire within the array. The form and complexity of these models can be arbitrarily chosen to account for large flow angles and flow interference between wires. A method to efficiently perform the numerical inversion of the

calibration equations to extract the velocity vector is also developed which can be used regardless of the complexity of the response models or the probe geometry.

## WIRE RESPONSE MODELING

In the use of hot-wires, the wire response is interpreted using the concept of effective cooling velocity,  $Q$ . The cooling velocity associated with  $U$  is defined as the magnitude of a velocity vector having a direction normal to the wire within the plane defined by the wire supports that would yield the same heat transfer from the wire as  $U$ . It is assumed that the anemometer output voltage,  $e$ , depends on some general angular response model and on the wire sensitivity relating it to the cooling velocity. We will show that the probe response ( $Q$ ) to velocity magnitude ( $U_{mag}$ ) and velocity direction ( $U/U_{mag}$ ) can be decoupled by determining  $f(U_{mag})$  and  $f(U/U_{mag})$  separately.

Given a global coordinate system defined by  $x$  in the mean flow direction,  $y$  in the vertical direction, and  $z$  in the spanwise direction, the orthogonal velocity components associated with this coordinate system ( $u, v, w$ ) can be transformed into a local coordinate system defined by the wire and its supports. The two geometric parameters required to define the new coordinates are  $\theta$ , the angle at which the wire is swept back from an orientation perpendicular to the  $x$  axis, and  $\omega$ , the angle the wire is rotated about the  $x$  axis, measured clockwise from the  $y$  axis, with a zero degree rotation corresponding to an orientation where the longer of the two supports is directly below the shorter one. The new coordinate system is defined with one axis parallel to the wire, one normal to the wire in the plane of the prongs, and the third one (binormal) completing an orthogonal set. The terms  $U_l$ ,  $U_n$ , and  $U_b$  are the velocity components in these directions as shown in Figure 1. In terms of the velocity vector ( $u, v, w$ ) and the wire orientation  $\theta$  and  $\omega$ , these velocity components are:

$$U_b = v \sin\omega - w \cos\omega \quad (1)$$

$$U_t = u \sin\theta - v \cos\omega \cos\theta - w \sin\omega \cos\theta \quad (2)$$

$$U_n = u \cos\theta + v \cos\omega \sin\theta + w \sin\omega \sin\theta \quad (3)$$

Experiments on heat transfer from yawed cylinders (Morgan, 1975) have yielded approximations for the cooling velocity as a function of the velocity terms above. The most commonly accepted form is Jorgensen's equation (Jorgensen, 1971):

$$Q^2 = K_1 U_t^2 + K_2 U_b^2 + K_3 U_n^2 \quad (4)$$

The values of  $K_1$ ,  $K_2$ , and  $K_3$  can be approximated based on a physical argument. Insensitivity to tangential velocities implies  $K_1 = 0$ . Equal sensitivity to the normal and binormal components implies  $K_2 = K_3 = 1.0$ . These values are commonly assumed because they greatly simplify equation solutions (Chang *et al*, 1988; Choi, 1989; and others). It is usually recognized that this form suffers from several shortcomings, particularly to represent data at large flow angles. However due to its simplicity and general acceptance, it will be used as a starting point for our hot-wire response analysis.

It has been found (Balint *et al*, 1989) that the "constants"  $K_1$ ,  $K_2$  and  $K_3$  should be allowed to vary with the flow angle to better represent data at large flow angles. An alternate way to capture these effects is to add additional terms in the Jorgensen's model involving higher powers of  $U_n$ ,  $U_b$  and  $U_t$ . However, those higher powers of the velocity components must be appropriately rescaled by the velocity magnitude  $U_{mag}$  to allow the separation of sensitivities to velocity magnitude and flow angle. The expanded model can be summarized as follows:

$$Q^2 = K_1 U_t^2 + K_2 U_b^2 + K_3 U_n^2 + K_4 \frac{U_t^4}{U_{mag}^2} + K_5 \frac{U_b^4}{U_{mag}^2} + K_6 \frac{U_n^4}{U_{mag}^2} + \dots \quad (5)$$

By considering a spherical coordinate system rather than a rectangular one, it can be seen that the three velocity components,  $u$ ,  $v$  and  $w$ , can be expressed in terms of the velocity magnitude  $U_{mag}$  times functions of two flow angles with respect of the probe axis  $\phi$  and  $\psi$ , as shown in Figure 2. This signifies that the velocity magnitude can be factored out of the three velocity components. Similarly, the velocity magnitude can also be factored out of the  $U_n$ ,  $U_b$  and  $U_t$  components since those are linearly related to  $u$ ,  $v$  and  $w$  (Equations 1-3). Since  $U_{mag}$  can be factored out of the three velocity components, Equation 5 can be divided to by  $U_{mag}^2$  to yield a right hand side which does not depend on the velocity magnitude but only on the flow angles  $\phi$  and  $\psi$ :

$$\left[ \frac{Q}{U_{mag}} \right]^2 = K_1 \left[ \frac{U_t}{U_{mag}} \right]^2 + K_2 \left[ \frac{U_b}{U_{mag}} \right]^2 + K_3 \left[ \frac{U_n}{U_{mag}} \right]^2 + \dots$$

$$= f(\phi, \psi) \quad (6)$$

This separation of the velocity magnitude from the directional sensitivity allows the dissociation of the probe calibration procedure into an angular calibration test and a sensitivity determination with respect to the velocity magnitude. It is important to note that the separation is allowed by the form of the wire response model. The Jorgensen equation is only appropriate for flow angles and magnitudes in the range for which the response model was designed. A typical correlation (Morgan, 1975) indicates a similar model is accurate for  $U_t / \sqrt{U_n^2 + U_b^2} < 2.75$ ,  $l/d = 200$ , and Reynolds number based on wire diameter between 1 and 12. When using a  $5\mu m$  diameter hot-wire, these Reynolds numbers correspond to velocity magnitudes between 3.4m/s and 43.2m/s.

Since the angular response is primarily governed by the geometry of the probe array, the Jorgensen's model is used as a base from which more detailed response models are determined. These more detailed models are used to capture effects of wake and prong interferences as well as model variation with flow angle. The response model will not change over time so the full response of a probe in terms of velocity magnitude and angles needs to be performed

only once (or rarely). With the angular response established, the probe can be calibrated against velocity magnitude at a fixed orientation (corresponding to its intended use). This procedure leads to considerable simplifications for the use and calibration of such triple wire probes and is justifiable as long as the response models are accurate in the range of flow angles and magnitudes where the probe is used.

## MODEL EVALUATION AND TESTING

In order to determine the best combination of variables and their powers for the response model, experiments were conducted to establish the relationship between the anemometer output voltage and the flow direction and magnitude. The low turbulence wind tunnel at The Ohio State University in the Department of Mechanical Engineering was used with a special positioning mechanism mounted in its test section. This mechanism consisted of a rod with one end fixed in space and the other sliding inside a ball joint attached to a precision, computer-controlled traversing mechanism. This allowed the rod to be oriented at any angular position with respect the free-stream velocity. A probe holder was attached to the rod to secure the probe parallel to the rod. The probes were connected to Constant Temperature Anemometers operating with overheat ratio ranging from 1.3 to 1.6 depending on the probe. The output of each anemometer was fed to a King's law type analog linearizer. The purpose of such circuits was not to linearize the hot-wire signals *per se*, but to maximize the sensitivity of the digital acquisition system at the higher flow velocities. This procedure degrades the signal somewhat in terms of the noise contamination, but the minimum signal to noise ratio for the circuitry was found to be around 500 which is acceptable for our needs.

Several triple-wire probes having a variety of wire arrangements were studied. Probes 1 and 2 (manufactured by Auspex) were of identical design having a common central prong, with the three wires swept at approximately 45

degrees, and equally spaced 120 degrees from each other. Probe 3 (TSI, Model 1295AV) had three wires swept 45 degrees but mounted on separate prongs. Two of the wires were arranged in one plane as a regular X-wire array and the third wire was mounted behind the other wires in a plane perpendicular to the X-wire plane. Figure 3 depicts the geometry of this probe. For the remainder of this paper, only the results of probe 3 will be shown. Equivalent or better results were obtained with probes 1 and 2 for reasons that will be discussed later.

Before attempting to determine how the wires in the probe array respond to variations in the flow direction, a sensitivity calibration was conducted. A standard experiment to determine the anemometer circuitry response to cooling velocity is to mount the wire in a flow of known velocity with the wire oriented in a specific position. While varying the speed, a data base can be established for voltage output versus velocity for one specific wire orientation. This yields a functional dependence between the anemometer output voltage,  $e$ , and a rough estimate for the cooling velocity,  $Q_{ref}$ , using a response model with assumed constants.

$$Q_{ref} = f(e) \quad (7)$$

The resulting calibration curves ( $Q_{ref}$  versus  $e$ ) served as a reference to compare wire response during an experiment with wire response during the angular calibration tests. As expected, the curves are approximately linear due to the preconditioning through the analog linearizer. A cubic polynomial is fit to the data using a least square procedure for a continuous approximation of  $Q_{ref}$  over the range of an anemometer outputs. This adds to the uncertainty in measuring the cooling velocity but this portion of the experimental approach is very accurate. Typically, errors in the curve fit are less than 0.25%.

The angular calibration was conducted by varying the probe orientation through a range of angles with respect to the flow and the velocity magnitude. At each calibration point, the free-stream velocity and the probe orientation

were converted to  $(u,v,w)$  in the frame of reference of the probe. The resulting sets of  $(u,v,w)$  and output voltages were recorded for later processing. Typically, the velocities were varied over a three-dimensional grid defined by a range of flow angles of  $\pm 20^\circ$  in the horizontal direction,  $\pm 35^\circ$  in the vertical direction, and a range of free-stream velocities commensurate with the intended use of the probes. This is near the cone of acceptance for the probes in certain directions. Each of the three independent variables was divided into at least five divisions yielding a minimum total of 125 data calibration points. The uncertainty in probe positioning,  $\pm 0.4^\circ$ , was found to be the most significant source of error in this calibration.

The angular calibration was used to define the model which best represents the data. As a first approximation, a comparison was made between  $Q_{ref}$  and Jorgensen's form of  $Q$  with all model constants assumed to be equal to reasonable values ( $K_1 = 0.1$ ,  $K_2 = 1.0$ , and  $K_3 = 1.0$ , for example). This yielded a plot of  $Q$  versus  $Q_{ref}$  as shown in Figure 4 for wire 3 (the wire most strongly affected by prong interference and wire wakes). If the sensitivity calibration and model were exact, there would be a linear relation between  $Q_{ref}$  and  $Q$ . As can be seen in Figure 4, some function  $Q = F(Q_{ref})$  can be fit to the data points. Since the points almost fall on a straight line, a quadratic polynomial was deemed sufficient to approximate the data and was determined by a least square procedure. The average error is 1.6% with a maximum error of 7.9%. It can be noted that there remains a significant amount of scatter around the fitted line. This can be attributed to the fact that the assumed model is not exact. To improve the model,  $Q$  is replaced by the response model to obtain:

$$Q^2 = K_1 U_t^2 + K_2 U_b^2 + K_3 U_n^2 = F^2(Q_{ref}) = A + B Q_{ref} + C Q_{ref}^2 \quad (8)$$

One constant in  $F^2$  or  $Q^2$  must be fixed in order to determine the others. Fixing the  $U_n$  coefficient to 1.0 and letting all the others vary is consistent with the concept of cooling velocity. Reordering Equation 8 yields,

$$U_n^2 = K_1 U_t^2 + K_2 U_b^2 - B Q_{ref} - C Q_{ref}^2 - A \quad (9)$$

all the constants in which can be determined using a least squares procedure. For wire 3 the equation was found to be

$$Q^2 = 0.063 U_i^2 + 1.03 U_b^2 + 1.00 U_n^2 = -121.0 + 11.5 Q_{ref} - 1.52 Q_{ref}^2 \quad (10)$$

The curve  $Q = F(Q_{ref})$  is shown in Figure 5a. It can be noted that the scatter of the fit has been considerably reduced from Figure 4 by finding the "best" constants in the model and the function  $F$ . The average error has been reduced to 0.96% with a maximum of 5.0%. Figure 5b represents the data obtained for wire 1 and is more typical of the collapse using this procedure. It has an average error of 0.66% with a maximum of 2.8%. Wire 3 (Figure 5a) exhibits the worst behavior, as compared to other wires in the array, due to its inherent asymmetry with respect to spanwise velocity and the upstream interference of wires 1 and 2. For the other types of probes investigated, Figure 5b is more representative of the response of all the wires.

The geometric constants describing the probe geometry,  $\theta_i$  and  $\omega_i$ , have been assumed to be their nominal design values in the analysis above. A further refinement of the method is obtained by calculating the error of the curve fit  $Q = F(Q_{ref})$  for a range of geometries around the design values and picking the geometry which yields the smallest error. Typically, the "improved" values of the wire angles specifying the geometry of the probe are found to be within a few degrees for their design values. In actuality, they may not be descriptive of the actual geometric constants of the probe but may represent physical aberrations such aerodynamic prong interference.

As Figure 5b illustrates, there remains little scatter in the experimental data. Further improvement can sometimes be obtained by adding additional terms in the model as stated in Equation 5. In the case of our probe, the third wire is mounted behind the X-array and is more sensitive to a positive  $w$  component than a negative one due to the inherent asymmetry of the design with

respect to the spanwise direction. For the third wire, the additional terms in the model are helpful in further reducing the error. On the other hand, the additional terms do not contribute to any significant improvement for wires 1 and 2 (X-array). The response model for wire 3 can be improved by adding a higher order tangential term to compensate for the asymmetry. This is equivalent to Equation 5, with  $K_5$  and  $K_6$  set to 0.0. As shown in Figure 6, the collapse of the data is slightly better than in Figures 4 and 5a having an average error of 0.65% and a maximum of 4.4%.

It has been suggested that if the Jorgensen's response model is used in its basic form, the constants  $K_1$ ,  $K_2$ , and  $K_3$  are not really constant. As noted earlier, the variation of these values with flow direction can be accounted for by the addition of higher order terms to the response model. For example, consider the case where the tangential component of velocity had increasing influence on the heat transfer as the flow became more tangent to the wire. The Jorgensen response equation could be written with a variable  $U_t$  coefficient as,

$$Q^2 = K_3 U_n^2 + K_b U_b^2 + K_t \left[ 1.0 + K_{tt} \left( \frac{U_t^2}{U_{mag}^2} \right) \right] U_t^2 \quad (11)$$

This equation is mathematically equivalent to Equation 5 with different coefficients. If the values of  $K$ 's are assumed to vary with velocity magnitude, the procedure to separate angular dependence from velocity magnitude dependence no longer works. Fortunately, the dependence of the values of  $K$ 's on the velocity is small over the range of velocities considered as is evident from Figures 5 and 6.

## VELOCITY EXTRACTION

With an acceptable response model established, the problem now becomes one of extracting the three velocity components from the three wire outputs.

When in use, each wire will output a voltage  $e$  from which  $F(Q_{ref})$  can be computed. It then remains to determine  $U$  by inverting the three model equations. This has been successfully accomplished in the past using special purpose hardware, special analytical approaches, and iterative techniques, but to analyze the amount of data required for high order statistical moments on large experimental grids accurately, more efficient solution techniques are required. One such approach which has been successfully implemented for single sensors is the table lookup method. In principle, this approach could be generalized to the three-dimensional problem by using a set of three-dimensional tables. However, the memory requirements to store a finely resolved set of tables are prohibitive and coarser tables give rise to significant interpolation errors. In an effort to maximize the table resolution and reduce the error, a more sophisticated method is used which transforms the three-dimensional problem into a two-dimensional one. This approach is possible since the form of the model was selected such that the velocity magnitude could be scaled out, yielding a two-dimensional problem which depends only on the flow direction. Similar variable transformations were proposed by Lekakis *et al.* (1989).

All discussions that follow rely on the assumption that the response model is accurate over the range of velocity magnitudes and directions in which the probe is to be used. The validity of this assumption is based on the accuracy of the model determination discussed in the preceding section.

Taking the Jorgensen's model as an example, the instantaneous velocity magnitude can be factored out to yield:

$$(Q_1/U_{mag})^2 = K_{11}(U_t/U_{mag})^2 + K_{12}(U_b/U_{mag})^2 + K_{13}(U_n/U_{mag})^2 \quad (12)$$

$$(Q_2/U_{mag})^2 = K_{21}(U_t/U_{mag})^2 + K_{22}(U_b/U_{mag})^2 + K_{23}(U_n/U_{mag})^2 \quad (13)$$

$$(Q_3/U_{mag})^2 = K_{31}(U_t/U_{mag})^2 + K_{32}(U_b/U_{mag})^2 + K_{33}(U_n/U_{mag})^2 \quad (14)$$

It can be shown by geometrical transformation equations that the right hand side of each equation is only a function of two velocity direction variables

only. By taking the ratio between Equations 12 and 14, a new variable was defined that is independent of velocity magnitude,

$$Q_{R1} = Q_1/Q_3 \quad (15)$$

Similarly, two additional variables can be defined by:

$$Q_{R2} = Q_2 / (Q_1^2 + Q_3^2)^{1/2} \quad (16)$$

$$Q_{mag} = \sqrt{Q_1^2 + Q_2^2 + Q_3^2} \quad (17)$$

The velocity components  $u$ ,  $v$  and  $w$  can be transformed in a similar way to yield two directional variables that are closely related to the flow direction:

$$D_{R1} = v/u = \tan(\psi) \quad (18)$$

$$D_{R2} = w/(u^2 + v^2)^{1/2} = \tan(\phi) \quad (19)$$

To complete the set of equations, the velocity magnitude can be related to the magnitude of the cooling velocities by:

$$D_{R3} = U_{mag}/Q_{mag} \quad (20)$$

This equation is derived by summing Equations 12, 13, and 14 and taking the square root.  $D_{R3}$  is defined so that it is a function of the velocity direction only, as were the other variables.

With the form of the model and all its constants determined from the angular calibration experiments, a data base can be generated by varying the  $U$  over a specified range commensurate with the calibration data and computing the corresponding  $Q$  values. This data base is determined computationally and made as fine as possible, typically using 176,400 data points. Applying the appropriate variable transformations described above, the computational data is changed to the three variables  $D_{R1}$ ,  $D_{R2}$ , and  $D_{R3}$  as a function of  $Q_{R1}$  and  $Q_{R2}$ . These three variables are depicted in Figure 7a through 7c as contours plots and gray level maps. The figures can be thought of as the top surface of a three-dimensional body. Only the parts of the surface having normals with components out of the page are considered. The portions of the body concealed

behind the top surface represent alternate values of the velocity variables corresponding to given values of  $Q_1$ ,  $Q_2$ , and  $Q_3$ . These multiple solutions occur at high angles of the flow direction where, because of the non-linear behavior of the model equations, the solution manifolds fold back on themselves and the equations yield multiple solutions.

To determine this cone of acceptance of the probe, an experiment can be performed where a probe is exposed to steadily increasing flow angles, and the trajectory in the variable space ( $Q_{R1}, Q_{R2}$ ) traced. The path begins near the center of the shaded space and progresses toward the edge of the region. At some flow angle, the path turns around and proceeds back into the shaded region. Where the path reverses is the boundary of the region. The flow angles that correspond the boundary defines the cone of acceptance. It can also be noted that the boundary of that domain coincide with regions where the isocontours of one of the variables become very close together.

The location of the velocity variables in  $Q_{R1}-Q_{R2}$  parameter space can be illustrated by plotting points with coordinates ( $Q_{R1}, Q_{R2}$ ) corresponding to all the calibration velocity triplets. This type of plot was used to evaluate the probe performance (see the section on errors). Figure 8 shows such a plot with the data points corresponding to the uniform distribution of  $u$ ,  $v$ , and  $w$  from the angular calibration. The calibration data does not span the entire cone of acceptance for the probe which is represented by the solid line. The response models were applied beyond the range of calibration data in order to fully examine the equation behavior. For this reason, the outer edges of the figure represent an extrapolation of the response models in flow regimes where they have not been proven to be accurate.

Figure 9 shows the distribution of points in the computed data base which spans the entire cone of acceptance of the probe. For clarity, only a small subset of the data base is actually plotted. The distribution of the points is heavily skewed to one side as a result of the probe geometry. The location of the

velocity point  $(u,0,0)$  is found at  $(Q_{R1}, Q_{R2}) \approx (1.0, 0.707)$ . The most limiting bounds on the cone of acceptance occur when the flow causes large  $Q_{R2}$  or small  $Q_{R1}$ . The effect of these problems is to limit probe use to flows not having strong  $v$  and  $w$  components and to reduce probe accuracy for certain flow angles. Probes of type 1 and 2 do not exhibit this strong favoritism to one side and do not have as limiting of a cone of acceptance due to their more symmetrical geometry.

To generate the tables for the lookup procedure, the following procedure was used. The data base was sorted by  $Q_{R1}$  and  $Q_{R2}$  and a uniform grid was overlaid on the data for each velocity variable  $(D_{R1}, D_{R2}, D_{R3})$  as shown in Figure 9. Since the computed points are not equally spaced in this parameter space, an interpolation procedure was used to calculate the table values on the regular grid. The interpolated values were obtained by a weighted average of the neighboring points closest to that grid location, with the weights defined as a function of the distance between each data point and the grid point. In this fashion, evenly spaced two-dimensional tables were constructed for the variables  $D_{R1}$ ,  $D_{R2}$  and  $D_{R3}$ . As will be addressed in more details shortly, very little error is introduced by this interpolation scheme owing to the density of the data distribution.

The use of the tables is strictly limited to the range of the  $U$  used in its generation and the boundary of the single solution domain. Sets of cooling velocity ratios out of the range of the tables yield an error in the table lookup which must be accounted for on an *ad hoc* basis in order not to contaminate the measurements during an actual experiment. By calibrating the probes over a sufficiently large range of flow angles for the intended use, such errors are rare and can be flagged appropriately.

To use the tables, the following extraction procedure is used. Measured voltages are converted to  $Q_{ref}$  using the sensitivity polynomial calibration of each of the three hot-wires. These are then converted to  $F(Q_{ref})$  to yield the

estimated cooling velocities,  $Q$ . These three cooling velocities are then transformed to the variables  $Q_{R1}$ ,  $Q_{R2}$ , and  $Q_{mag}$ . By table lookup and bilinear interpolation between table values, the  $D_{R1}$ ,  $D_{R2}$  and  $D_{R3}$  velocity components are then determined. Transforming these velocity variables back to the usual velocity components is performed by a simple coordinate transformation. Specifically, these equations are as follows:

$$u = \frac{D_{R3} Q_{mag}}{\sqrt{1 + (1 + D_{R1}^2) D_{R2}^2 + D_{R1}^2}} \quad (21)$$

$$v = D_{R1} u \quad (22)$$

$$w = D_{R2} \sqrt{u^2 + v^2} \quad (23)$$

Since all these computational steps are explicit and simple, their implementation is computationally very efficient. This fact is the chief advantage of a table look-up procedure. A summary flow chart of the overall calibration procedure, table generation and velocity extraction is given in Figure 10.

## ERRORS

The calibration method described in the previous paragraphs model involves assumptions, interpolations, and curve fits. This results in significant uncertainties which need to be quantified. Selecting the best model for the wire response offers the most flexibility in reducing the method errors. Figures 4, 5 and 6 illustrate how these errors can be reduced by first selecting the best constants for the basic model, and then by adding appropriate terms to the model when it is warranted. The average error of the curve fit, in terms of  $Q$ , with the assumed constants in the model for Figure 4 is 1.6% of full scale with a maximum error of 7.86%. As mentioned before, these errors are for wire 3 (worst wire). The average errors for the other wires are of the order of 1%.

To quantify the errors in terms of velocity, the following procedure was used. For each data point in the angular calibration data base, the velocity vector,  $U$ , was extracted from the actual anemometer voltages using the procedures of the previous section. Since the actual velocities,  $U_a$ , are known from the probe positioning, a measure of the overall error can be defined:

$$\epsilon^2 = \frac{[(u_a - u)^2 + (v_a - v)^2 + (w_a - w)^2]}{[u_a^2 + v_a^2 + w_a^2]} \quad (24)$$

These overall errors represent the errors compounded through the fitting of the model and its inversion through the table lookup procedure and interpolation. The average error in the extracted velocity using the assumed model constants is 2.6% with a maximum of 12.1%. By finding the best constants for the model, the average error for wire 3 (Figure 5a) can be reduced to 0.96% of full scale with a maximum of 5.0%. Similarly, the average errors for the other wires are reduced to values of the order of 0.7% as exemplified by the excellent collapse of the data in Figure 5b (wire 1). Finally, by including additional terms in the model for wire 3 (Figure 6), the average error can be reduced to 0.7% with a maximum of 4.4%. These additional terms can play an important role when the range of flow angles is large for the geometry of the probe. The error magnitudes are commensurate with the error usually encountered with single or X-wire probes.

The distribution of errors is shown in Figure 8 for the model used in Figure 5b. Each of the symbols in Figure 8 represents the velocity error corresponding to an individual calibration data point. It can be seen that most of the errors are below 2% except in a few regions of the parameter space.

Finally, a potential source of errors stems from the table generation, table look-up and interpolation procedures. To investigate this type of errors, a computational experiment was conducted. Velocity vectors were selected over the range of  $U$  used during the model testing. Using the response model, the

cooling velocities were calculated and inverted back through the table look-up procedure. The velocity vector determined in this way,  $U$ , was compared to the initial input,  $U_a$ , and the error determined as before. Through the numerical experiments, it was found that tables with a resolution of  $200 \times 200$  are sufficient to insure an accuracy of the order of 0.03% for the average error with a maximum of the order of 0.1%. In other words, the numerical errors associated with the velocity extraction by the table look-up and calibration method are negligible with respect to the model errors.

#### APPLICATION TO MEASUREMENTS IN TURBULENT BOUNDARY LAYERS

These calibration and extraction procedures were tested in a realistic situation by taking data in a turbulent boundary layer. The experiment was conducted in a zero-pressure gradient, flat plate boundary layer at a Reynolds number based on momentum thickness of the order of 4000. Long records of the outputs of the three anemometers were digitally acquired at a sampling frequency of 2 viscous time units ( $\Delta t^+ = 2$ ) and stored to disk for later processing. This was repeated for a range of heights in the boundary layer in order to obtain profiles of the statistics of the three velocity components.

Figure 11a depicts the mean profiles of the streamwise ( $u$ ), normal ( $v$ ) and spanwise ( $w$ ) velocities plotted against  $y/\delta$ , where  $\delta$  is the 99% boundary layer thickness. As expected, the streamwise velocity profile is in good agreement with other measurements and the normal and spanwise are extremely close to zero. It should be noted that these two quantities were not forced to zero, but calculated directly from the data. This indicates that the probe calibration performs well, including in regions characterized by strong spatial velocity gradients and turbulence intensities. Figure 11b depicts the profiles of the streamwise ( $u'$ ), normal ( $v'$ ) and spanwise ( $w'$ ) turbulence intensities. Again, the data is in good agreement with results previously reported in the literature. Owing

to the size of the probe and its supports, no data was gathered in the near wall region. The profile of the normalized cross-correlation,  $R_{uv}$ , is shown in Figure 11c. The correlation coefficient,  $R_{uv}$ , has the value of -0.41 throughout the log layer which is as expected.

## CONCLUSIONS

In conclusion, an experimental approach to calibrate triple hot-wire probes with arbitrary geometry has been designed and tested. This method provides a way to optimize the constants in the conventionally accepted model and to include additional terms in the model to further reduce the errors. This procedure decouples the angular calibration from the sensitivity to the velocity magnitude, in a manner similar to that used by Lekakis *et al.* The decoupling considerably reduces the complexity of the calibration and velocity extraction procedures.

By scaling out the velocity magnitude, the three-dimensional velocity extraction problem can be reduced to a set of two-dimensional problems, which are then solved by a table look-up procedure. The table look-up approach has the advantage of allowing for arbitrarily complex response model equations to be solved provided they follow the rules described. This was found to be important when wire and prong interference changes the nature of the flow within a probe array. This method is computationally efficient and does not require the numerical inversion of the non-linear model equations.

## ACKNOWLEDGMENT

This research was supported by the Air Force Office of Scientific Research under the Grant 89-0434, monitored by Dr. J. McMichael. Their support is gratefully acknowledged.

## REFERENCES

- Balint, J. L., Vukoslavcevic, P., and Wallace, J. M., 1989, Private Communication.
- Chang, P. H., Adrian, R. J., and Jones, B. G., 1984, "Comparison Between Triple-Wire and X-Wire Measurement Techniques in High Intensity Turbulent Shear Flow," *Symposium on Turbulence*, Science Press, Princeton 1983, 206.
- Choi, W. C., 1989, MS thesis, The Ohio State University.
- Jorgensen, F. E., 1971, "Directional Sensitivity of Wire and Fiber-film Probes," *DISA*, Vol. 11, 31.
- Lekakis, I. C., Adrian, R. J., and Jones, B. G., 1989, "Measurement of Velocity Vectors With Orthogonal and Non-Orthogonal Triple-Sensor Probes," *Experiments in Fluids*, 7, 228.
- Lekakis, I. C., PhD Thesis, The University of Illinois, 1988.
- Morgan, V. T., 1975, "The Overall Convective Heat Transfer from Smooth Circular Cylinders," *Advances in Heat Transfer*, Vol. 11, 199.
- Russ, S., and Simon, T. W., 1990, "Signal Processing Using the Orthogonal Triple-wire Equations," *Flow Lines*, TSI inc., Winter, 3.
- Vukoslavcevic, P., Balint, J. L., and Wallace, J. M., 1987, "A Multi-Sensor Hot-Wire Probe to Measure Vorticity and Velocity in Turbulent flows," *ASME Symposium on Thermal Anemometry*, Cincinnati, June 1987.
- Yavuzkurt, S., Crawford, M. E., and Moffat, R. J., 1977, "Real-Time Hot-Wire Measurements in Three-Dimensional Flow," *Symposium on Turbulence*, Science Press, Princeton 1979, 265.

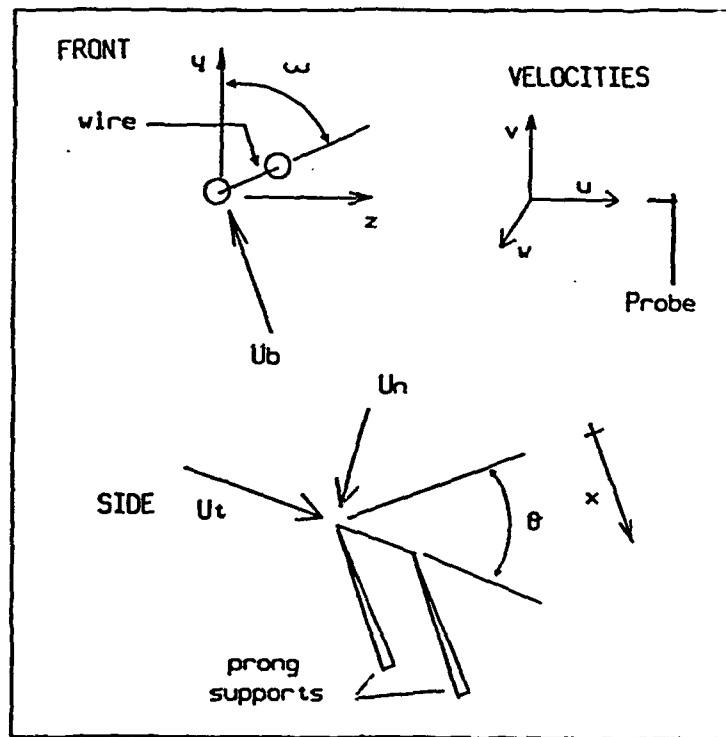


Figure 1 - Definition of Global and Local Coordinate Systems

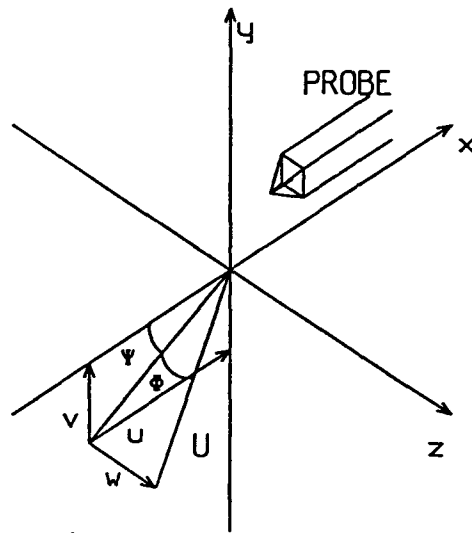
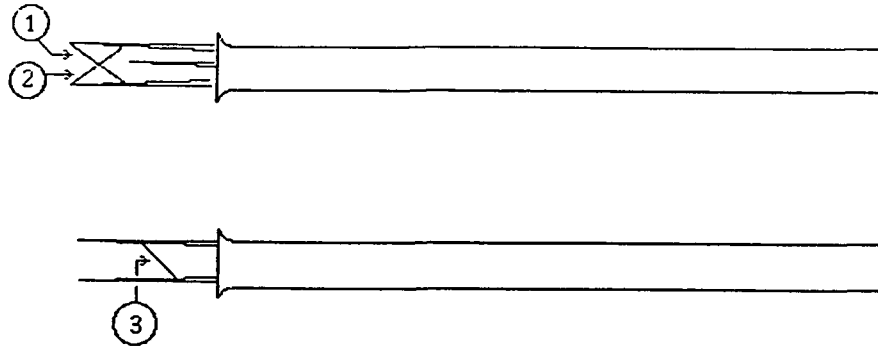


Figure 2 - Definition of Flow Direction in Spherical Coordinates

## TSI 128AU-20 TRIPLE-WIRE PROBE



## WIRE ORIENTATIONS

WIRE	SWEEP	ROTATION
1	45	180
2	45	0
3	45	90

Figure 3 - Geometry of Probe 3

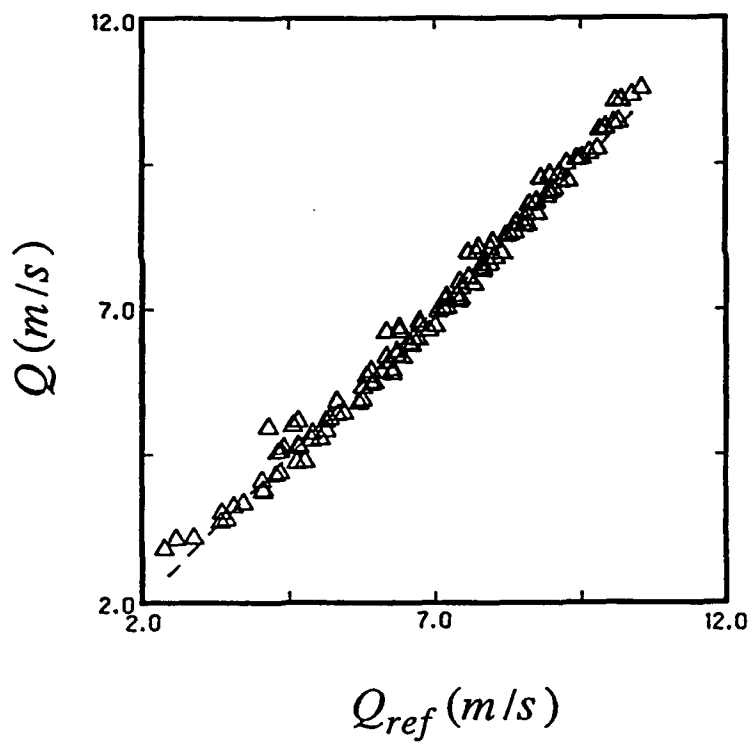


Figure 4 - Calibration Curve for Wire 3 with Assumed Constants in Model

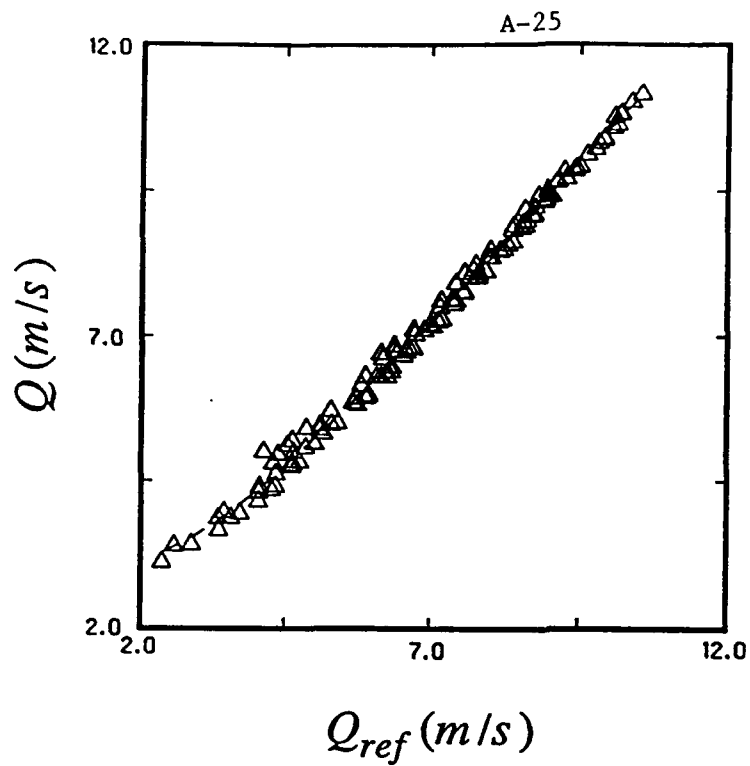
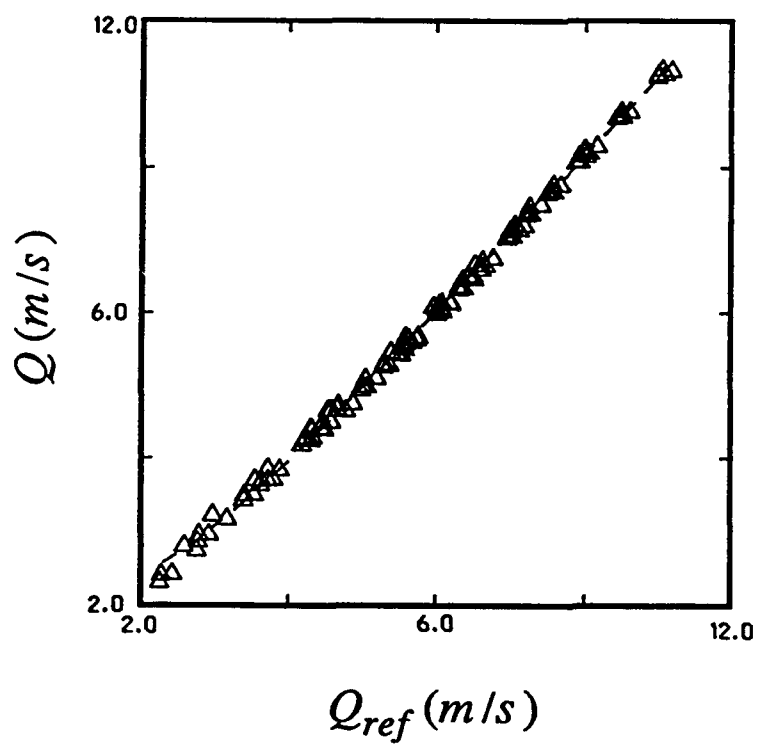


Figure 5 - Calibration Curve with Optimal Constants in Model:  
a) Wire 3



b) Wire 1

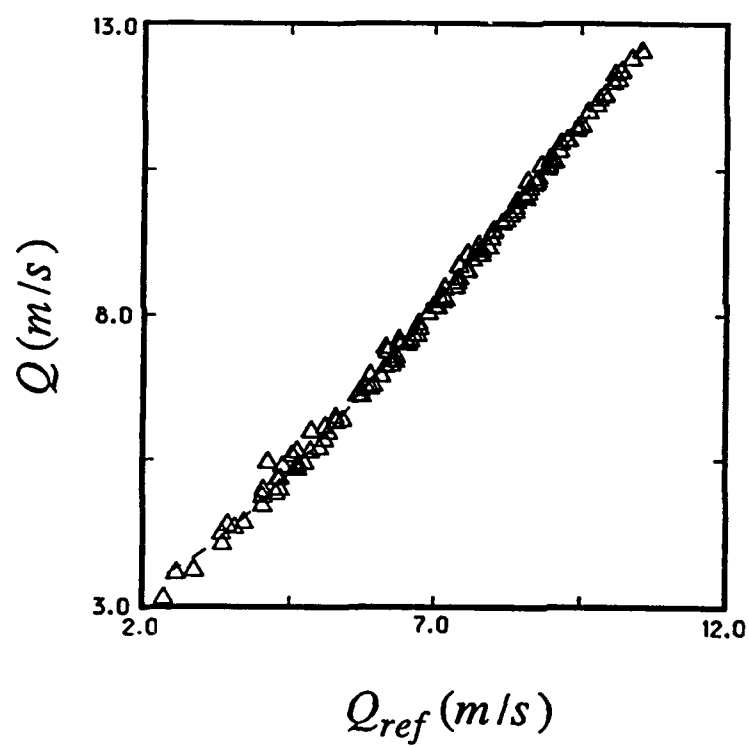


Figure 6 - Calibration Curve for Wire 3 with Additional Terms in Model

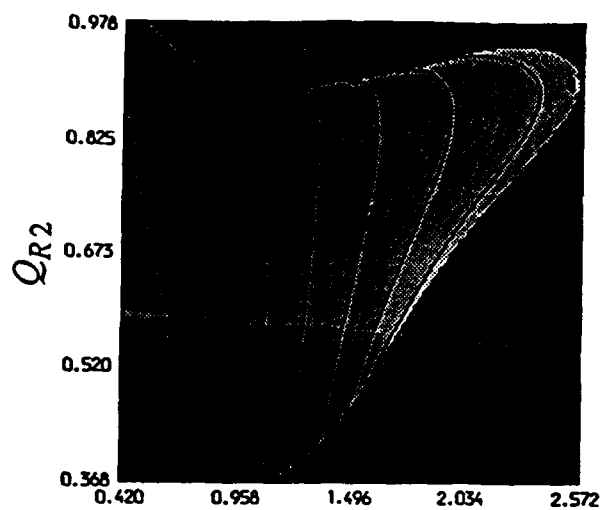
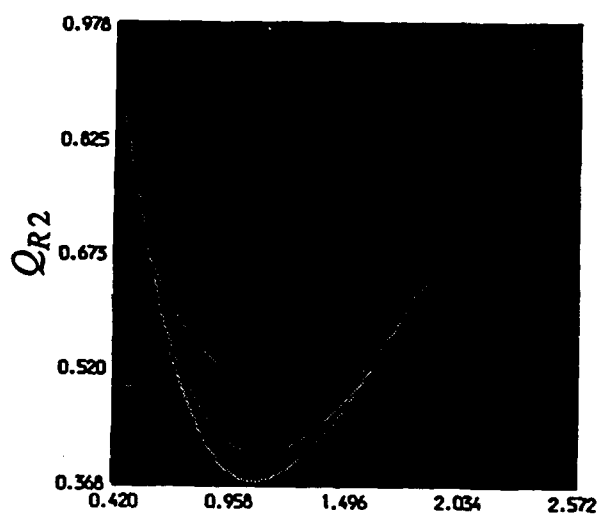
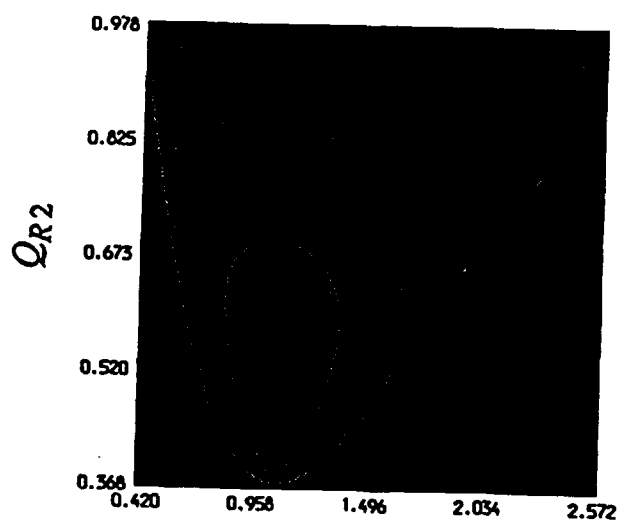


Figure 7 - Isocontours of Velocity Components as a Function of Cooling Velocity Direction:

a)  $D_{R1}$



b)  $D_{R2}$



c)  $D_{R3}$

$Q_{R1}$

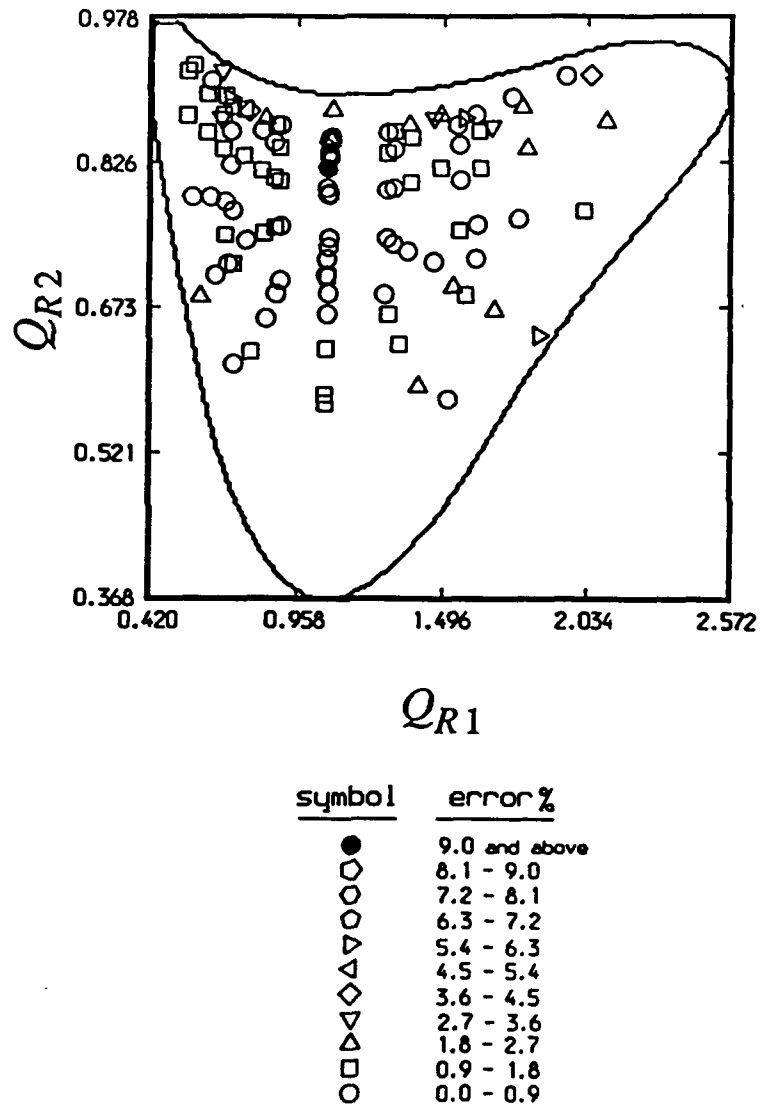


Figure 8 - Distribution of Calibration Data Points as a Function of Cooling Velocity Direction

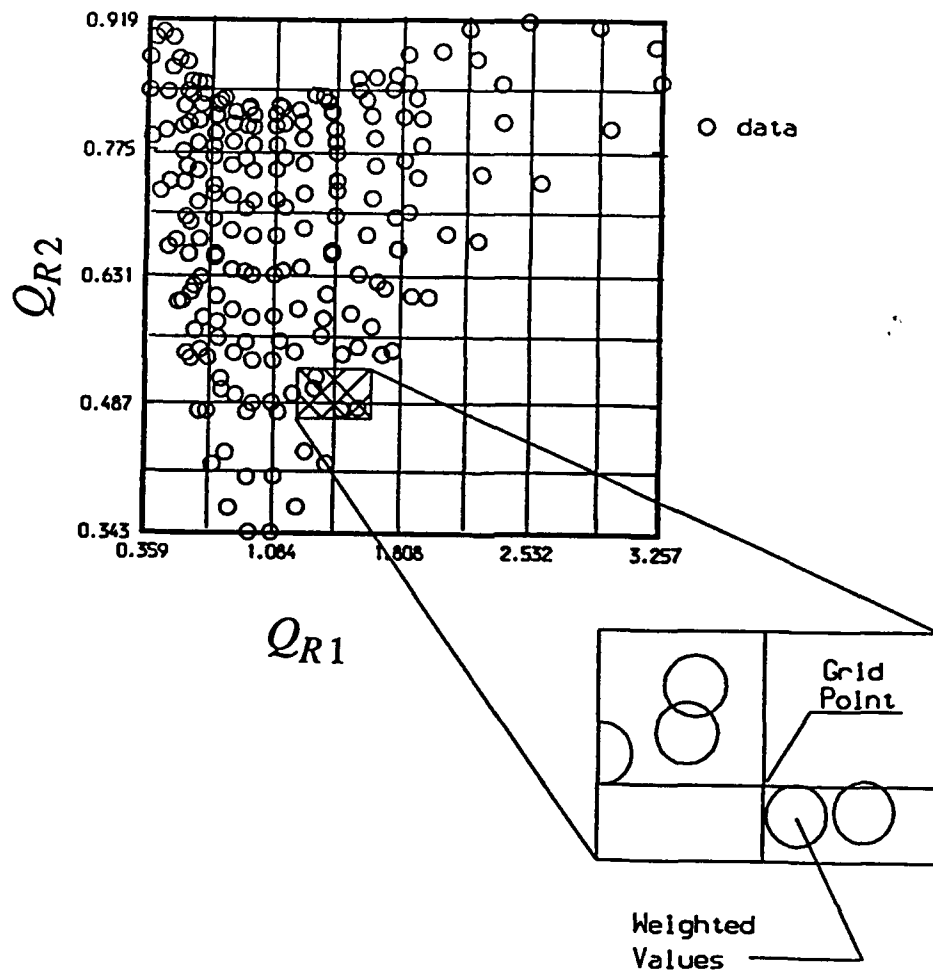


Figure 9 - Table Generation Procedure

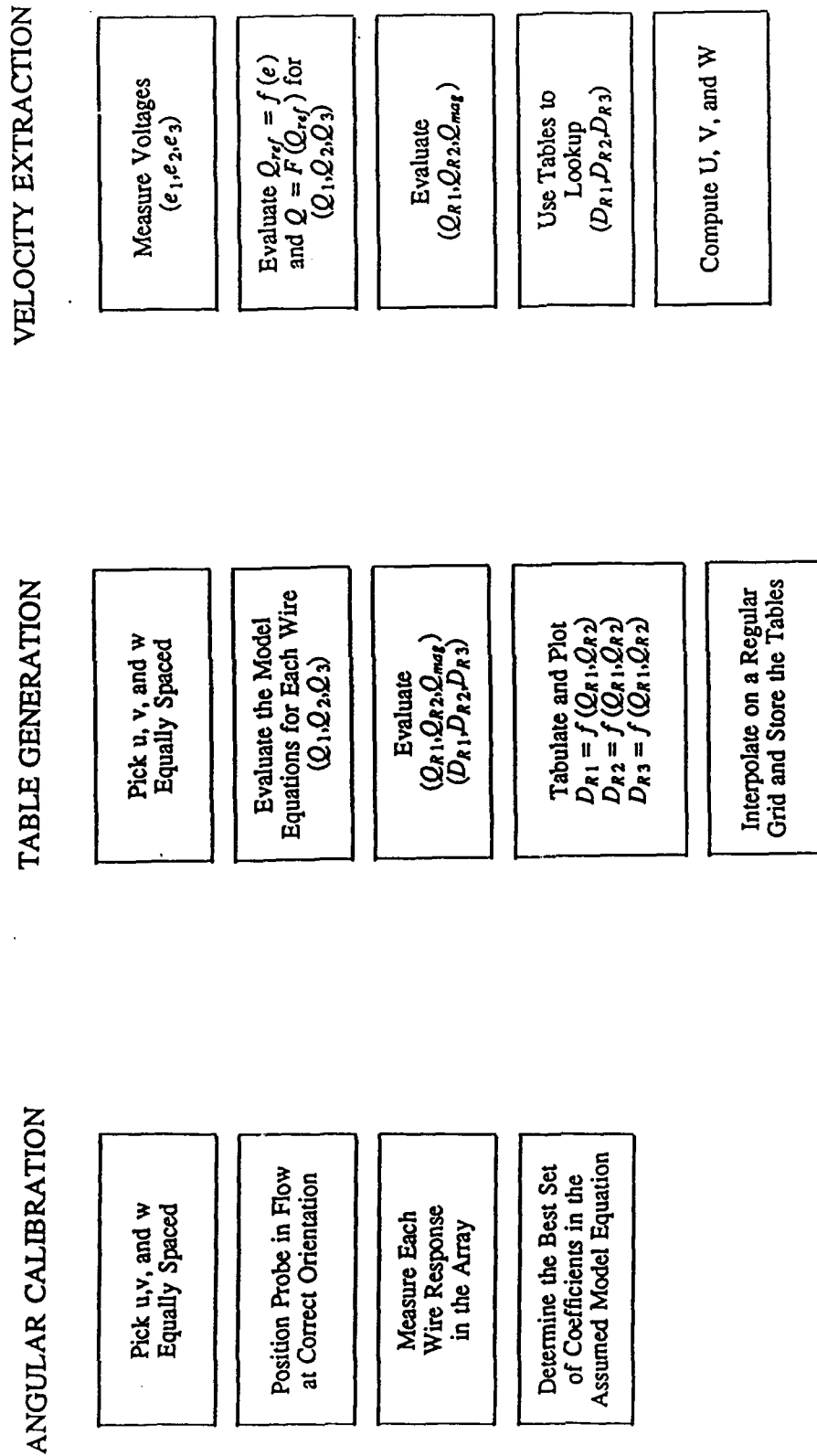


Figure 10 - Flow Chart of Calibration, Table Generation and Velocity Extraction Procedure

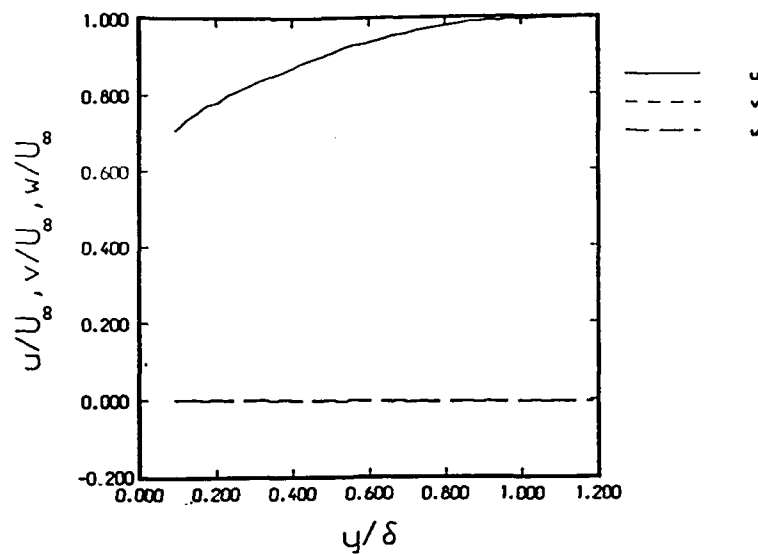
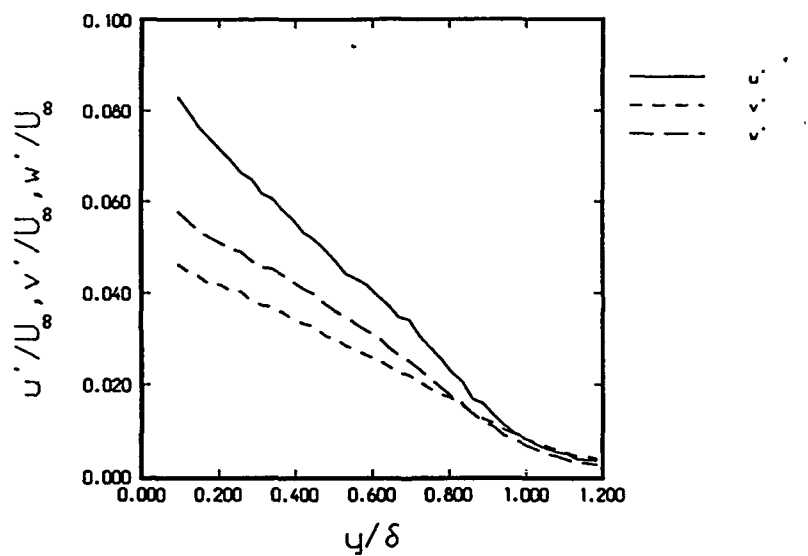
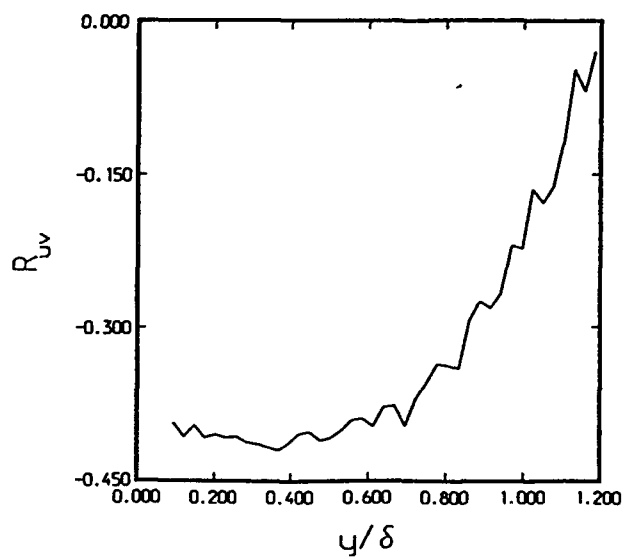


Figure 11 - Turbulent Boundary Layer Profiles:  
a) Mean Velocity



b) Turbulence Intensity



c) Cross-Correlation Coefficient

## **Appendix B**

Paper presented to 29th AIAA Aerospace Sciences Meeting, Reno,  
Nevada (1991): *Detailed Documentation of the Near Field Effects*  
of Large Eddy Break Up Devices on the Oncoming Vortical Structures  
in Turbulent Boundary Layers, N. Trigui and Y. G. Guezennec



**AIAA 91-0519**

**Detailed Documentation of the Near Field  
Effects of Large Eddy Break Up Devices  
on the Oncoming Vortical Structures  
in Turbulent Boundary Layers**

**N. Trigui and Y. G. Guezennec**

**Ohio State University**

**Columbus, OH**

**29th Aerospace Sciences Meeting**

**January 7-10, 1991/Reno, Nevada**

# DETAILED DOCUMENTATION OF THE NEAR FIELD EFFECTS OF LARGE EDDY BREAK UP DEVICES ON THE ONCOMING VORTICAL STRUCTURES IN TURBULENT BOUNDARY LAYERS

N. Trigui\* and Y. G. Guezennec\*\*  
The Ohio State University  
Columbus, Ohio

## Abstract

The near field effect of a single Large Eddy Break Up device (LEBU) on the oncoming vortical structure in a turbulent boundary layer was investigated in great details by measuring the full two-point space-time correlation tensor. In addition to conventional turbulence moments, spatial and temporal integral scales were determined. The stochastic estimation technique was used to reconstruct estimates of the full three-dimensional spatio-temporal evolution of the vortical structures as they pass over the manipulator: the name "Large Eddy Break Up" device is indeed justified by the results obtained here. It was found that in addition to the obvious inhibition of the normal velocity component by the LEBU, a number of other interrelated mechanisms are at play.

## Nomenclature

$C_f$	Skin friction coefficient
$h$	LEBU height
$l$	LEBU chord length
$R_{\alpha\beta}$	Correlation between $\alpha$ and $\beta$
$Re_\theta$	Reynolds number based on momentum thickness
$t$	Time
$T$	Integral time scale
$u$	Streamwise velocity
$v$	Normal velocity
$w$	Spanwise velocity
$x$	Streamwise coordinate
$x_L$	Downstream location of LEBU
$y$	Wall normal coordinate
$z$	Spanwise coordinate
$U_\infty$	Free-stream velocity
$\alpha$	LEBU angle of attack
$\delta$	Boundary layer thickness
$\delta_2, \theta$	Momentum thickness
$\delta_L$	Boundary layer thickness at LEBU position
$\Delta t$	Time separation
$\Delta x$	Streamwise separation
$\Delta z$	Spanwise separation
$\xi$	Non-dimensional distance downstream of LEBU
	$(x - x_L) / \delta_L$

## Subscripts

o Refers to regular case

## Introduction

The effect of Large Eddy Break-Up (LEBU) devices on turbulent boundary layers has been studied extensively in the past decade. These studies were first aimed at investigating the potential of these devices for viscous drag reduction. Among these studies, one can cite the investigations by Corke *et al.*<sup>1,2</sup>, Hefner *et al.*<sup>3</sup>, Bertelrud *et al.*<sup>4</sup>, and many others. The results obtained varied considerably from one study to another and were sometimes conflicting. While there was general agreement about the ability of these devices to produce sizable local skin friction reduction, there was considerable controversy to the extent, if any, of the net drag reduction potential of these devices. This prompted a different type of studies aimed at optimizing the geometry of the LEBU's, as the parametric investigation of Plesniak and Nagib<sup>5</sup>. These investigations indicated the marked sensitivity of the drag reduction results to the geometry of the LEBU's and identified the acceptable parameters to achieve drag reduction.

However, it also became clear that a more detailed understanding of the effects of these manipulators on the turbulence structure was required to further optimize these devices and make them less sensitive to minute geometrical changes. A number of studies dealt with documenting the changes in the various turbulence characteristics downstream of the LEBU's and identifying some possible mechanisms for these changes. Such studies have been conducted by Guezennec and Nagib<sup>6</sup>, Chang and Blackwelder<sup>7</sup>, Lemay *et al.*<sup>8</sup>, Trigui and Guezennec<sup>9</sup>, and others. This time however, the results of the different studies were in good agreement, namely that through an inhibition of the entrainment process, the LEBU's reduces the scales of the eddies in the outer and logarithmic region, which results in a drastic decrease of the momentum transport and therefore a decrease in the local skin friction. This conclusion was further supported by the failure of the LEBU's to produce any skin friction reduction in fully developed turbulent channel flow as recently reported by Prabhu *et al.*<sup>10</sup>.

Various mechanisms have been proposed for the modification of the boundary layer by the LEBU's<sup>6</sup>, such as direct inhibition of the normal velocity component by the manipulator, and the interaction of the shed vorticity in the wake of the LEBU with the turbulent boundary layer to name a few. However, these mechanisms are primarily inferred from measurements taken downstream of the LEBU's where it is hard to quantify exactly the relative role of these various processes. While the direct inhibition of the normal velocity component by the LEBU's is probably the most dominant mechanism in the immediate vicinity of the LEBU's, there is no detailed documentation of the near field of the manipula-

\* Graduate Student, Mechanical Engineering  
\*\* Assistant Professor, Mechanical Engineering,  
Member AIAA

tor and the alteration of the vortical structures. A more fundamental understanding of these mechanisms is essential for future design of manipulators that possess stronger and longer lasting effects on the turbulence structure. Furthermore, unlike the initial focus of the earlier work on drag reduction, there is a renewed interest in these devices for a variety of applications ranging from local skin friction reduction, to alteration of the transport of scalar contaminants, heat transfer applications, turbulence suppression for optical applications, boundary layer self-noise and drag reduction applications involving a combinations of techniques. Experimental investigations of some of these effects have been conducted by Trigui and Guezennec<sup>9,11</sup>, Lindemann<sup>12</sup>, Sommer and Petrie<sup>13</sup>, Keith *et al.*<sup>14</sup>, and others.

Up to date, all investigations (except one flow visualization study<sup>15</sup> to the authors knowledge) have been conducted downstream of the manipulators. From such studies, it is very difficult, if not impossible, to unravel the detailed mechanisms by which the LEBU's actually alter the turbulence structure. In particular, it is impossible to separate the effects of the manipulators on the oncoming large scale structures from the effects of the shed vorticity on what is remaining of these structures downstream of the manipulators.

This paper is part of a larger study<sup>16</sup> in which the near field of the LEBU's, both upstream and downstream, was investigated in great detail to elucidate these key questions. This paper will concentrate on the effect of a single LEBU on the oncoming large scale structures in the boundary layer before it reaches the trailing edge of the manipulator. In addition to presenting some of the usual one- and two-point statistical turbulence measurements, a detailed documentation of the effects of the LEBU on the large-scale vortical structures will be presented through a reconstruction of conditionally-averaged three-dimensional velocity field around the manipulators.

### Experimental Procedure

The boundary layer investigated was nominally a zero pressure gradient, flat plate boundary layer with a free-stream velocity of 10 m/s and Reynolds number based on momentum thickness ranging from 2000 to 8000. A flat plate manipulator was placed 1.2 m from the leading edge at a small angle of attack of approximately 2 degrees. This location,  $x_L$ , corresponds to a Reynolds number based on momentum thickness  $Re_\theta$  of about 2500. The LEBU was made out of 5 cm wide, 0.127 mm thick blued spring steel strip. It was suspended 1.9 cm above the plate and was carefully tensioned to avoid any vibration. The regular boundary layer thickness,  $\delta_0$ , at that location was nominally 2.5 cm. In other words, the LEBU configuration corresponded to a chord length of  $2\delta_0$  and a height of  $0.75\delta_0$ . A schematic diagram of the boundary layer test plate and of the LEBU configuration is given in Figure 1. For more details, the reader is referred to Trigui<sup>16</sup>.

The boundary layer characteristics were documented by acquiring a set of velocity profiles on the plate centerline at various downstream stations. The location of the various

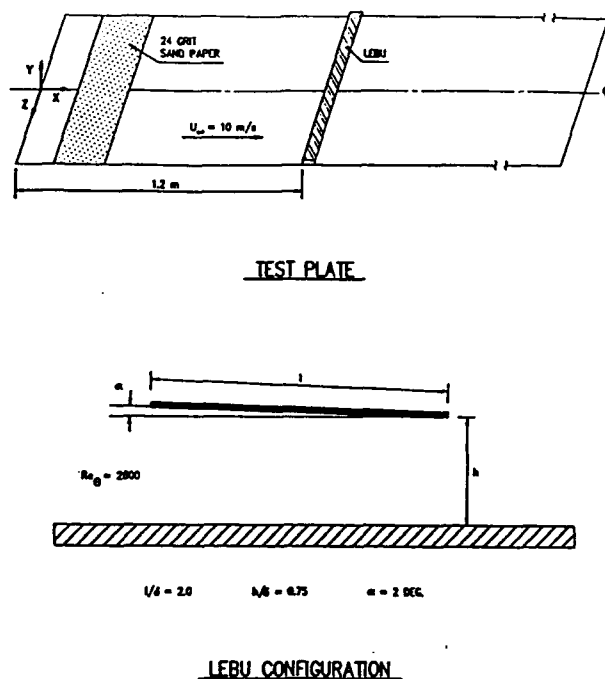


Fig. 1. Schematic Diagram of the Boundary Layer Test Plate and LEBU Configuration.

measurement stations ranged from  $\xi = 0.5$  to 53.0, where  $\xi$  is defined as the non-dimensional distance downstream of the trailing edge of the LEBU. A total of 49 points was collected in each profile. The points were equally spaced over a distance ranging from 100 wall units to 1.5 boundary layer thickness from the wall. At each point, long time records of the three velocity components was acquired with a triple hot-wire probe at a frequency of 7,000 Hz. A total of 50,000 samples was acquired in each record.

The main part of the experiment consisted in acquiring six simultaneously sampled hot-wire signals: three velocity components at a fixed reference point ("detection probe") and three velocity components at a mapping probe traversed over a coarse three-dimensional sampling grid. In order to study the evolution of the large-scale vortical structures as they pass over the manipulator, the fixed probe was positioned  $0.635\text{ cm}$  ( $0.25\delta_0$ ) upstream of the leading edge of the manipulator at the same height. A mapping was performed on a  $3 \times 15 \times 31$  mesh in the streamwise, normal and spanwise directions, respectively. The first cross-stream ( $y$ - $z$ ) plane corresponded to a zero streamwise separation between the detection and the mapping probes. The second and third cross-stream planes corresponded to separation of  $1.27\text{ cm}$  and  $2.54\text{ cm}$  ( $0.5$  and  $1.0\delta_0$ ), respectively.

In each of the cross-stream planes, the mapping span a total distance ranging from  $0.508\text{ cm}$  to  $3.81\text{ cm}$  away from the surface of the plate in the normal direction, and  $3.81\text{ cm}$  on either side of the test plate centerline in the spanwise direction. These distances correspond to distances ranging from  $0.2\delta_0$  to  $1.5\delta_0$  in the normal direction, and from  $-1.5\delta_0$  to  $1.5\delta_0$  in the spanwise direction. The spatial resolution in either the normal or spanwise direction was therefore equal to

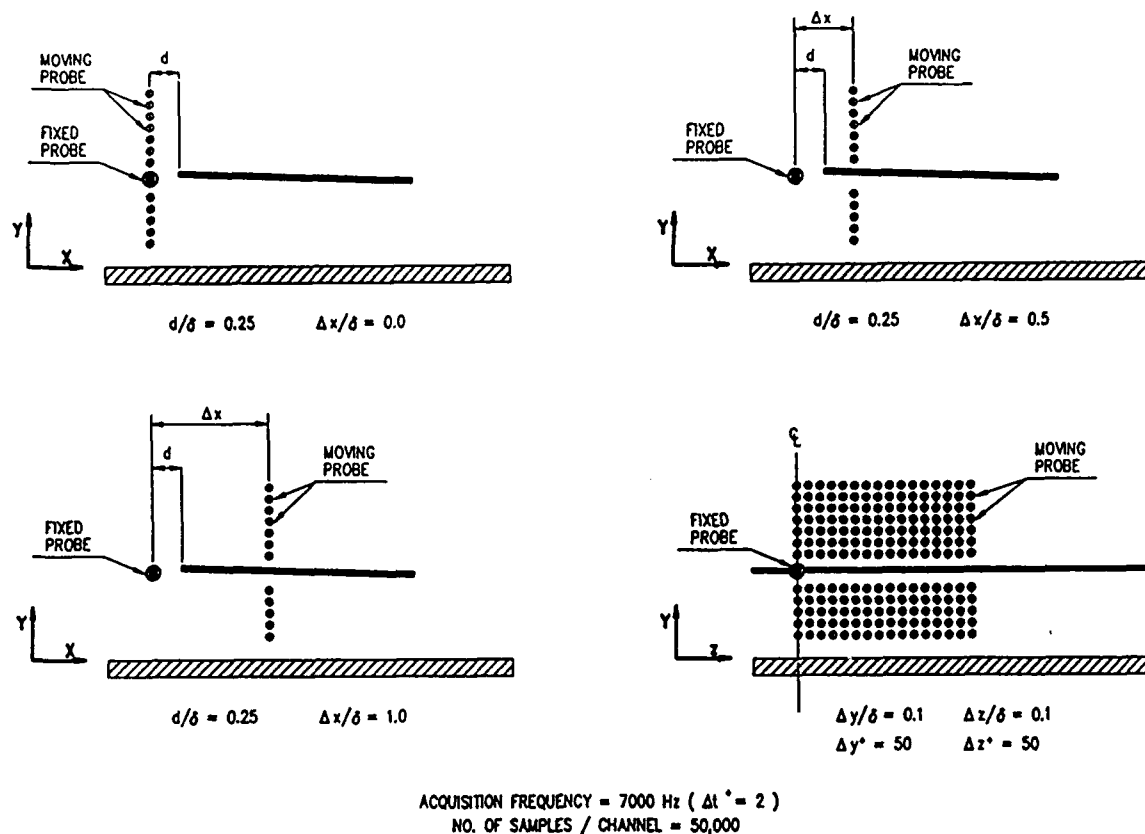


Fig. 2. Schematic Diagram of the Data Acquisition Mapping.

0.254 cm ( $0.1\delta_0$ ). As mentioned above, the spatial resolution in the streamwise direction was much coarser, namely 1.27 cm ( $0.5\delta_0$ ). The data acquisition grid is schematically shown in Figure 2. At each grid point, long time records of the six velocity components were acquired at a frequency of 7,000 Hz, corresponding to 2 viscous unit time units between samples. A total of 50,000 samples was acquired at each spatial point.

The local skin friction coefficient along the plate was evaluated using various methods. In the regular boundary layer case, the friction velocity was determined from a standard Clauser plot with the usual constants and from a two-dimensional momentum balance equation. In the manipulated case, since it has been shown by that the constants in the "law of the wall" do not hold in non-equilibrium boundary layers, only the two-dimensional momentum balance was used to compute the local skin friction coefficients along the plate. The practical implementation of the momentum balance technique was similar to that used by Corke *et al.*<sup>2</sup> and Plesniak *et al.*<sup>5</sup>. Although such technique is inherently inaccurate, it is the only tool available for reducing the data in manipulated, non-equilibrium turbulent boundary layers short of direct measurement by local skin friction balances<sup>17</sup>. In order to validate the use of the two-dimensional balance technique, velocity profiles were acquired at different spanwise locations on either side of the plate centerline and at few downstream locations. It was found that the boundary layer thickness did not vary by more than 3% over the span of

interest. Furthermore, the skin friction results obtained from this technique were only used to perform a relative comparison between the regular and manipulated cases, hence minimizing the inherent inaccuracies of the technique.

In addition to all the usual statistical quantities, such as means, and first and second order moments, all nine components of the space-time correlation tensor were computed, yielding  $R_{\alpha\beta}(\Delta x, \Delta y, \Delta z; \Delta t)$  in both the regular case and the manipulated case. From this, inference about the underlying spatio-temporal structure of the flows can be made, and other quantities such as convection velocities, integral scales in space and time can be computed in the usual fashion. Furthermore, a more physical interpretation of these extensive correlation measurements can be made by using a tool called the stochastic estimation technique. This technique was first introduced by Adrian and his co-workers<sup>18,19,20</sup>. Recently, it has been used extensively in the context of boundary layers to obtain estimates of conditional eddies (in the sense of classical conditional ensemble averages) by extracting information from the (unconditional) two-point correlation tensor. This technique is very powerful and convenient when dealing with a three- or four-dimensional data base, particularly to investigate a large number of "conditions". For more details about the derivation and the use of the technique, the reader is referred to recent applications to turbulent boundary layers<sup>21,22</sup>.

## Results

The detailed documentation of the characteristics of the regular and manipulated boundary layers can be found elsewhere<sup>16</sup>. The results are similar in character to those reported by other investigators for similar cases. As an example, the downstream evolution of the skin friction ratio between the manipulated and regular case is shown in Figure 3. A maximum of about 20% local skin friction decrease is obtained and the effect slowly relaxes up to  $\xi = 50$ .

A comparison of the downstream evolution of the various integral time scales is shown in Figure 4. The left column represents the integral time scale associated with the streamwise velocity fluctuations, while those associated with the normal and spanwise velocity fluctuations are shown in the center and right columns, respectively. All time scales are made non-dimensional with the local mean velocity at that height and the momentum thickness,  $\delta_2$ . In effect, these can also be interpreted as non-dimensional length scales by the use of Taylor's hypothesis. The normal distance from the wall is also made non-dimensional with the momentum thickness. A decrease of about 20% is observed for the integral scale associated with the streamwise velocity,  $T_u$ , and this decrease appears to persist up to the last measurement station at  $\xi = 53$ . On the other hand, the integral scales associated with the normal and spanwise velocity,  $T_v$  and  $T_w$ , respectively, are very significantly reduced in the upper part of the boundary layer immediately behind the LEBU. This effect is definitely less pronounced below the LEBU. This

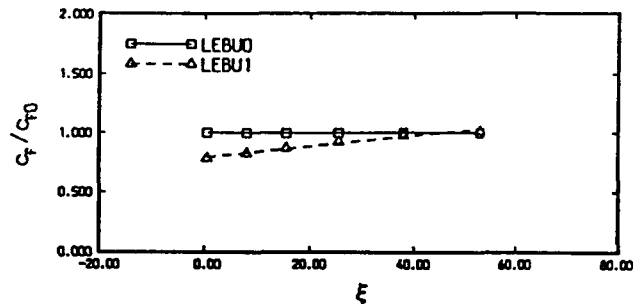


Fig. 3. Comparison of the Downstream Evolution of the Skin Friction Coefficient between Regular and LEBU case.

indicates that different mechanisms are at play above and below the manipulator. However, both  $T_v$  and  $T_w$  relax much faster than  $T_u$  with downstream distance, with  $T_v$  returning to regular values by  $\xi = 53$ . These relaxation effects are similar to those reported in the literature for the turbulence intensity profiles. It should also be noted that all three integral scales are drastically reduced in the near wake of the LEBU. This can be attributed to the generation of small scales in the near wake of the manipulator which dominate the boundary layer fluctuations.

To understand what is happening to oncoming large scale structures in the immediate vicinity of the LEBU, all

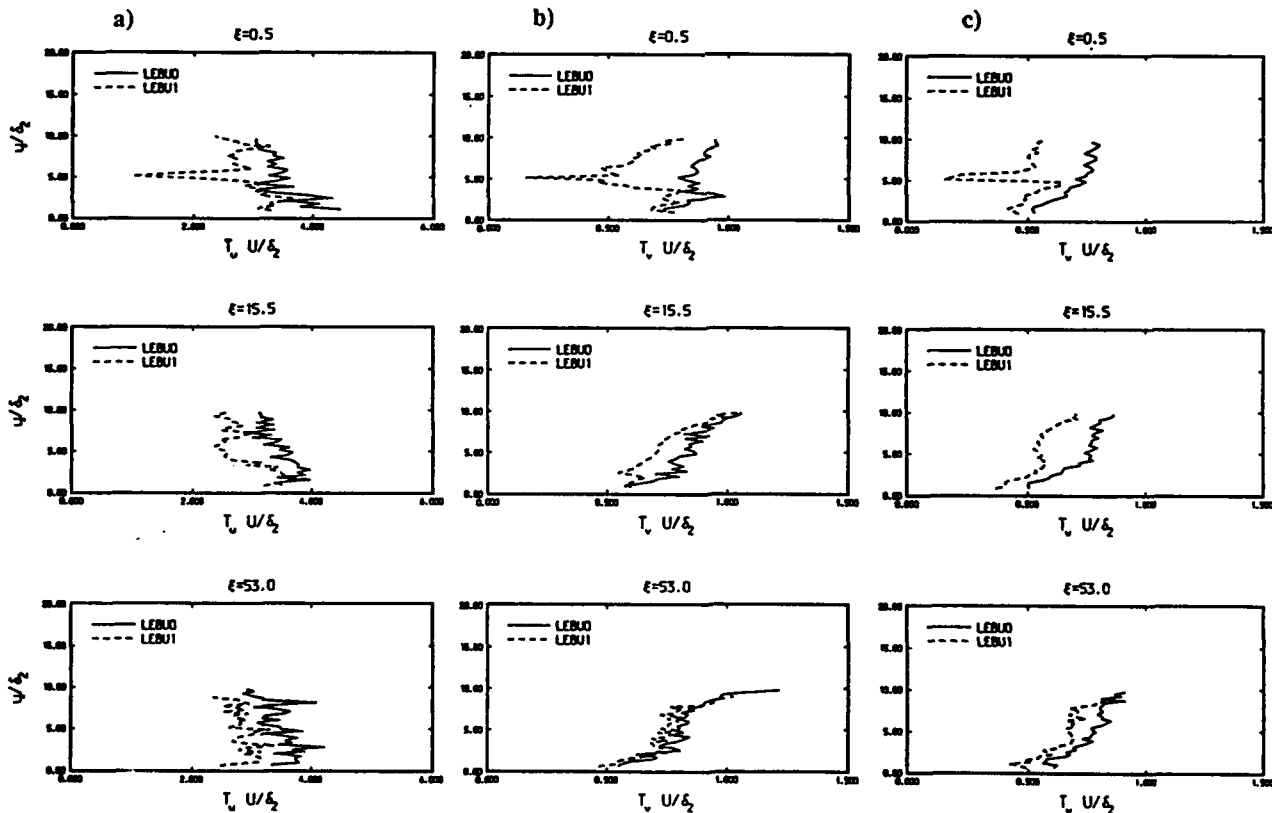


Fig. 4. Comparison of the Downstream Evolution of the Integral Time Scales of the Three Velocity Components between Regular and Manipulated case: a) Streamwise velocity, b) Normal Velocity and c) Spanwise Velocity.

nine components of the space-time correlation tensor were measured with respect to a fixed point located just upstream of the manipulator, as described in the previous section. A comparison between the regular and the manipulated case is shown in Figures 5, 6 and 7 for the  $R_{uu}$ ,  $R_{vv}$  and  $R_{ww}$  components, respectively. In each figure, iso-correlation contours are shown in the  $t$ - $z$  plane. The time axis is made non-dimensional with  $U_\infty$  and  $\delta_0$  and the spanwise axis non-dimensionalized by  $\delta_0$ . In each Figure, the left column represent the regular case at  $y/\delta_0 = 0.6$ , while the middle column represents the LEBU case at  $y/\delta_0 = 0.6$  (just below the LEBU) and the right column corresponds to the LEBU case at  $y/\delta_0 = 0.9$  (just above the LEBU). In all three figures, the top line represents a streamwise separation  $\Delta x/\delta_0 = 0$ , while the middle line corresponds to  $\Delta x/\delta_0 = 0.5$  and the bottom line corresponds to  $\Delta x/\delta_0 = 1.0$ .

As expected, Figure 5a shows that Taylor's hypothesis holds quite nicely for the streamwise velocity correlation  $R_{uu}$  in the regular case. The convection velocity is slightly less than  $U_\infty$  as expected at that height in the boundary layer, and the structures do not significantly decay in space-time over a distance of a boundary layer thickness. A similar behavior is observed in Figures 6a and 7a for the normal and spanwise velocity correlations,  $R_{vv}$  and  $R_{ww}$ , respectively. However,  $R_{vv}$  does decay appreciably more than the other two. For the manipulated case below the LEBU, the streamwise velocity correlation (Figure 5b) indicates a similar convection velocity and a very slight strengthening of the  $u$  perturbation as it

passes under the LEBU. This can possibly be attributed to the very small angle of attack of the manipulator contributing to a small contraction effect. On the other hand, the streamwise velocity correlation above the LEBU (Figure 5c) exhibits a convection velocity faster than  $U_\infty$  probably due to the acceleration of the flow above the leading edge of the manipulator. Furthermore, the streamwise velocity perturbation decays rather strongly in space-time, thereby invalidating the use of Taylor's hypothesis even over short distance in the immediate vicinity of the LEBU. The difference in convection velocity between the top and bottom side of the LEBU contributes to the decorrelation of the remnants of the structures over the manipulator, ultimately prohibiting their reconnection downstream of the device. This difference in convection velocity is clearly linked to the circulation around the device and partially legitimizes the use of small positive angles of attack and sufficient long chord length<sup>5</sup>. It should also be noted that the correlation contours are slightly pinched in the spanwise direction both above and below the LEBU, i.e. the manipulator decreases slightly the spanwise length scale of the structures<sup>7,23</sup>.

On the other hand, the normal velocity correlations,  $R_{vv}$ , exhibits similar behavior above and below the LEBU (Figures 6b and 6c). The structures decay very rapidly, perhaps more so on the top side. Again, this points to the lack of validity in applying Taylor's hypothesis even over short distances in the immediate vicinity of the manipulator. It also confirms that the direct inhibition of the normal velo-

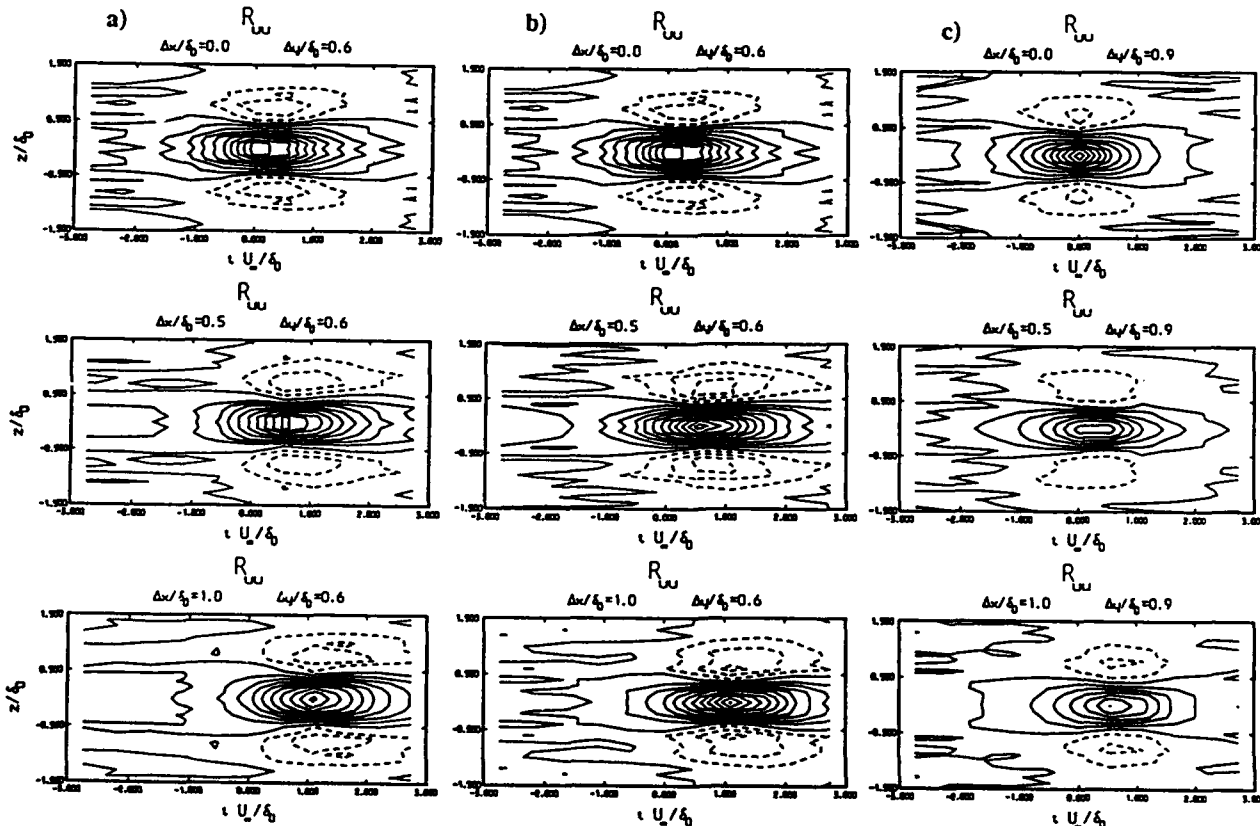


Fig. 5. Comparison of the Space-Time Correlation Maps of the Streamwise Velocity for: a) Regular Case at  $y/\delta = 0.6$ , b) LEBU Case at  $y/\delta = 0.6$  and c) LEBU Case at  $y/\delta = 0.9$ .

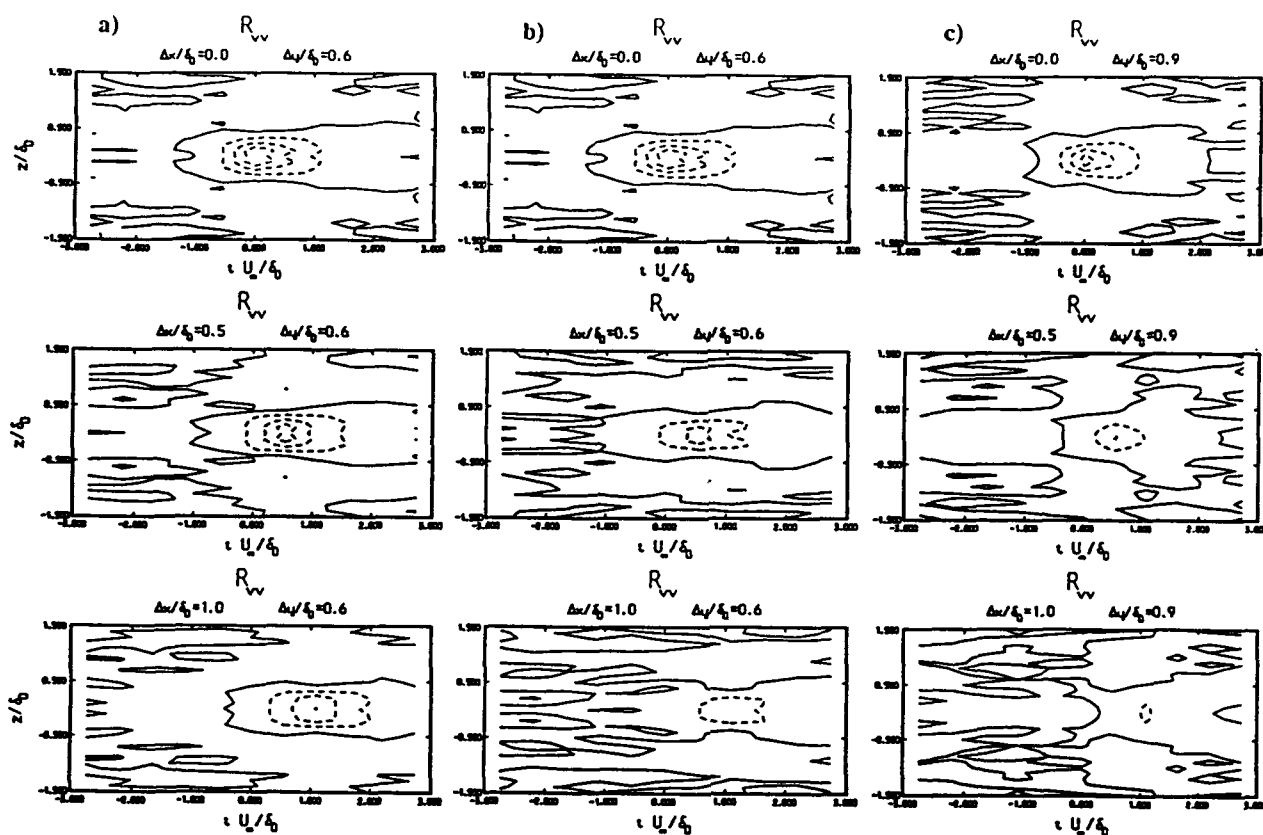


Fig. 6. Comparison of the Space-Time Correlation Maps of the Normal Velocity for:  
a) Regular Case at  $y/\delta = 0.6$ , b) LEBU Case at  $y/\delta = 0.6$  and c) LEBU Case  
at  $y/\delta = 0.9$ .

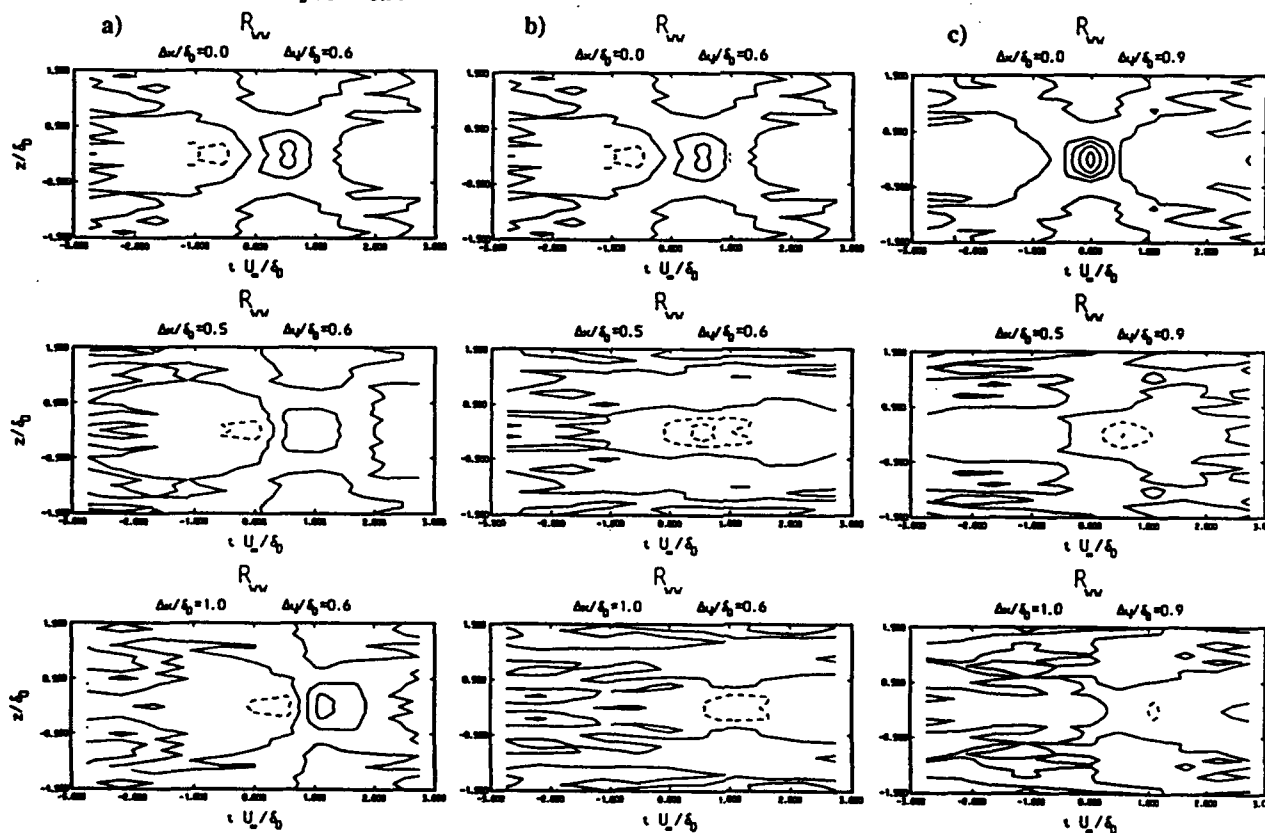


Fig. 7. Comparison of the Space-Time Correlation Maps of the Spanwise Velocity for:  
a) Regular Case at  $y/\delta = 0.6$ , b) LEBU Case at  $y/\delta = 0.6$  and c) LEBU Case  
at  $y/\delta = 0.9$ .

city component by the LEBU is felt immediately and contributes very significantly to the decay of the vortical structures over distances of the order of less than a boundary layer thickness (less than half a chord length in this case).

The spanwise velocity correlations,  $R_{ww}$ , exhibit a very interesting behavior as shown in Figures 7b and 7c. Not only the perturbation does not remain correlated as it travels over the LEBU, but it becomes anti-correlated. This behavior can probably be attributed to a "splating" effect or the formation of a new vortical structure on the surface of the LEBU due to the newly imposed no-slip boundary condition. It is needless to say that the concept of Taylor's hypothesis loses all its meaning in this case.

To further illustrate the structural changes to the vortical eddies passing over the LEBU, the stochastic estimation technique was used as a tool to reconstruct estimates of the

three-dimensional conditional velocity field associated with a typical perturbation impinging on the leading edge of the manipulator. As described in the previous section, the complete space-time correlation tensor is used as a basis to determine the linear stochastic estimation coefficients. For further details about the application and validity of the stochastic estimation technique to boundary layers, the reader is referred to the work of Guezennec<sup>21</sup> and Guezennec and Trigui<sup>22</sup>. The choice of the "condition" is not critical to the conclusions being drawn here. As an example, the case of an inrush of high-speed potential fluid towards the wall was chosen as the relevant "condition". The magnitude of  $u$  was chosen to be equal to one r.m.s. value,  $\sigma_u$ , and the magnitude of  $v$  was chosen to be minus one r.m.s. value,  $\sigma_v$ . The magnitude of  $w$  was chosen to be zero (hence yielding spanwise-symmetric structures), although more likely values will be randomly ranging within plus or minus one r.m.s.,  $\sigma_w$ , and would yield strongly asymmetric structures as pointed

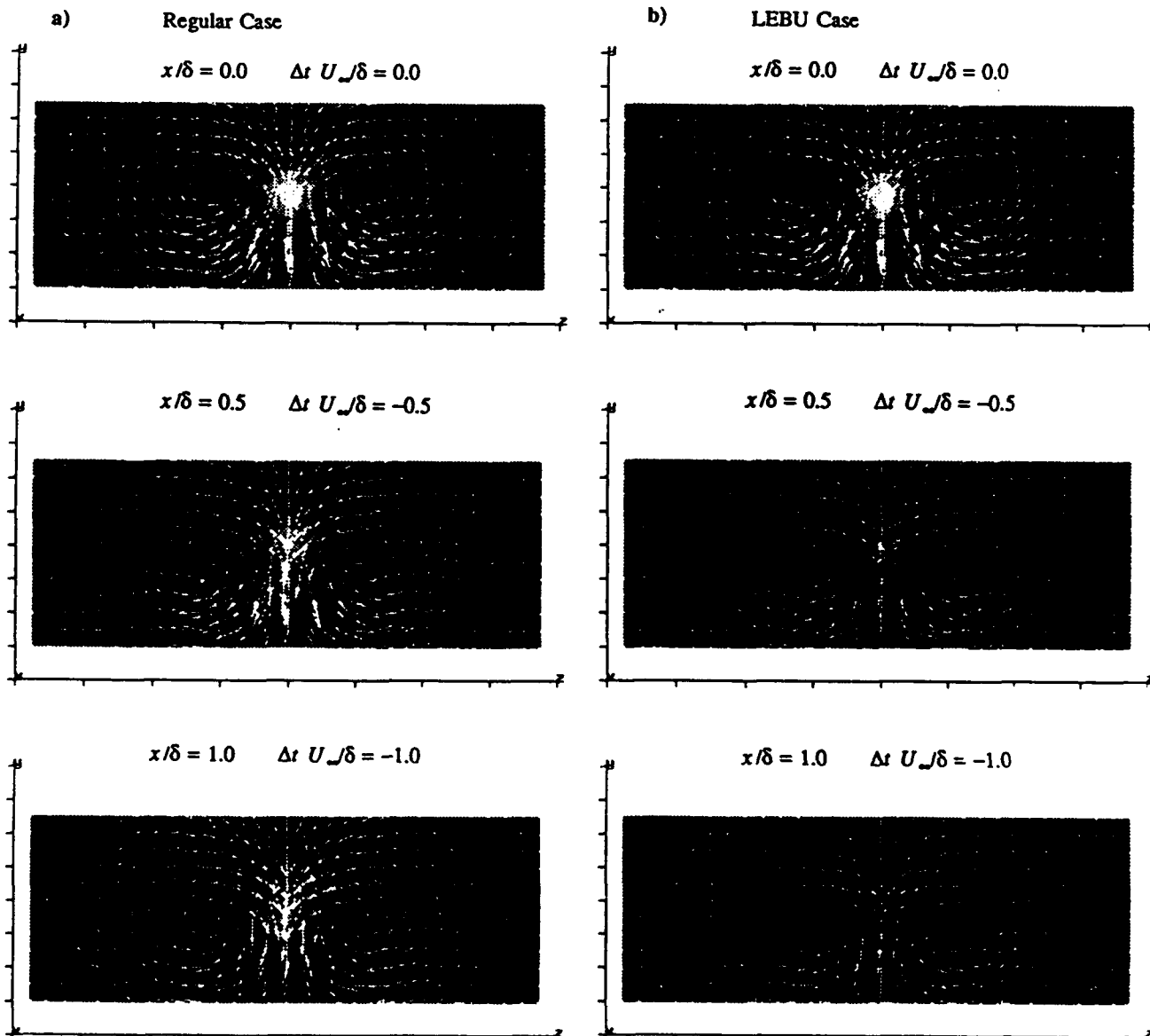


Fig. 8. Comparison of the Space-Time Evolution of Reconstructed Velocity Field for:  
a) Regular Case and b) LEBU Case.

out by Choi and Guezennec<sup>24</sup> (not shown here). Figure 8 shows a comparison between the space-time evolution of such a conditional structure between the regular case (left column) and the LEBU case (right column). The top line correspond to a streamwise separation  $\Delta x/\delta_0 = 0.0$ , i.e. upstream of the manipulator and hence both cases are identical. The middle line represents the case where  $\Delta x/\delta_0 = 0.5$  and  $\Delta t U_\infty/\delta_0 = -0.5$ , whereas the bottom line represents the corresponding case for  $\Delta x/\delta_0 = 1.0$  and  $\Delta t U_\infty/\delta_0 = -1.0$ . Since this is a space-time representation, it should not be interpreted as a physical spatial structure, but rather as an illustration of the concepts discussed in the previous three Figures. In all Figures, the cross-stream plane ( $y-z$ ) is shown with arrows representing the  $v$  and  $w$  velocity components in that plane. The gray level background represents the magnitude of the streamwise velocity perturbation, with white corresponding to a high positive perturbation, mid-gray to a zero perturbation and black to a high negative perturbation. The scale of the arrows and gray levels is kept fixed for all plots. As described earlier, Taylor's hypothesis is quite valid in the regular case, with the structure looking essentially identical for all three space-time locations and the amplitude of the perturbation slightly decaying for  $u$  and  $w$  and more significantly for  $v$ . On the contrary in the LEBU case, the strength of the vortical motion is considerably weakened by the the first position over the LEBU and the strength of the  $u$  perturbation has decayed particularly above the LEBU near the outer edge of the boundary layer. Again, it should be re-emphasized that this is *not* a spatial representation of the eddies over the LEBU.

Such a representation is given in Figure 9, which depicts a comparison between the regular and manipulated case for the spatial structure with zero time delay, i.e. a true spatial structure with no use of Taylor's hypothesis. Again, the "condition" is the same as the one investigated in the previous Figure. The regular case exhibits a pair of counter-rotating eddies which are inclined over the wall at a shallow angle. By the last station ( $\Delta x/\delta_0 = 1.0$ ), the eddies are not identifiable since they have reached the outer edge of the boundary layer. In the LEBU case, we can observe the formation of a secondary pair of eddies on the top of the manipulator at  $\Delta x/\delta_0 = 0.5$  due to the "splatting" effect inferred earlier. The remnant of the original eddy passing below the manipulator is reasonably unaffected at that station, but represents more of a fossil perturbation not associated any more with a vortical structure. By the last station ( $\Delta x/\delta_0 = 1.0$ ), the remaining perturbation is considerably weaker than in the regular case.

### Conclusions

In summary, the very near field effects of a single Large Eddy Break Up device on the oncoming vortical structures in a turbulent boundary layer was investigated with very detailed three-dimensional measurements of all velocity components. It was found that the structure of the boundary layer is affected very rapidly and in many ways by the presence of the LEBU. Since all three components of the velocity correlations exhibit a different behavior as the vortical large-scale structures pass over the LEBU, the term "Large Eddy Break Up" device can be better understood. The mechanisms

at play are rather complex, ranging from the "simple" inhibition of the normal velocity component of the eddies, to the formation of new or distorted eddies by the "splatting" and the no-slip condition on the manipulator surface, and to the shearing by different convection velocities of an otherwise fossilized streamwise velocity perturbation. Furthermore, all those changes happen over a distance of the order of a boundary layer thickness or less. While this does not elucidate all aspects of the role of the LEBU for the manipulation of turbulent boundary layers, it characterizes in a very detailed fashion the initial effects on the boundary layer. It is clear that these effects are so drastic that the outer structure of the boundary layer is annihilated for practical purposes by the time the turbulence reaches the trailing of the LEBU. The additional mechanisms occurring immediately downstream of the manipulator and the interaction of the wake of the LEBU with the boundary layer turbulence, as well as the relaxation of these effects with downstream distance have been investigated and are described elsewhere<sup>16</sup>.

### Acknowledgment

This work was partially supported by the National Science Foundation under Grant MSM-8709154 and the Air Force Office of Scientific Research under Grant 89-0434. Their support is gratefully acknowledged.

### References

- 1 Corke, T. C., Guezennec, Y. G. and Nagib, H. M. "Modification in Drag of Turbulent Boundary Layers Resulting from Manipulation of Large-Scale Structures," NASA CR-3444, July 1981.
- 2 Corke, T. C., Nagib, H. M. and Guezennec, Y. G. "A New View on Origin, Role and Manipulation of Large Scales in Turbulent Boundary Layers," NASA CR-165861, February 1982.
- 3 Hefner, J. N., Anders, J. B., and Bushnell, D. M. "Alteration of Outer Flow Structures for Turbulent Drag Reduction," AIAA 21st Aerospace Sciences Meeting, January 1983, AIAA Paper 83-0293.
- 4 Bertelrud, A., Truong, T. V., and Avellan, F. "Drag Reduction in Boundary Layers Using Ribbons," AIAA 9th Atmospheric Flight Mechanics Conference, August 1982, AIAA Paper 82-1370.
- 5 Plesniak, M., and Nagib, H. M. "Net Drag Reduction in Turbulent Boundary Layers Resulting from Optimized Manipulation," AIAA Shear Flow Control Conference, Boulder Colorado, 1985, Paper 85-0518.
- 6 Guezennec, Y. G., and Nagib, H. M. "Documentation of Mechanisms Leading to Net Drag Reduction in Manipulated Turbulent Boundary Layers," *AIAA J.*, Vol. 28, 1990, pp. 245-252.
- 7 Chang, S. I. and Blackwelder, R. F. "Modification of Large Eddies in a Turbulent Boundary Layer," *J. Fluid Mech.*, Vol. 213, pp. 419-442, 1990.

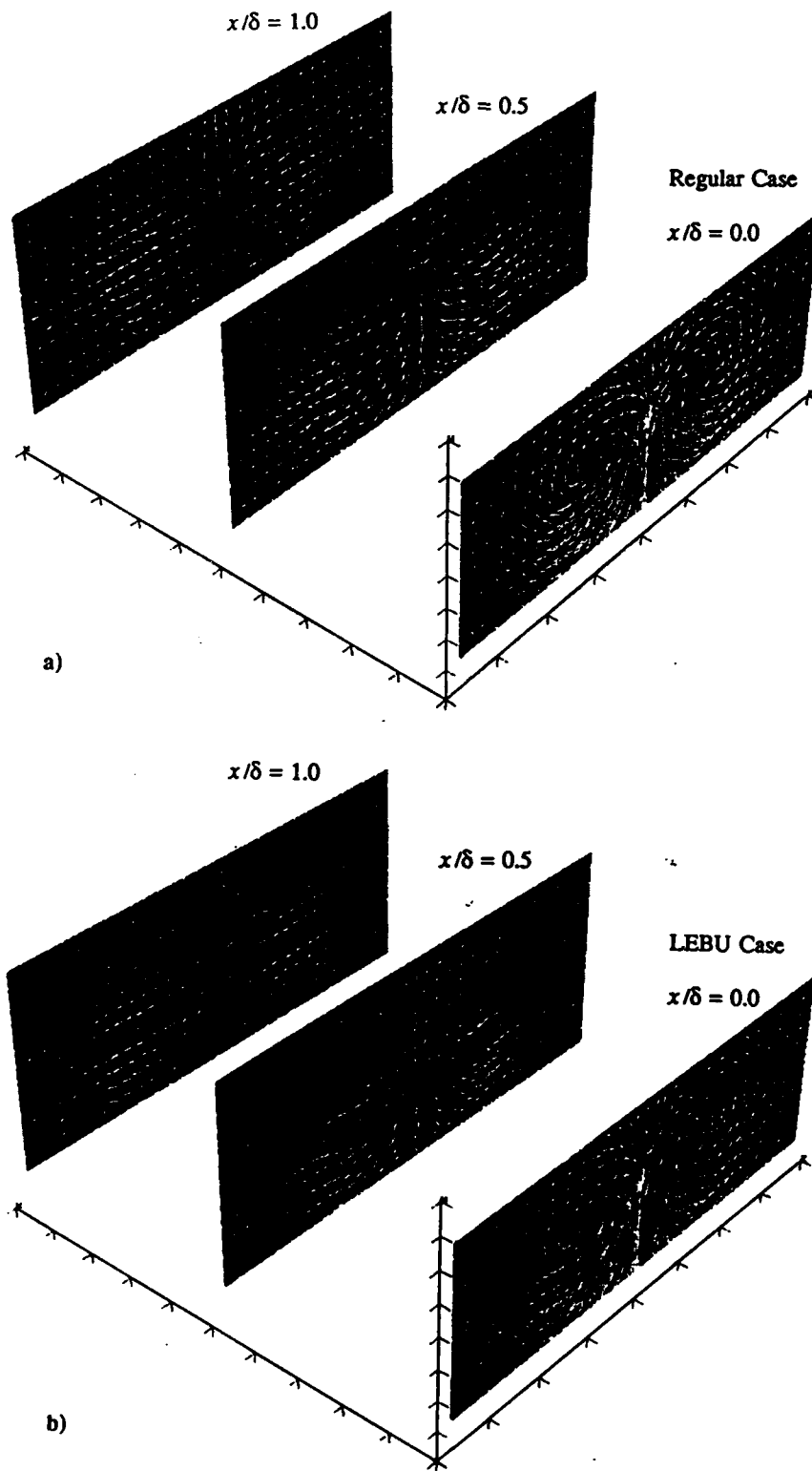


Fig. 9. Comparison of the Spatial Evolution of the Reconstructed Velocity Field for: a) Regular Case and b) LEBU Case.

- <sup>8</sup> Lemay, J., Delville, J., and Bonnet, J. P. "Turbulent Kinetic Energy Balance in a LEBU Modified Turbulent Boundary Layer", *Experiments in Fluids*, Vol. 9, pp. 301-308, 1990.
- <sup>9</sup> Trigui, N. and Guezennec, Y. G. "Turbulence Modification by Large Eddy Breakup Devices in a Passively Heated Turbulent Boundary Layer", *Proc. Joint ASME/CSME Symposium on Turbulence*, Toronto, Canada, June 1990, FED Vol. 94, pp. 17-22 (also submitted to *Experiments in Fluids*, 1990).
- <sup>10</sup> Prabhu, A., Vasudevan, B., Kailasnath, R. S., and Narasimha, R. *Turbulence Management and Relaminarization*, Vol. 97, Heidelberg, Springer.
- <sup>11</sup> Trigui, N. and Guezennec, Y. G. "Heat Transfer Reduction in Manipulated Turbulent Boundary Layers", *Int. J. Heat and Fluid Flow*, Vol. 11, 1990, pp. 214-219.
- <sup>12</sup> Lindemann, A. M. "Turbulent Reynolds Analogy factors of Stacked Large Eddy Break-Up Devices", *J. of Spacecraft and Rockets*, Vol. 23, pp. 348-350, 1986.
- <sup>13</sup> Sommer, S. T. and Petrie H. L. "Diffusion of slot injected drag reducing polymer solution in a LEBU modified turbulent boundary layer", *Proc. Symposium on Turbulence*, Rolla, Missouri, September 1990, pp. A10(1-8).
- <sup>14</sup> Keith, L. W., Ciesluk, A. J., and Barclay, J. J. "Hydrodynamic Measurements of the Wall Pressure Field Downstream of a Large Eddy Breakup Device", *Proc. of the Second Symposium on Performance Enhancement for Marine Applications*, Newport, Rhode Island, October 1990, pp. 199-207.
- <sup>15</sup> Savory, E., Toy, N., and Tahouri, B. "Visualization of the Flow Regime around Tandem LEBU Manipulators", *Proc. of the Second Symposium on Performance Enhancement for Marine Applications*, Newport, Rhode Island, October 1990, pp. 211-218.
- <sup>16</sup> Trigui, N. "Detailed Documentation of the Effects of Large Eddy Breakup Devices on Turbulent Boundary Layers", Ph.D. Thesis, The Ohio State University, March 1991.
- <sup>17</sup> Nguyen, V. D., Dickinson, J., Anderson, J., Haeberle, D., Larose, J., Boisvert, L. M., Chalifour, Y., and Jaen, Y. "Some Experimental Observations of the Law of the Wall Behind Large-Eddy Breakup Devices Using Servo-Controlled Skin Friction Balances", AIAA 22nd Aerospace Sciences Meeting, Reno, Nevada, Paper 84-0346, 1984.
- <sup>18</sup> Adrian, R. J., "On the Role of Conditional Averages in Turbulent Theory", *Proc. of the Fourth Symposium on Turbulence*, University of Rolla-Missouri, 1976.
- <sup>19</sup> Adrian, R. J., "Conditional Eddies in Isotropic Turbulence", *Phys. Fluids*, Vol. 22, 1979, pp. 2065-2070.
- <sup>20</sup> Tung, T. C. and Adrian, R. J., "Higher Order Estimates of Conditional Eddies in Isotropic Turbulence", *Phys. Fluids*, Vol. 23, 1980, pp. 1469-1470.
- <sup>21</sup> Guezennec, Y. G. "Stochastic Estimation of Coherent Structures in Turbulent Boundary Layers", *Physics of Fluids A*, Vol. 1, pp. 1054-1061, 1989.
- <sup>22</sup> Guezennec, Y. G. and Trigui, N. "Reconstruction of the Pseudo-Dynamics of Turbulent Boundary Layers by Multi-Point Stochastic Estimates" submitted to *Physics of Fluids A*, 1991.
- <sup>23</sup> Lemay, J., Savill, A. M., Bonnet, J. P., and Deville, J. "Some Similarity between Turbulent Boundary Layers manipulated by thin and thick flat plate manipulators", *Turbulent Shear Flows*, Vol. 6, pp. 179-193, Heidelberg, Springer.
- <sup>24</sup> Choi, W. C. and Guezennec, Y. G. "On the Asymmetry of Coherent Structures in Turbulent Boundary Layers", *Phys. Fluids A*, Vol. 2, 1990, pp. 628-630.

## **Appendix C**

Transparencies presented at the 1991 AFOSR Meeting on Turbulence  
Structure and Control, Columbus, Ohio (1991): The Stochastic  
Estimation: A Versatile Tool to Study and Predict (?) Turbulent Flows,  
Y. G. Guezennec, T. J. Gieseke W. C. Choi and N. Trigui

# **The Stochastic Estimation: A Versatile Tool to Study Turbulent Flows**

**Yann G. Guezennec**

**W. C. Choi**

**N. Trigui**

**T. Gieseke**

**Mechanical Engineering Department  
The Ohio State University**

**Supported by:  
AFOSR 89-0434  
ONR N00014-90-J-1499**

## **NEW DIRECTIONS FOR RESEARCH IN TURBULENT FLOWS**

- **Scientific Needs**

- Understand routes to chaos, transition
- Understand mechanisms for the sustainment of turbulence

- **Technological Needs**

- Develop better transition/turbulence models for flow prediction
- Develop transition/turbulence control schemes to achieve  
desired characteristics

- **A few facts about transition/turbulence**

- Unsteady, three-dimensional flow fields
- Complex interaction between the various terms
- Existence and importance of organized/coherent structures
- Relative lack of formalism to incorporate heuristic ideas  
into models or dynamics
- Lack of universality among flow fields/researchers/models

## IMPLICATIONS FOR RESEARCH IN TURBULENT FLOWS

- Structures/flow features are very diverse. Therefore they must be "captured" in the most generic way to avoid bias.
- Structures are inherently unsteady and three-dimensional. Therefore, the methods for their "capture" and study must respect those attributes.
- We must incorporate organized/coherent structures into a quantitative formalism to obtain dynamics. Therefore, we must evolution equations for these structures.

## POSSIBLE APPROACHES

- Stochastic estimation → Pseudo-dynamics, p.d.f. models, L.E.S subgrid models(?). *(wall region)*
- Proper Orthogonal Decomposition (POD) → *?* Dynamical systems approach

## EXPERIMENTAL NEEDS

- Measure 3-D space(-time) two-point correlation tensor since all structural information is imbedded in it. Study non-canonical cases. Use either/both approaches to extract specific structures and study them.

## THEORETICAL/NUMERICAL NEEDS

- Use experimental data to study the following:
  - Three-dimensional structure (velocity/vorticity fields)
  - Contributions to the overall flow (kinetic energy, Reynolds stress, production...)
  - Dynamics (evolution in time, regular/chaotic behavior, origin of chaotic behavior...)
  - Control of the dynamics
  - Sensitivity of results (indirectly of correlation tensor) to Reynolds number, non-canonical forcing...

**NECESSITY TO COMBINE  
EXPERIMENTAL/THEORETICAL/NUMERICAL/VISUALIZATION  
EFFORTS TO ENCOMPASS THE WHOLE PROBLEM**

## **DRAWBACKS OF CONVENTIONAL CONDITIONAL AVERAGING TECHNIQUES**

- The conditional average decays to zero away from the detection point.
- The choice of the "condition" is difficult. Results obtained depend directly on the condition selected.
- Strictly kinematic description of the flow.
- Tedious to implement for many different "conditions" for a 3-D data base.

## STOCHASTIC ESTIMATION OF CONDITIONAL AVERAGES

→ Least-square estimation of conditional averages (Adrian, 1976, 1979, 1980, etc..).

Conditional average of  $u$  at  $x+r$  given condition at  $x$ :

$$\bar{u}(x;r) = \langle u(x;r) \mid u(x) \rangle$$

Assume a linear estimate for  $\bar{u}(x;r)$ :

$$u_i(x;r) = A_{ij}(r) u_j(x) + O[u^2(x)]$$

Determine  $A_{ij}(r)$  by least-square procedure:

$$e_i = \langle [A_{ij}(r)u_j(x) - u_i(x+r)]^2 \rangle \quad \text{Min.}$$

Minimize the error with respect to the unknown coefficients  $A_{ij}(r)$ :

$$\frac{\partial e_i}{\partial A_{ij}(r)} = 0 \rightarrow \langle u_j(x)[A_{ik}(r)u_k(x) - u_i(x+r)] \rangle = 0$$

which yields:

$$\langle u_j(x)u_k(x) \rangle A_{ik}(r) = \langle u_j(x)u_i(x+r) \rangle$$

The determination of the coefficient  $A_{ij}(r)$  requires the use of the 2-point 2nd order spatial correlation tensor.

## ESTIMATION PROCEDURE

- Measure the 2-point spatial correlation tensor.
- Solve linear systems of equations for the  $A_{ij}(r)$  coefficients for each  $r$ .
- Select condition vector(s) at  $x$
- Reconstruct the linear estimate of the conditional velocity field around  $x$

## GENERALIZATION TO INCLUDE TIME DEPENDENCE

Conditional average of  $u$  at  $x+r$  and  $t+\tau$  given condition at  $x$  and  $t$ :

$$\bar{u}(x,t;r,\tau) = \langle u(x+r; t+\tau) | u(x,t) \rangle$$

Assume a linear estimate for  $\hat{u}(x,t;r,\tau)$ :

$$u_i(x,t;r,\tau) = A_{ij}(r,\tau) u_j(x,t) + O[u^2(x,t)]$$

Determine  $A_{ij}(r,\tau)$  by least-square procedure:

$$e_i = \langle [A_{ij}(r,\tau) u_j(x,t) - u_i(x+r,t+\tau)]^2 \rangle \quad \text{Min.}$$

Minimize the error with respect to the unknown coefficients  $A_{ij}(r,\tau)$ :

$$\frac{\partial e_i}{\partial A_{ij}(r,\tau)} = 0$$

which yields:

$$\langle u_j(x,t) u_k(x,t) \rangle A_{ik}(r,\tau) = \langle u_j(x,t) u_i(x+r,t+\tau) \rangle$$

The determination of the coefficient  $A_{ij}(r,\tau)$  requires the use of the 2-point 2nd order space-time correlation tensor.

## ESTIMATION PROCEDURE

- Measure the 2-point space-time correlation tensor.
- Solve linear systems of equations for the  $A_{ij}(r,\tau)$  coefficients for each  $r$  and each  $\tau$ .
- Select condition vector(s) at  $x$
- Reconstruct the linear estimate of the conditional velocity field around  $x$  and  $t$ .

## GENERALIZATION TO HIGHER ORDER ESTIMATES

Assume a higher order expansion for the estimate of  $\hat{u}(x;r)$ :

$$u_i(x;r) = A_{ij}(r) u_j(x) + B_{ijk}(r) u_j(x) u_k(x) + C_{ijkl}(r) u_j(x) u_k(x) u_l(x) + \dots$$

Determine  $A_{ij}(r)$ ,  $B_{ijk}(r)$ ,  $C_{ijkl}(r)$ , ... by least-square procedure:

$$e_i = \left\langle \left[ \hat{u}_i(x;r) - u_i(x+r) \right]^2 \right\rangle \quad \text{Min.}$$

Minimize the error with respect to the unknown coefficients  $A_{ij}(r)$ ,  $B_{ijk}(r)$ ,  $C_{ijkl}(r)$ , ...:

$$\frac{\partial e_i}{\partial A_{ij}(r)} = \frac{\partial e_i}{\partial B_{ijk}(r)} = \frac{\partial e_i}{\partial C_{ijkl}(r)} = \dots = 0$$

which yields:

$$\begin{aligned} \langle u_j(x) u_k(x) \rangle &= A_{jk}(r) + \langle u_j(x) u_k(x) u_l(x) \rangle B_{ijk}(r) + \\ &\quad \langle u_j(x) u_k(x) u_l(x) u_m(x) \rangle C_{ijkl}(r) = \langle u_j(x) u_i(x+rx) \rangle \end{aligned}$$

$$\begin{aligned} \langle u_j(x) u_k(x) u_l(x) \rangle &= A_{jk}(r) + \langle u_j(x) u_k(x) u_l(x) u_m(x) \rangle B_{ijk}(r) + \\ &\quad \langle u_j(x) u_k(x) u_l(x) u_m(x) u_n(x) \rangle C_{ijkl}(r) = \langle u_j(x) u_k(x) u_i(x+rx) \rangle \end{aligned}$$

etc...

or symbolically represented as:

$$[A][C] = [B]$$

where  $[A]$  represents the matrix of moments of order up to  $2^n$  at the reference point  $x$ ,  $[C]$  is the unknown coefficients in the stochastic estimation expression (functions of  $r$ ) and  $[B]$  represents the two-point,  $n$ -th order spatial correlations.

B

# STOCHASTIC ESTIMATION OF TWO-POINT CONDITIONAL AVERAGES

→ Adrian, 1987.

Conditional average of  $u$  at  $r$  given condition at  $x_1$  and  $x_2$ :

$$\bar{u}(r; x_1, x_2) = \langle u(r) | u(x_1), u(x_2) \rangle$$

Assume a linear estimate for  $\bar{u}(r; x_1, x_2)$ :

$$u_i(r; x_1, x_2) = A_{ij}(r) u_j(x_1) + B_{ij}(r) u_j(x_2) + O[u^2]$$

Determine  $A_{ij}(r)$  and  $B_{ij}(r)$  by least-square procedure:

$$e_i = \langle [\hat{u}_i(r) - u_i(r)]^2 \rangle \quad \text{Min.}$$

Minimize the error with respect to the unknown coefficients  $A_{ij}(r)$  and  $B_{ij}(r)$ :

$$\frac{\partial e_i}{\partial A_{ij}(r)} = \frac{\partial e_i}{\partial B_{ij}(r)} = 0$$

which yields symbolically:

$$[A][C] = [B]$$

where  $[A]$  is a matrix formed by the second order one- and two-point correlation with point  $x_1$  and  $x_2$ ,  $[C]$  represent the unknowns coefficients  $A_{ij}$  and  $B_{ij}$ , and  $[B]$  represent the two-point spatial correlation between points  $r$  and  $x_1$  and between points  $r$  and  $x_2$ .

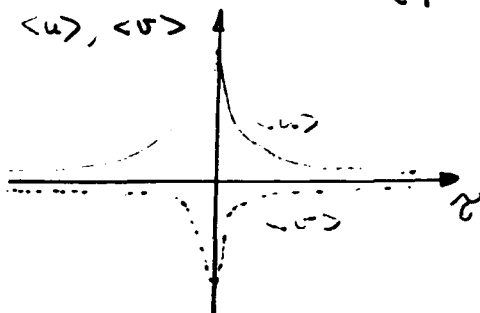
- If the two reference points are only displaced in the homogeneous direction(s) with respect to each other, all quantities in the matrix  $[A]$  and the right-hand side  $[B]$  can be written from the 2-point spatial correlation tensor  $R_{ij}(r; x)$ .

- This procedure allows to defined structures of a specific scale (forced by the separation between  $x_1$  and  $x_2$ ).

→ • Generalization of this procedure to form non-linear, time-dependent estimates of multi-point conditional averages can similarly be obtained.

## "CONVENTIONAL" ENSEMBLE AVERAGING TECHNIQUES

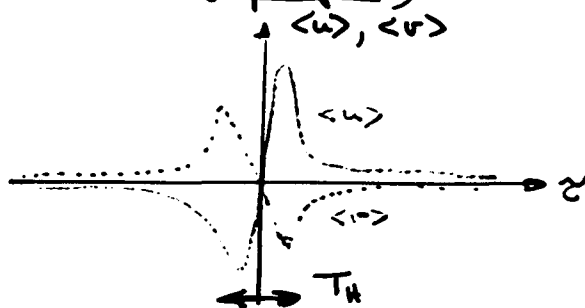
- 1 POINT CONDITIONAL AVERAGES  
(quantum technique, u-level, ...)



The characteristic size (in space and/or time) of the structures reconstructed is commensurate with the integral scale of the variable reconstructed — i.e. "large" structure viewed in isolation

- "1 1/2" or 2 POINT CONDITIONAL AVERAGES  
(VITA / VISA, ...)

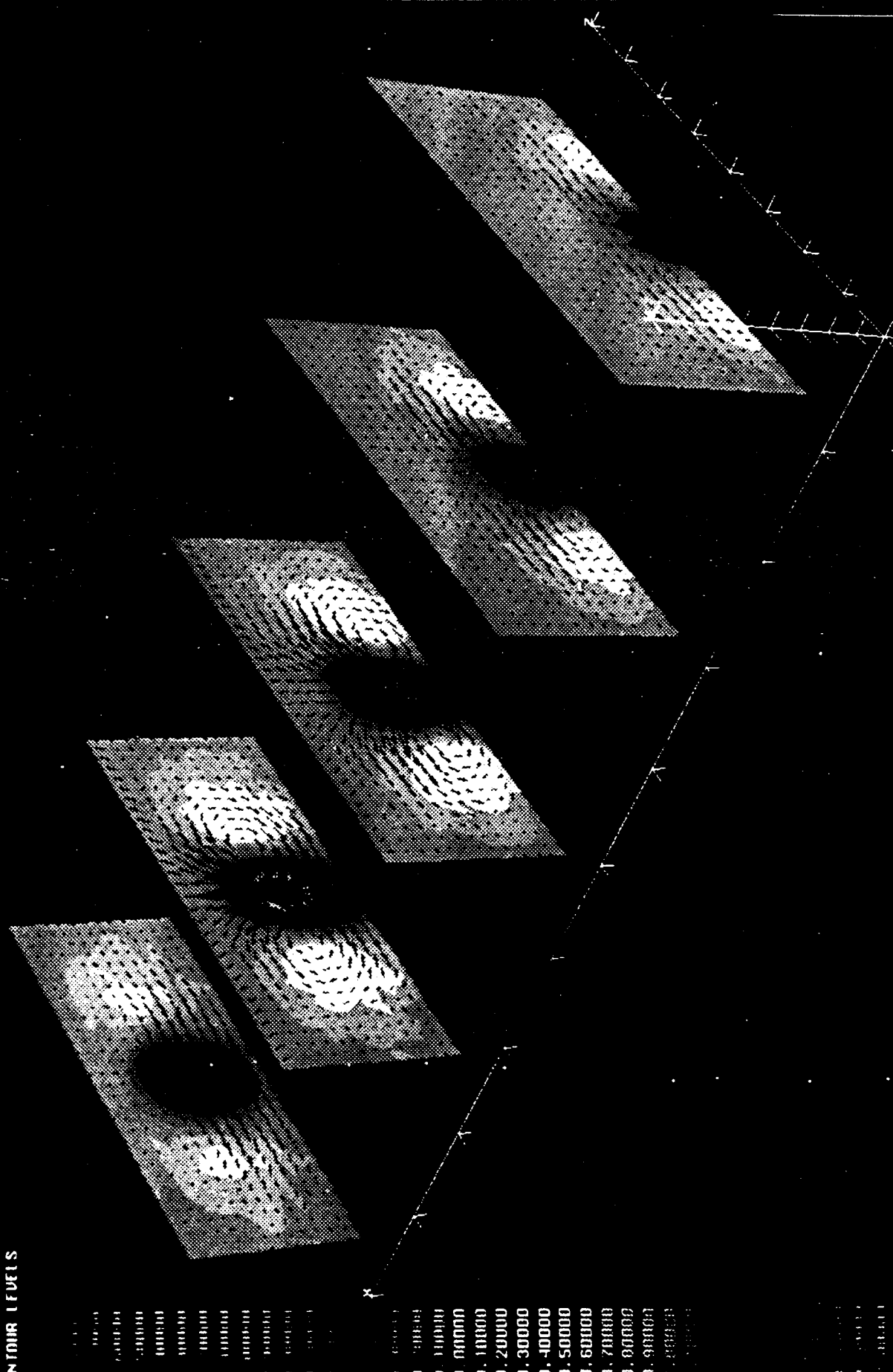
One detection point, but sharp change over a short (specified) time scale



The 1 1/2 or 2 point techniques yield much sharper features since a time/length scale is imposed in addition to the integral scale of the variable reconstructed.

**INDIAN FUELS**

### One-point Condition

$$t2 \text{ U/delta} = -.5$$


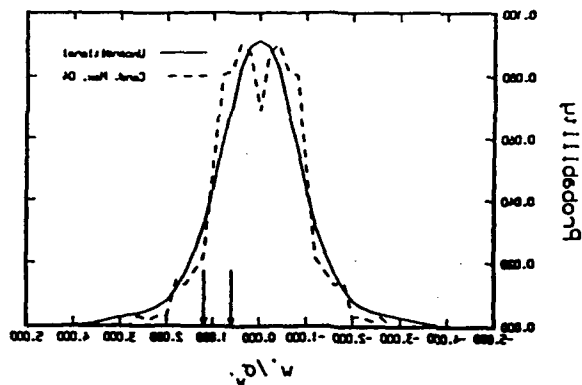


FIG. 1. The probability density function of spanwise velocity fluctuations at  $x^+ = 50$  unperturbed and conditioned on the  $Q^*$  event.

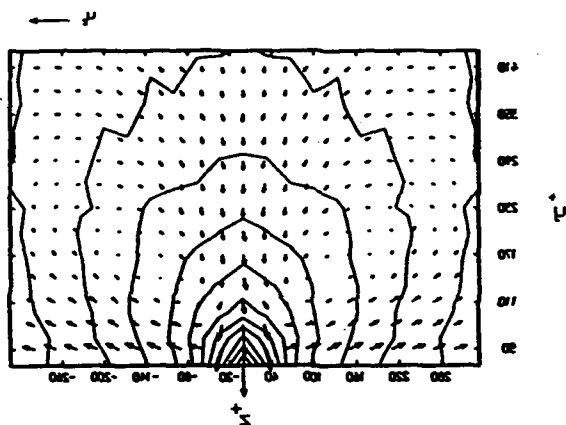


FIG. 2. The vector map of normal and spanwise velocity perturbation and contours of streamwise velocity perturbation for the symmetric  $Q^*$  event ( $w = 0w^*$ ) at  $x^+ = 0$ .

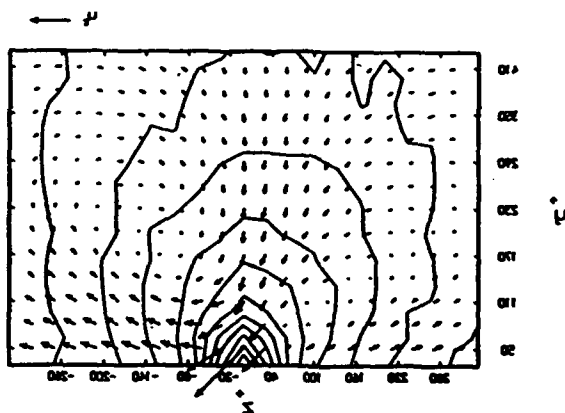


FIG. 3. The vector map of normal and spanwise velocity perturbation and contours of streamwise velocity perturbation for the weakly asymmetric  $Q^*$  event ( $w = 1.23w^*$ ) at  $x^+ = 0$ .

## **GOAL**

Design a tool which can be implemented with experimental data to examine the instantaneous spatial structure of the flow and its evolution in time.

**PSEUDO-DYNAMICS → REALISTICALLY ANIMATED  
KINEMATICS**

### MULTIPOINT CONDITIONAL AVERAGES

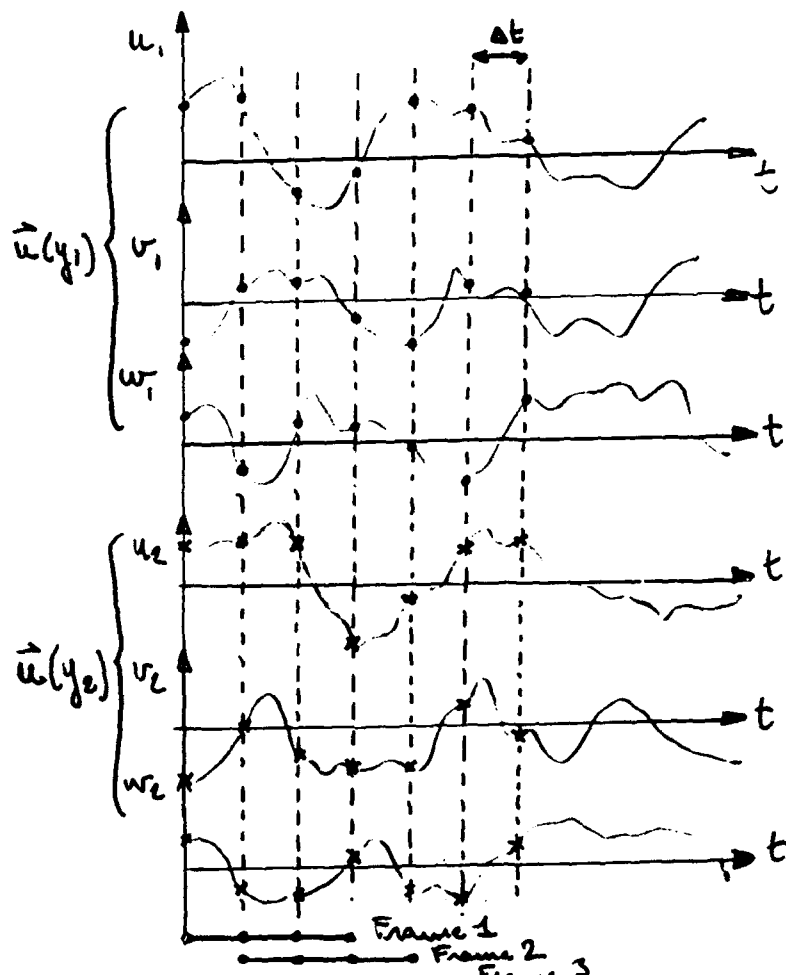
- Easy to implement with the stochastic estimation formalism -- Nearly impossible to implement by conventional ensemble averages.
- Control over time/length scale(s) of observation. Study the interaction of structures rather than unrealistic structures in isolation.

### PSEUDO-DYNAMICS → REALISTICALLY ANIMATED KINEMATICS

- Choice of "conditions": Measured time series at the reference points to get pseudo-dynamics, i.e. a time dependent kinematical representation of the flow consistent with a measured realization of the flow at several points.

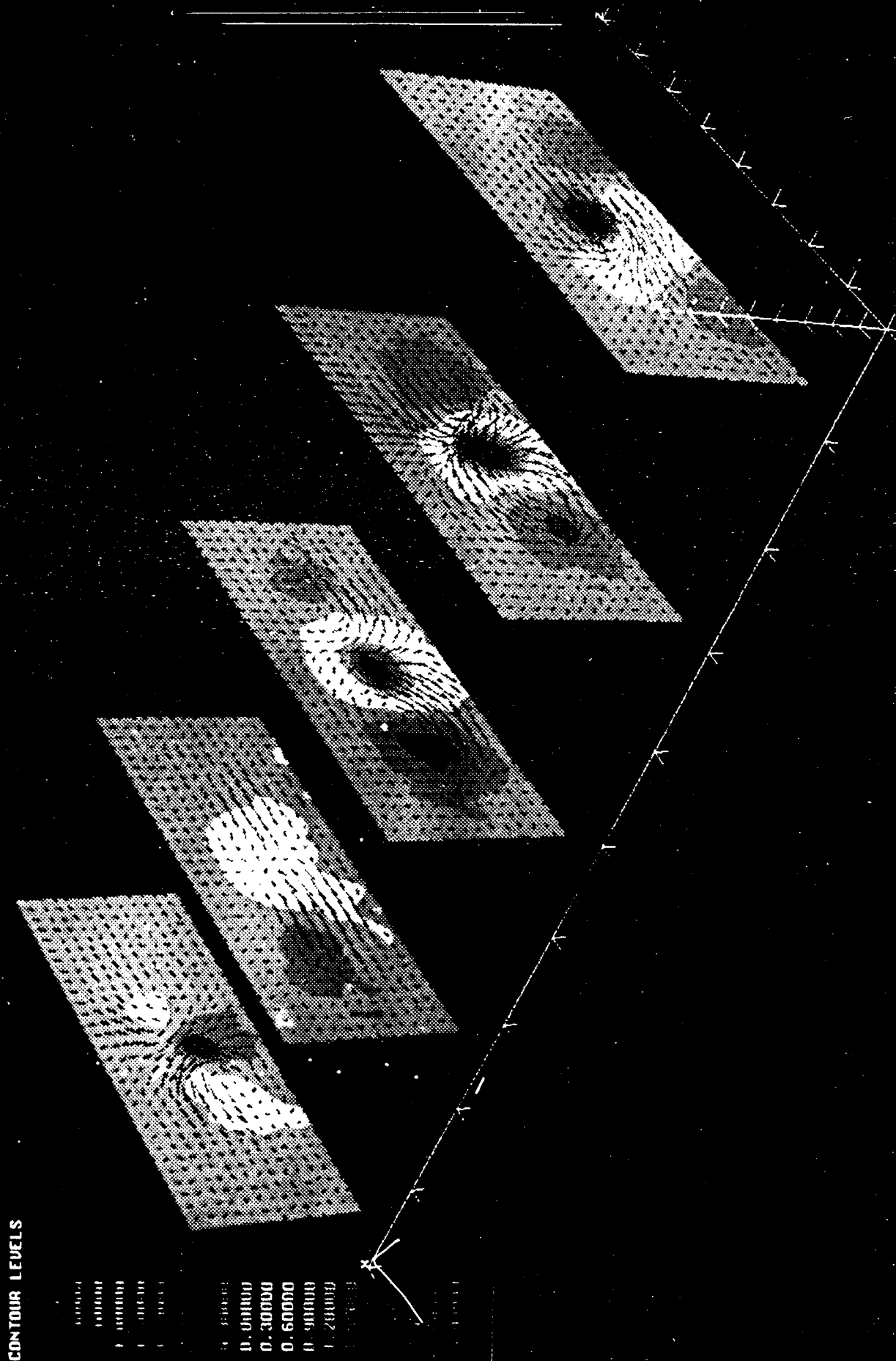
### EXAMPLE IN THE WAKE

4 points separated in time



In example  $y_1$  at peak riv.  
 $y_2$  in center  
 $\Delta t = 10 \Delta t_s$  (1000 Hz)

### Five-point Condition



### Five-point Condition

[illegible]

### Five-point Condition

[illegible]

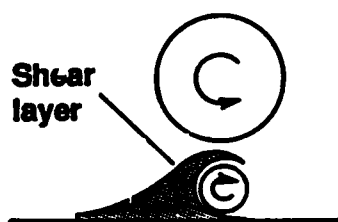
1.20000  
0.90000  
0.60000  
0.30000  
0.00000  
1.00000

### Five-point Condition

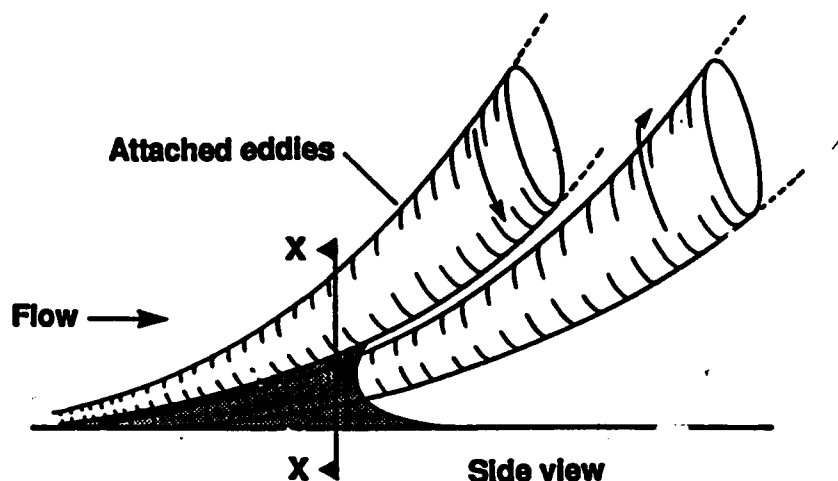
## CONTINUUM LEVELS

Year	1990	1991	1992	1993	1994	1995	1996	1997	1998	1999	2000	2001	2002	2003	2004	2005	2006	2007	2008	2009	2010	2011	2012	2013	2014	2015	2016	2017	2018	2019	2020	2021	2022	2023	2024	2025	2026	2027	2028	2029	2030	2031	2032	2033	2034	2035	2036	2037	2038	2039	2040	2041	2042	2043	2044	2045	2046	2047	2048	2049	2050	2051	2052	2053	2054	2055	2056	2057	2058	2059	2060	2061	2062	2063	2064	2065	2066	2067	2068	2069	2070	2071	2072	2073	2074	2075	2076	2077	2078	2079	2080	2081	2082	2083	2084	2085	2086	2087	2088	2089	2090	2091	2092	2093	2094	2095	2096	2097	2098	2099
1990	1990	1991	1992	1993	1994	1995	1996	1997	1998	1999	2000	2001	2002	2003	2004	2005	2006	2007	2008	2009	2010	2011	2012	2013	2014	2015	2016	2017	2018	2019	2020	2021	2022	2023	2024	2025	2026	2027	2028	2029	2030	2031	2032	2033	2034	2035	2036	2037	2038	2039	2040	2041	2042	2043	2044	2045	2046	2047	2048	2049	2050	2051	2052	2053	2054	2055	2056	2057	2058	2059	2060	2061	2062	2063	2064	2065	2066	2067	2068	2069	2070	2071	2072	2073	2074	2075	2076	2077	2078	2079	2080	2081	2082	2083	2084	2085	2086	2087	2088	2089	2090	2091	2092	2093	2094	2095	2096	2097	2098	2099

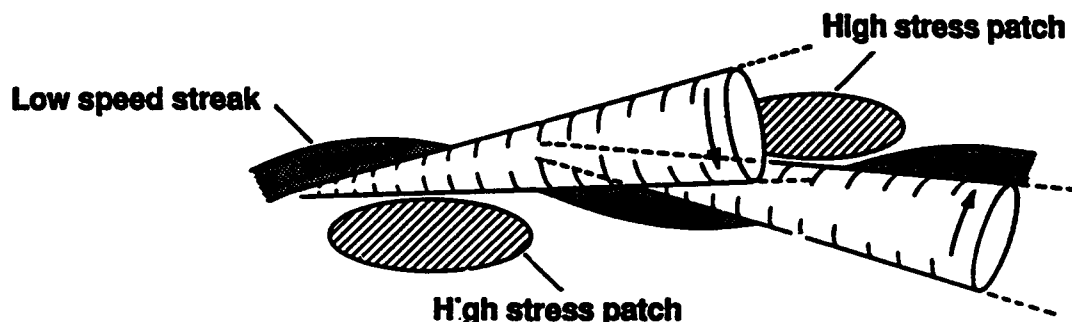
0. 30000  
0. 00000  
0. 30000  
0. 60000  
0. 90000  
1. 20000



Section XX



Side view



Plan view

STRETCH

# VELOCITY

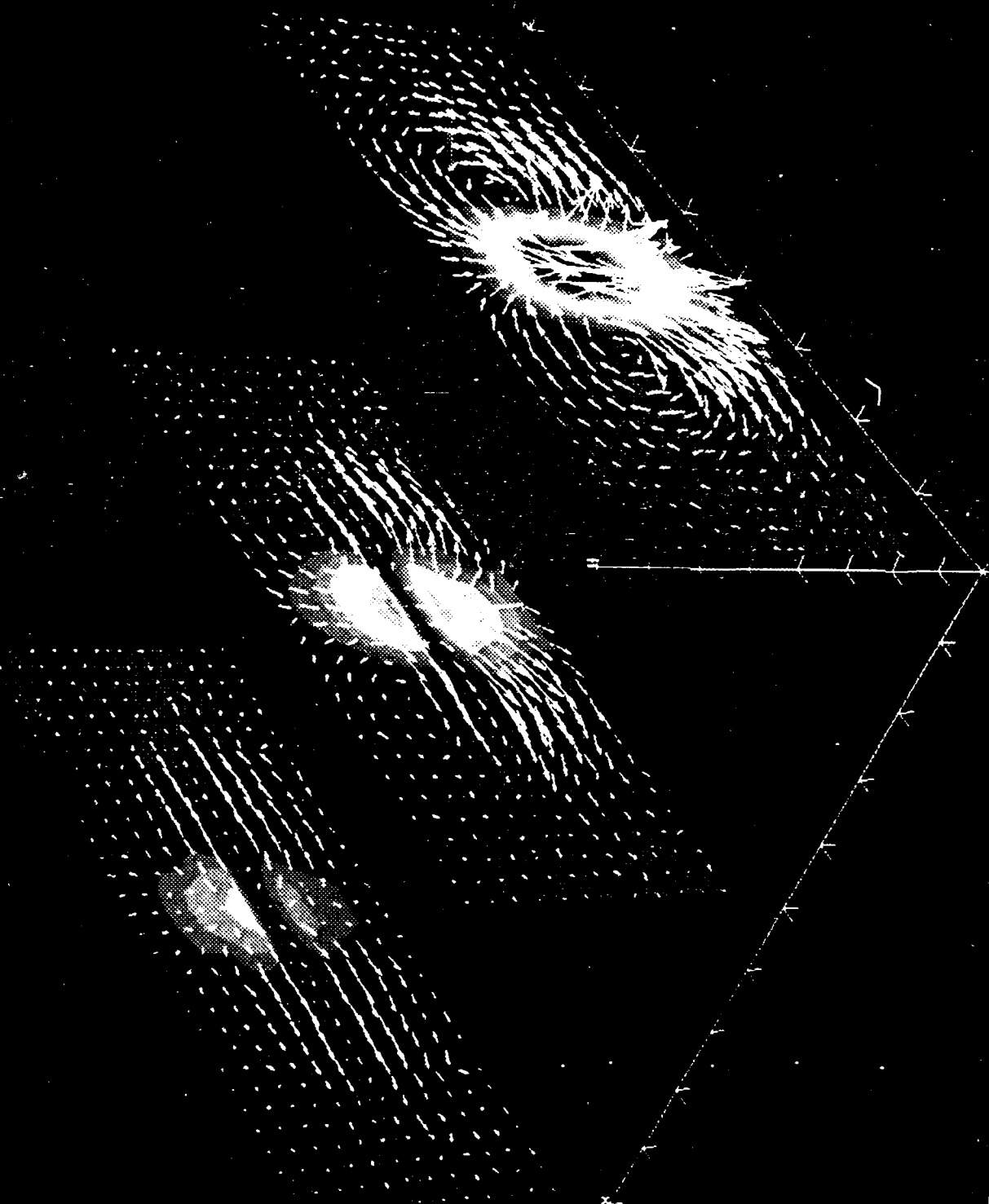
Manipulated Case

$X/\delta = 0.0, 0.5, 1.0$      $t/\delta = 0$

CONTOUR LEVELS

0.00000  
0.10000  
0.20000  
0.30000  
0.40000  
0.50000

0.60000  
0.70000  
0.80000  
0.90000  
1.00000





CONTINUUM LEVELS



X = 0.5 Time = -0.5

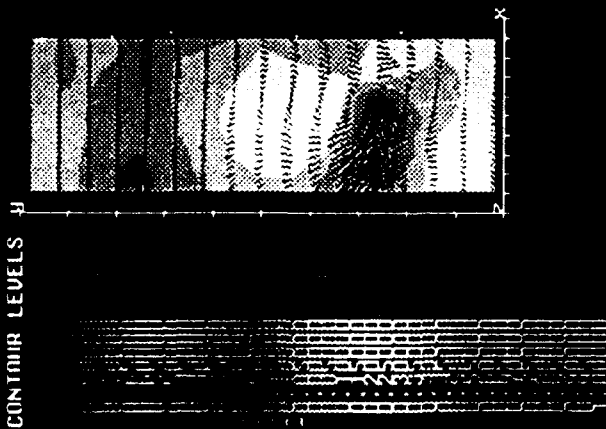


VELOCITY  
Manipulated Case  
X = 0.5 Time = -0.5

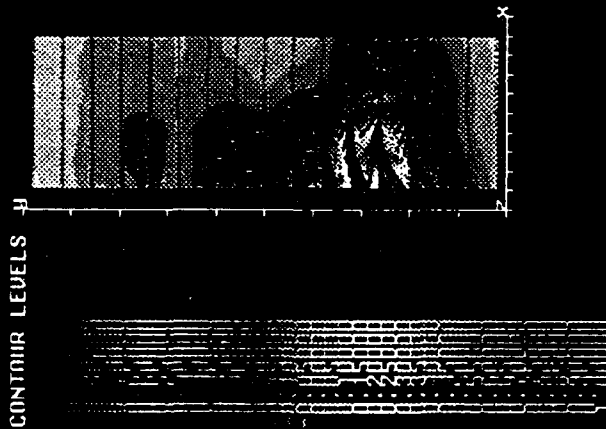
CONTINUUM LEVELS



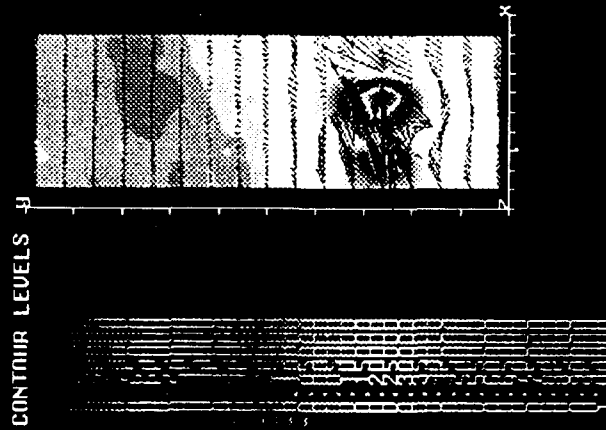
VEL Y  
Four points Condition  
Contours of u



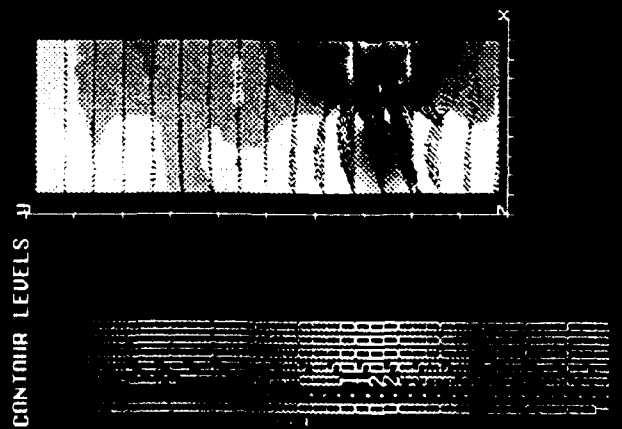
VEL X  
Four points Condition  
Contours of u



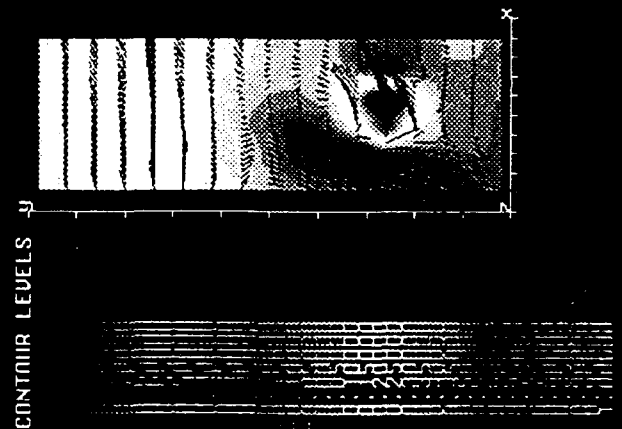
VELOCITY  
Four points Condition  
Contours of u



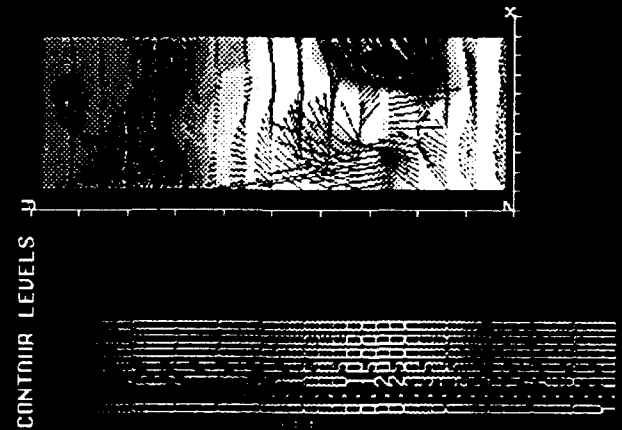
VELOCITY  
Four points Condition  
Contours of u



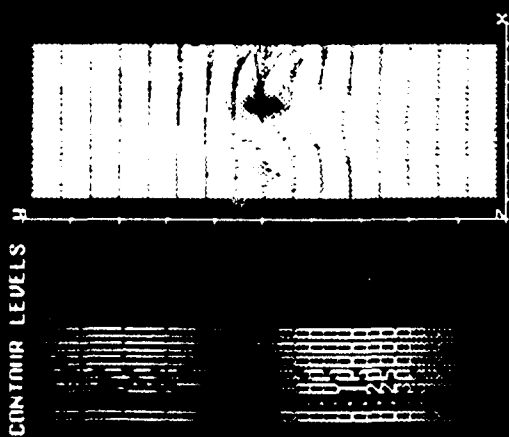
VELOCITY  
Four points Condition  
Contours of u



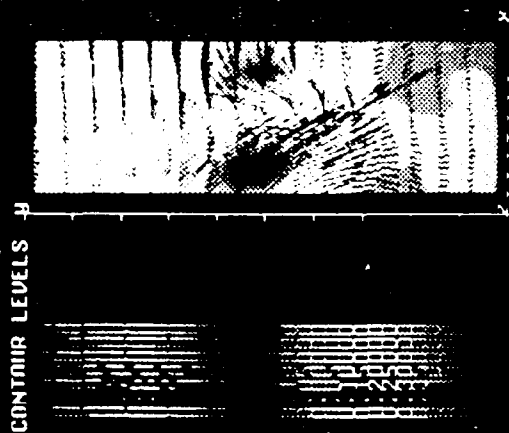
VELOCITY  
Four points Condition  
Contours of u



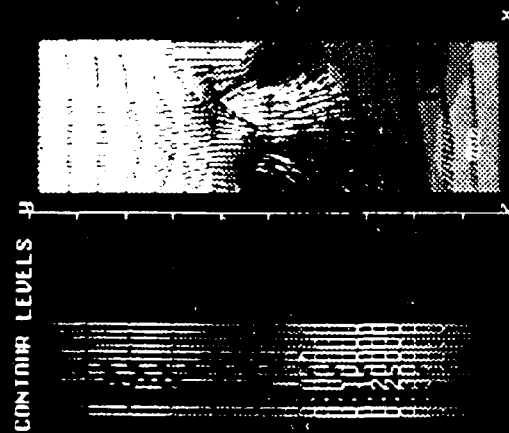
VELOCITY  
Four points Condition  
Contours of  $u$



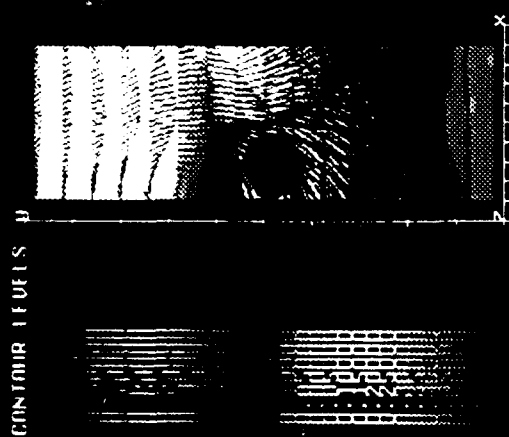
VELOCITY  
Four points Condition  
Contours of  $u$



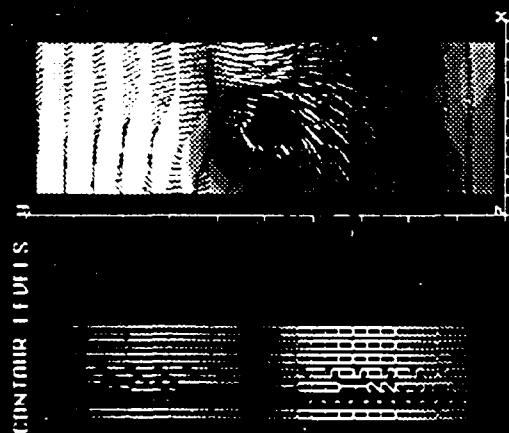
VELOCITY  
Four points Condition  
Contours of  $u$



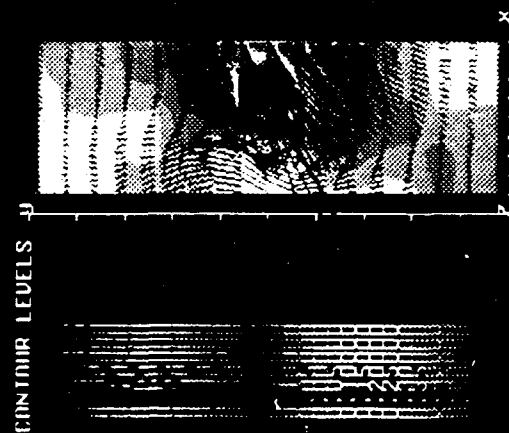
VELOCITY  
Four points Condition  
Contours of  $u$



VELOCITY  
Four points Condition  
Contours of  $u$



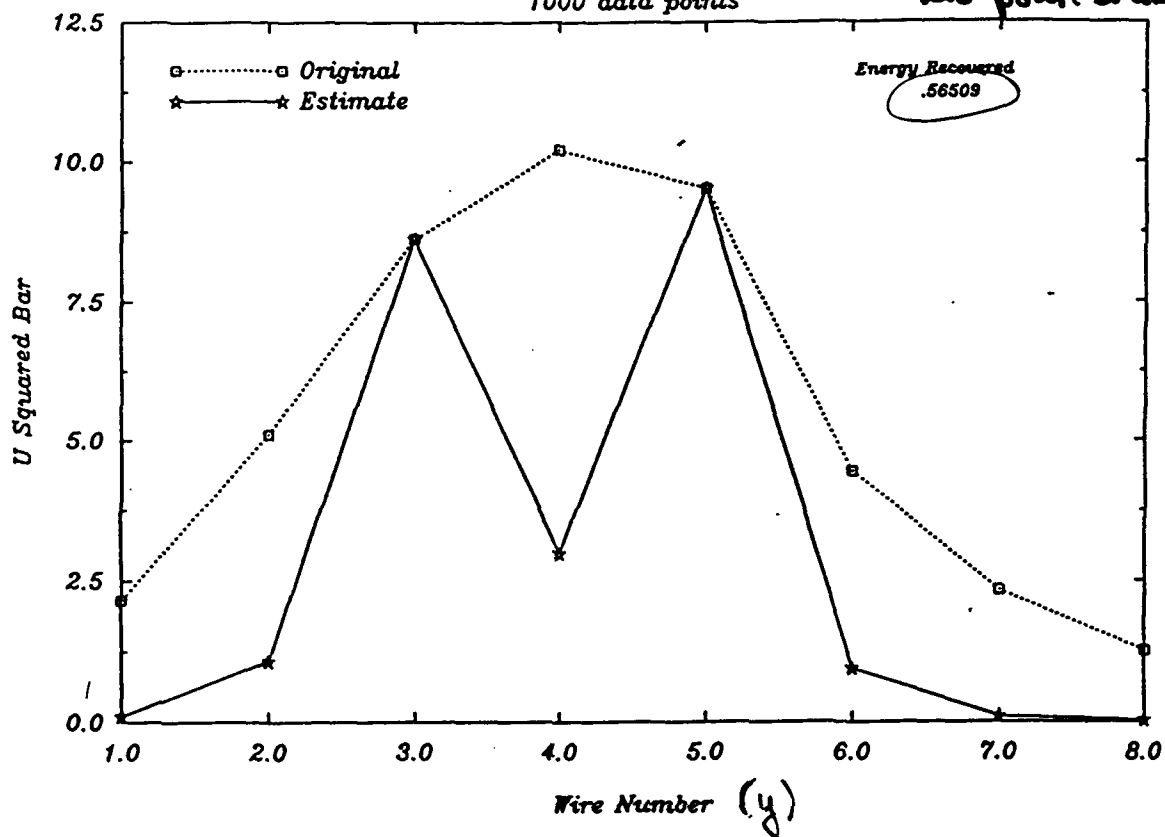
VELOCITY  
Four points Condition  
Contours of  $u$



Estimate Using Wires 3 & 5

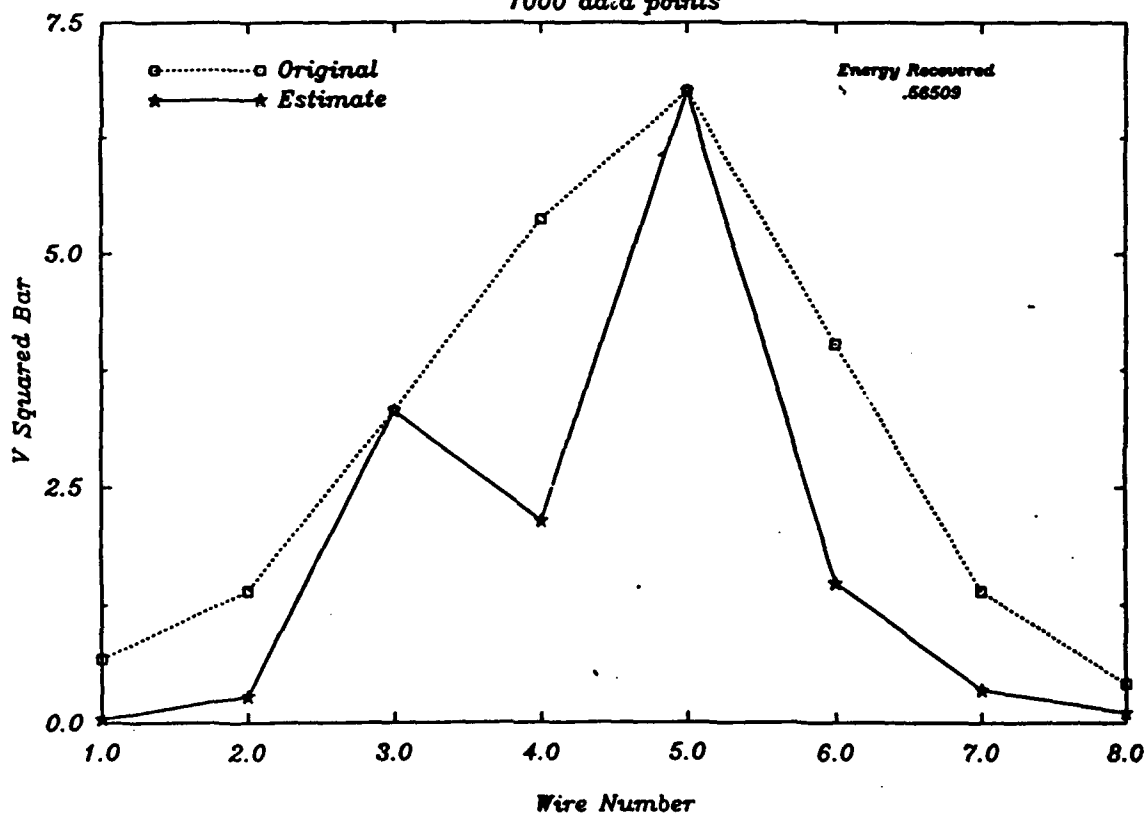
1000 data points

two point estimation



Estimate Using Wires 3 & 5

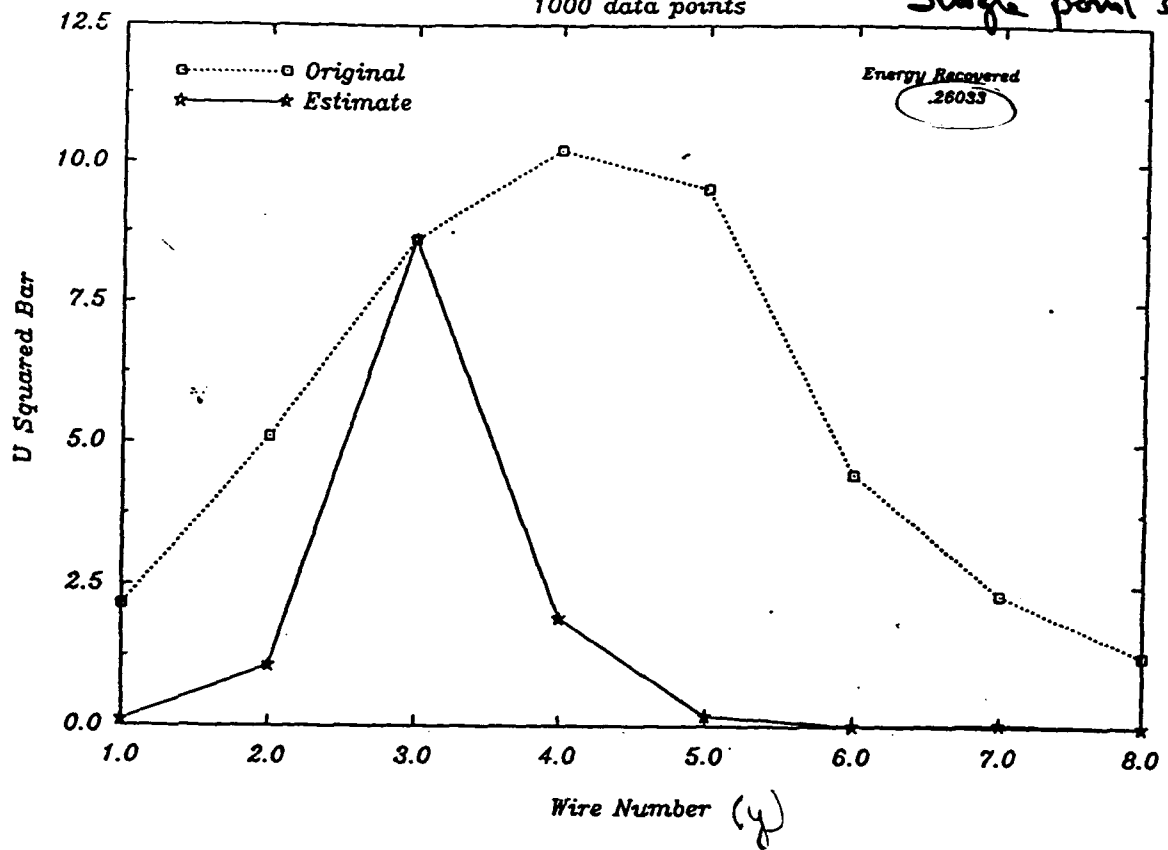
1000 data points



## Estimate Using Wire 3

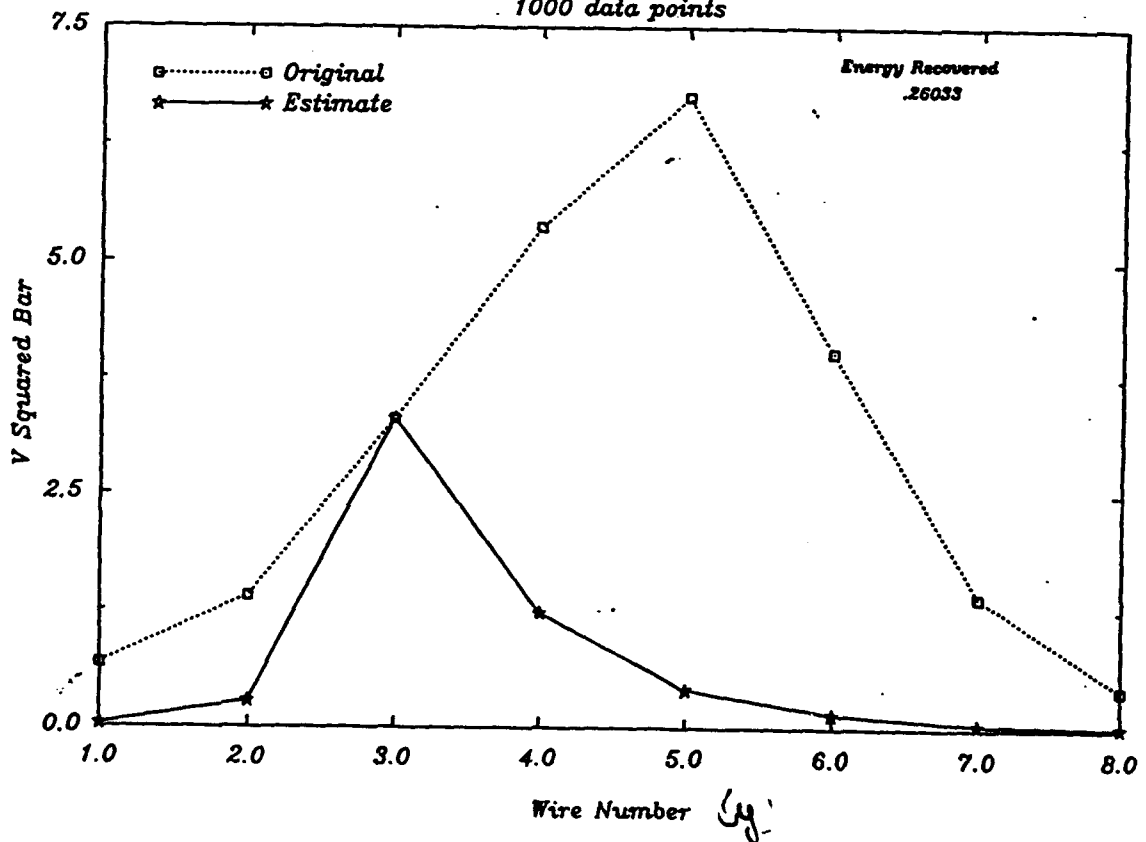
1000 data points

Single point estimate



## Estimate Using Wire 3

1000 data points



# DYNAMICS OF STRUCTURES / STOCHASTIC ESTIMATION APPROACH

- Measure  $R_{ij}(\Delta x, y, y', \Delta z)$
- Fourier Transform in homogeneous directions  $\begin{cases} \Delta x \rightarrow k_x \\ \Delta z \rightarrow k_z \end{cases}$   
to get  $\tilde{R}_{ij}(k_x, y, y', k_z)$
- Perform multipoint (in  $y$ ) stochastic estimate
- Project velocity field (Fourier Transformed) on estimates

$$(*) \quad \tilde{u}_i(k_x, y, k_z, t) = \sum_{j,k} a_{ijk}(k_x, y, k_z) \tilde{u}_j(k_x, y_k, k_z, t)$$

Stochastic estimate coef.  $\rightarrow \psi_{jk}^{k_x, k_z}(y)$

"Modes"  
(alike P.O.D) modes)

- Project (\*) on Navier Stokes equations

$\Downarrow$   
Truncate to get dynamical system (\*\*)

NOTE : (\*) represents pseudo dynamics if  $\tilde{u}_j(k_x, y_k, k_z, t)$  is measured

(\*\*) represents truly dynamics